Phenomenology of top-philic axion-like particles

Supervisor:	Submitted by:
Prof. Davide Pagani	**Simone Tentori**
Co-supervisor:	
Prof. Fabio Maltoni	

"Do the bop, bop, bop to the top."

Sharpay Evans -
High School Musical

1

Abstract

Axion like particles (ALPs), i.e., pseudo-scalar bosons interacting via derivative couplings, are a generic feature of many new physics scenarios, including those addressing the strong-CP problem and/or the existence of dark matter. Their phenomenology is very rich, with a wide range of scales and interactions being directly probed at very different experiments, from accelerators to observatories. In this thesis, we explore the possibility that ALPs might indirectly affect precision collider observables. In particular, we consider an ALP that preferably couples to the top quark (top-philic) and we study new-physics one-loop corrections to processes involving top quarks in the final state. Our study stems from the simple, yet non-trivial observation that one-loop corrections are not infrared divergent even in the case of negligible ALP masses and therefore can be considered on their own. We compute the one-loop corrections of new physics analytically in key cases involving top quark pair production and then implement and validate a fully general next-to-leading-order model in MadGraph5_aMC@NLO, which allows to compute virtual effects for any process of interest. A detailed study of the expected sensitivity to virtual ALPs in top-quark pair production at the LHC is performed.

Contents

Chapter 1

Introduction

Research in particle physics has achieved many fundamental results in the last fifty years culminating with the Higgs boson discovery in 2012 at the Large Hadron Collider (LHC) at CERN. The Higgs boson was the last particle predicted by the Standard Model (SM) left to be observed. A new era towards identifying what is beyond the SM has therefore started. The SM, as it is, presents theoretical limitations and leaves several open questions vis-à-vis observations, that will be faced in the next decades. A concise summary of these problems can be found in [1]. Among them, the strong CP problem emerges as a long-standing puzzle. Several solutions have been proposed in the literature, including the existence of a new particle, an axial pseudo-goldstone boson, coupling derivatively to the SM particles. Generic particles with this property are commonly referred to as ALPs (Axion Like Particles). While we will discuss the strong CP problem and the characteristic of these particles later in the introduction, it is worth mentioning ALPs could also play a role in the Dark Matter (DM) problem: in some scenarios, ALPs could contribute to a fraction or all of the cold DM.

ALPs can be searched for in a wealth of experiments, from accelerator based ones, such as fixed target experiments at high intensity, to astroparticle observatories, to astrophysical and cosmological observations. It is also possible to look for ALPs in collider experiments. In this case, ALPs could either introduce new exotic signatures (via real radiation) or modify SM predictions (via loops). The simplest possibility is looking for missing transverse energy or momentum in events. This implies a very precise reconstruction of the energy and momentum of the particles in the process. A second possibility is to look for indirect effects in high-precision observables, i.e., look for loop effects that modify observables such as the invariant mass or the pseudo-rapidity, or other distribution of final states that can be easily measured in colliders. The top-quark, as we will see later in this chapter, is a perfect probe to look for ALPs, mainly because it is produced with large rates at the LHC and it has a very distinctive signature, allowing almost background-free and very precise measurement of kinematic distributions. Top-quark-related measurements are so precise that have been proposed to indirectly constrain the Higgs Yukawa coupling at LHC, something that has been achieved recently by the CMS collaboration [2]. It is possible to look at EW loops containing the Higgs in the $t\bar{t}$ production in order to theoretically predict how different values of the Yukawa coupling would change top-quark kinematic distributions. One of the purposes of this work is to motivate doing a similar analysis for constraining the ALPs, considering a more general spin-0 particle, interacting with the top-quark as

$$\mathcal{L}_{\text{int}} = -X_0\bar{t}(g + i\tilde{g}\gamma_5)t \,. \tag{1.0.1}$$

The CP odd coupling to the fermion in Yukawa interaction is the distinctive sign of ALPs. To work in full generality and make connections with known results for the CP-even coupling, we consider the more general coupling above. This is also the approach followed in the literature in the context of the Higgs CP properties characterization [3] [4]. The choice of focusing on the top-quark interactions stems from the reasons stated before, on its rich phenomenology at the LHC, and from the possibility of accessing a lot of information from the final states, including measuring the top-quark spin correlation and studying how new physics (NP) next-to-leading order (NLO) processes would change it. There are also reasons from the model-building point of view, that are currently investigated[5].

In this chapter, we will be giving a brief introduction about ALPs particles. Later in the chapter, we will introduce top-quark properties and the key role it plays in Electroweak (EW) theory and in collider physics.

In the second chapter, we will analyze in detail the real-emission processes for vector, scalar and pseudoscalar particles, computing them in the soft limit. We will also run simulations to confirm our calculations.

In the third chapter, we will analyze in detail the virtual corrections to the process $q\bar{q} \to t\bar{t}$ due to the interaction in the Lagrangian (1.0.1). We will compute, in particular, the new-physics one-loop corrected amplitude in the scalar ($\tilde{g} = 0$) and in the pseudoscalar case ($g = 0$), with particular attention to the limit $m_{X_0} \to 0$, that will be related to the same limit in the real emission processes. In order to study the kinematical distribution of the $t\bar{t}$ in the process $pp \to t\bar{t}$ we have realized a UFO model, which is the standard way for implementing in Madgraghp5_aMC@NLO input parameters and Feynman rules for new interactions, including UV counterterms. For its validation, we will use the result for the one-loop corrected amplitude obtained from the $q\bar{q} \to t\bar{t}$ calculation.

In the fourth and final chapter, we will analyze the new-physics virtual correction to the process $pp \to t\bar{t}$. To this end, we will plot for different benchmark points of our model parameters g and $\tilde{g}$ the invariant mass distribution of the $t\bar{t}$ pair, the distribution of the transverse momentum $p_T(t)$, the distribution of the top-quark rapidity y_t and the distribution of the difference between $y_t - y_{\bar{t}}$. For each different benchmark point, we will discuss the new-physics NLO corrections, their implications and in particular their behaviour with respect to m_{X_0}.

1.1 ALPs, axial current and couplings

ALPs are one of the possible solutions to the strong CP problem, which consists of the fact that in the QCD Lagrangian it is possible to introduce a charge-parity (CP) violating term, but the experiments do not measure its phenomenological consequences: a non-vanishing neutron dipole moment. In the following we start describing the strong CP problem: in a general Lagrangian, any term allowed by the underlying symmetry group should be present. Defining the gluon field strength tensor $G_a^{\mu\nu} = \partial^\mu A_a^\nu - \partial^\nu A_a^\mu$ and the gluon dual field strength tensor $\tilde{G}^{\mu\nu} = \frac{1}{2}\epsilon^{\mu\nu\rho\sigma}G_{\rho\sigma}$, where A_a^μ is the gluon field, it is possible to adds in the QCD Lagrangian the term

$$\frac{\theta_{\text{QCD}}}{32\pi^2}\text{Tr}\, G_{\mu\nu}\tilde{G}^{\mu\nu}.$$

This term was initially discarded because it is a total derivative [6]

$$\text{Tr}\, G_{\mu\nu}\tilde{G}_{\mu\nu} = \partial_\mu \text{Tr}\left[\epsilon_{\mu\nu\lambda\sigma}A_\nu(\partial_\lambda A_\sigma + \frac{2}{3}A_\lambda A_\sigma)\right].$$

4

We know that in general total derivatives in Lagrangians can be neglected because the fields vanish at the boundaries. On the other hand, certain field configurations in non-abelian theories do not decrease fast enough at the boundaries to allow the removal of the total derivative. These configurations are non-trivial topological solutions to the field equations and are called solitons. It is possible to show [7] that the CP-violating term can be rewritten in terms of the quarks field. Doing this we obtain a new CP violating term in the Lagrangian

$$\delta\mathcal{L}_{\mathrm{CP}} = \bar{q}_{f_1} i\gamma_5 \theta_{f_1,f_2} q f_2,$$

where θ_{f_1,f_2} is a hermitian matrix with the indices indicating the quarks flavours, which contains the θ_{QCD} dependence.

The CP-violating term implies the existence of a non-vanishing neutron electric dipole moment given by the effective Lagrangian

$$\mathcal{L}_{\mathrm{EDM}} = -\frac{d_{\mathrm{N}}}{2}(\bar{\psi}_{\mathrm{N}} i\gamma^5 \sigma^{\mu\nu})\psi_{\mathrm{N}} F_{\mu\nu},$$

that is related to θ_{QCD} through

$$d_n = (2.4 \pm 1.0)\theta_{\mathrm{QCD}}\, 10^3 e\,\mathrm{fm}.$$

It is possible to experimentally measure the neutron electric dipole moment and the best current measurement leads to the bound [8]:

$$|\theta|_{\mathrm{QCD}} < 1.3\,10^{-10}. \tag{1.1.1}$$

In order to explain this unnaturally low value of θ_{QCD}, Peccei and Quinn proposed that this term arises from a spontaneously broken $U(1)_{\mathrm{A}}$ [9]. Weinberg and Wielzeck noted that this spontaneously broken symmetry can lead to a new pseudo-Nambu-Goldstone boson: the axion a. The axion-gluon interaction term will be

$$\mathcal{L}_{\mathrm{gga}} = -\frac{\alpha_s}{8\pi}\mathrm{Tr}\, G^{\mu\nu}\tilde{G}_{\mu\nu}\frac{a}{f_{\mathrm{a}}},$$

where f_{a} is a parameter related to the scale of the spontaneously broken symmetry. All the other terms in which a appears in the Lagrangian are of a derivative type so, except for the gluon term, we have a shift symmetry: $a \to a + f_{\mathrm{a}}$. We can use this shift symmetry to reabsorb θ_{QCD} in the original Lagrangian, this will leave $a/f_{\mathrm{a}} = \theta(t,x)$ as a dynamical phase. Vafa and Witten proved that in absence of other CP-violation sources, the QCD vacuum energy has an absolute minimum at $\theta = 0$ [10], so given enough time θ will relax to the minimum of its potential solving the so-called CP strong problem (the absence of the neutron dipole electric moment).

The tree-level potential of the QCD axion can be calculated with the methods developed in chiral perturbation theory, giving

$$V_{\mathrm{QCD}}(\theta) = -(m_\pi f_\pi)^2 \sqrt{1 - 4\frac{m_{\mathrm{u}} m_{\mathrm{d}}}{(m_{\mathrm{u}} + m_{\mathrm{d}})^2}\sin^2\left(\frac{\theta}{2}\right)}, \tag{1.1.2}$$

where $m_{\mathrm{u}}\, m_{\mathrm{d}}$ are the up quark and down quark masses, m_π is the pion mass and $f_\pi \approx 93\,\mathrm{MeV}$ is the pion decay constant. The oscillatory behaviour of the axion potential makes it a very good candidate for cold dark matter. We will not enter the details here but the general idea is that if we take a large f_A, the axion will be a very weakly coupled field and due to its oscillating potential will form an

axion-condensate with the exact same properties of dark matter. The QCD axion does not exhaust all the possibilities of axion-like particles (ALPs) and in the next paragraphs, we will present some toy models in which the pseudoscalar coupling arises. In particular, we will show that this coupling can arise in chiral theory with broken axial symmetry and that it can be written in two different ways that are equivalent for on-shell fermions.

1.1.1 Axial current in sigma models

Let's consider the following Lagrangian [11], in which a fermion ψ interacts with two spin-0 particles π and σ

$$\mathcal{L} = i\bar{\psi}\partial_\mu\gamma^\mu\psi + \frac{1}{2}\partial_\mu\pi\partial^\mu\pi + \frac{1}{2}\partial_\mu\sigma\partial^\mu\sigma - \bar{\psi}(g\sigma + ig\gamma_5\pi)\psi - V(\sigma,\pi), \tag{1.1.3}$$

where we can realize the following field transformations:

$$\begin{cases} \delta\psi = \frac{i}{2}\alpha\gamma_5\psi, \\ \delta\bar{\psi} = \frac{i}{2}\alpha\bar{\psi}\gamma_5, \\ \delta\sigma = \alpha\pi, \\ \delta\pi = -\alpha\sigma. \end{cases}$$

Using (A.0.6), the kinetic part of $\mathcal{L}$ transforms as

$$\begin{aligned} \delta\mathcal{L}_{\text{kin}} =&\, i\delta\bar{\psi}\partial_\mu\gamma^\mu\psi + i\bar{\psi}\partial_\mu\gamma^\mu\delta\psi + \partial_\mu\pi\partial^\mu\delta\pi + \partial_\mu\sigma\partial^\mu\delta\sigma = \\ =&\, -\frac{1}{2}\alpha\bar{\psi}\partial_\mu\gamma_5\gamma^\mu\psi - \frac{1}{2}\alpha\bar{\psi}\partial_\mu\gamma^\mu\gamma_5\psi - \partial_\mu\pi\partial^\mu\sigma + \partial_\mu\sigma\partial^\mu\pi = \\ =&\, -\frac{1}{2}\alpha\bar{\psi}\partial_\mu\gamma_5\gamma^\mu\psi + \frac{1}{2}\alpha\bar{\psi}\partial_\mu\gamma_5\gamma^\mu\psi = 0, \end{aligned} \tag{1.1.4}$$

while the interaction part, considering $\delta V(\sigma,\pi) = 0$, transforms as

$$\begin{aligned} \delta\mathcal{L}_{\text{int}} =&\, -2\bar{\psi}(g\sigma + ig\gamma_5\pi)\delta\psi - \bar{\psi}(g\delta\sigma + ig\gamma_5\delta\pi)\psi - \delta V(\sigma,\pi) \\ =&\, -a\bar{\psi}(ig\sigma - g\gamma_5\pi)\gamma_5\psi - \alpha\bar{\psi}(g\pi - ig\gamma_5\sigma)\psi = \\ =&\, -ig\alpha\sigma\bar{\psi}\gamma_5\psi + ag\pi\bar{\psi}\psi - \alpha\pi g\bar{\psi}\psi + ig\alpha\sigma\bar{\psi}\gamma_5\psi = 0. \end{aligned} \tag{1.1.5}$$

Of course, for this equality to work, we had to assume a potential that is invariant under the transformation in (1.1.1). The axial transformation we have written can then be associated with a conserved axial current. From Noether's theorem we have

$$J^\mu = \frac{\partial\mathcal{L}}{\partial\partial_\mu\phi_n}\frac{\delta\phi_n}{\delta\alpha}, \tag{1.1.6}$$

which for our Lagrangian this means

$$J^\mu = \frac{1}{2}\bar{\psi}\gamma_5\gamma^\mu\psi + \pi\partial^\mu\sigma - \sigma\partial^\mu\pi. \tag{1.1.7}$$

Using Noether theorem we know that $\partial_\mu J^\mu = 0$, so

$$0 = \frac{1}{2}\partial_\mu(\bar{\psi}\gamma_5\gamma^\mu\psi) + (\partial_\mu\pi\partial^\mu\sigma - \partial_\mu\pi\partial^\mu\sigma) - \sigma\Box\pi + \pi\Box\sigma = \frac{1}{2}\partial_\mu(\bar{\psi}\gamma_5\gamma^\mu\psi) - \sigma\Box\pi + \pi\Box\sigma = 0.$$

If the scalars are massless, using the equation of motion we find:

$$0 = \partial_\mu(\bar{\psi}\gamma_5\gamma^\mu\psi). \tag{1.1.8}$$

Now we can break this symmetry to obtain an effective theory in which only the effects of the pseudoscalar are visible up to a certain energy. Choosing the potential such that the minimum enforces $\langle\pi\rangle = 0$, $\langle\sigma\rangle = -v$, we can make a field redefinition $\sigma = \sigma' - v$. We then can keep only the pseudoscalar interaction up to a certain energy choosing the scalar potential in such a way that σ' has a large mass. With the new field, we obtain

$$\mathcal{L}_{\text{eff}} = i\bar{\psi}\partial_\mu\gamma^\mu\psi + \frac{1}{2}\partial_\mu\pi\partial^\mu\pi + \mathcal{L}_{\sigma'} - \bar{\psi}(gv + ig\gamma_5\pi)\psi - V(\pi), \tag{1.1.9}$$

$$\mathcal{L}_{\sigma'} = \frac{1}{2}\partial_\mu\sigma'\partial^\mu\sigma' - g\sigma'\bar{\psi}\psi - V(\sigma'). \tag{1.1.10}$$

With this mechanism, fermions obtain masses with value $m = gv$. Choosing a large value for the σ mass implies that it is possible to see the scalar σ or its effects only at very high energy. In this way, we have started with a Lagrangian that had a $U(1)_A$ symmetry and we have ended up with an effective low energy Lagrangian $\mathcal{L}_{\text{eff}}$ that has lost this symmetry. Neither to say, if we keep the whole $\mathcal{L}_{\text{eff}} + \mathcal{L}_{\sigma'}$ the $U(1)_A$ symmetry is still intact.

1.1.2 Pseudoscalar interaction arising from chiral interaction

We can consider a different type of model in which the pseudoscalar originates in a totally natural way. Consider a complex scalar H interacting with a fermion ψ with the following Lagrangian

$$\mathcal{L} = \partial_\mu H\partial^\mu H^* + i\bar{\psi}_L\partial_\mu\gamma^\mu\psi_L + i\bar{\psi}_R\partial_\mu\gamma^\mu\psi_R - y(H^*\bar{\psi}_L\psi_R + H\bar{\psi}_R\psi_L) - V(H).$$

We can consider a $U(1)_A$ transformation for which

$$\begin{cases} \delta\psi_L = -iq\alpha\psi_L, \\ \delta\psi_R = +iq\alpha\psi_R, \\ \delta H = 2iq\alpha H. \end{cases}$$

Using (1.1.6) we can find the conserved current

$$J^\mu = 2(H\partial^\mu H^* - H^*\partial^\mu H) - i(\bar{\psi}_L\gamma^\mu\psi_L - \bar{\psi}_R\gamma^\mu\psi_R),$$

which implies

$$\partial_\mu(\bar{\psi}_L\gamma^\mu\psi_L - \bar{\psi}_R\gamma^\mu\psi_R) = 0.$$

We can now promote the transformation parameter to a field:

$$\begin{cases} \psi'_L = e^{-iq\frac{\pi(x)}{f}}\psi_L \\ \psi'_R = e^{+iq\frac{\pi(x)}{f}}\psi_R \\ H' = e^{2iq\frac{\pi(x)}{f}}H, \end{cases}$$

the interaction Lagrangian remains the same, but we have a new kinetic term

$$\mathcal{L}'_{\text{kin}} = \partial_\mu H\partial^\mu H^* + i\bar{\psi}_L\partial_\mu\gamma^\mu\psi_L + i\bar{\psi}_R\partial_\mu\gamma^\mu\psi_R + \frac{q}{f}(\partial_\mu\pi)(\bar{\psi}_L\gamma^\mu\psi_L - \bar{\psi}_R\gamma^\mu\psi_R).$$

This term represents the interaction of the Goldstone boson π with the fermion ψ. We can rewrite this term in order to make explicit a $U(1)_A$-like current in the interaction

$$\frac{q}{f}(\partial_\mu \pi)(\bar{\psi}_{\mathrm{L}}\gamma^\mu \psi_{\mathrm{L}} - \bar{\psi}_{\mathrm{R}}\gamma^\mu \psi_{\mathrm{R}}) = \frac{q}{f}(\partial_\mu \pi)(\bar{\psi}\gamma^\mu \frac{1-\gamma_5}{2}\psi - \bar{\psi}\gamma^\mu \frac{1+\gamma_5}{2}\psi) =$$
$$= -\frac{q}{f}(\partial_\mu \pi)\bar{\psi}\gamma^\mu \gamma_5 \psi. \tag{1.1.11}$$

This gradient operator has dimension 5, so the interaction is not renormalizable, but, as we will see in the next section, it is possible to connect it to a dimension-4 Yukawa-like operator that is the same present in the CP-odd part of our model Lagrangian (1.0.1).

1.1.3 Gradient model and Yukawa model connection

Without considering any Goldstone boson or any connection to other theories we can simply insert in the Lagrangian a Yukawa interaction with a pseudoscalar coupling

$$\mathcal{L}_{\mathrm{yuk}} = -ig\pi\bar{\psi}\gamma_5 \psi, \tag{1.1.12}$$

this term is in some way connected to the gradient term we have presented in the previous section

$$\mathcal{L}_{\mathrm{grad}} = -\frac{q}{f}(\partial_\mu \pi)\bar{\psi}\gamma^\mu \gamma_5 \psi. \tag{1.1.13}$$

These two interactions are not the same and will, in general, give us different amplitudes. We can simply see this by writing down the Feynman rules for the two models
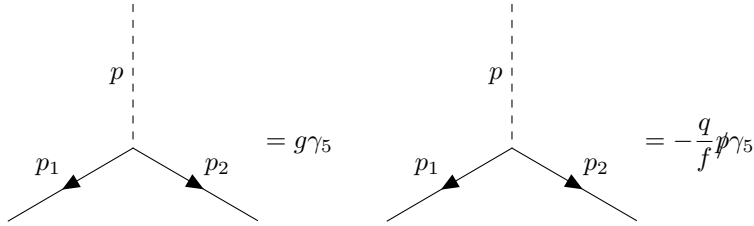
Figure 1.1.1: Feynman rules for the two vertices. Yukawa left, gradient right

However, these interactions can be related using the equations of motion (A.0.21) and (A.0.22)

$$-\frac{q}{f}(\partial_\mu \pi)\bar{\psi}\gamma^\mu \gamma_5 \psi = \frac{q}{f}\pi\partial_\mu(\bar{\psi}\gamma^\mu \gamma_5 \psi) = \frac{q}{f}\pi[(\partial_\mu \bar{\psi})\gamma^\mu \gamma_5 \psi - \bar{\psi}\gamma_5 \gamma^\mu(\partial_\mu \psi)] =$$
$$= \frac{2iqm}{f}\pi\bar{\psi}\gamma_5 \psi, \tag{1.1.14}$$

that is the same term of (1.1.13) if we define

$$g \equiv -\frac{2qm}{f}.$$

8

In (1.1.14) we have used the equation of motion for a free fermion, this only makes sense if we look at external legs, if we want an always valid relation we should look at the full Lagrangian and so the relation between the two operators is not valid anymore. Nevertheless, we can consider a process such as the real emission of a pseudoscalar from a fermion anti-fermion couple. In the soft momentum limit, the off-shell leg from which the pseudoscalar is emitted is almost on-shell and so the relation (1.1.14) is almost exact. We can consider now a general emission process of a particle π, from a fermion anti-fermion couple. In the case of π being a vector or a scalar, the real emissions process will induce an effect of order

$$g_\pi^2 \ln \frac{s}{m_\pi^2} \tag{1.1.15}$$

after the integration over the π momentum, where g_π^2 is the interaction coupling of π with the fermion, m_π is the mass of π and s is the fermion pair invariant mass. The case of a massless π case implies infrared divergences, and in general, the smaller m_π, the larger will be the effect of the emission.

The situation in the case of a pseudoscalar π is different. In this section, we have seen that the associated Feynman rule for a pseudoscalar interacting via a CP-odd Yukawa coupling is equivalent to another one with an overall factor p in front. For this reason, in the soft limit ($p \to 0$) the related real emission amplitude should vanish or give a constant term and therefore we expect the absence of infrared divergences. This property can be exploited from a phenomenological point of view: the mass of the pseudoscalar can be taken as small as we want without having divergent amplitudes, or equivalently large corrections due to real emission.

The behaving mentioned here will be the argument of the chapter 2, in which we will compute in detail real emission in the soft momentum approximation for the vector, scalar and pseudoscalar case.

1.2 Top-quark phenomenology

The top-quark t is the up-type quark of the third SM fermion family, which includes the bottom quark b, the tau lepton τ and the tau-neutrino ν_τ. It was discovered in 1995 by the CDF and D$\cancel{O}$ experiments [12] [13], the present measured mass value is $172.69 \pm 0.30\,\mathrm{GeV}$ [14]. To make the discovery the two experiments studied $p\bar{p}$ collisions at $\sqrt{s} = 1.8\,\mathrm{TeV}$ looking for the process $\bar{t}t \to W^+ b W^- \bar{b}$ and for the subsequent decays $W^+ b W^- \bar{b} \to \ell\nu q\bar{q}b\bar{b}$ and $W^+ b W^- \bar{b} \to \ell\nu\ell'\nu'b\bar{b}$.
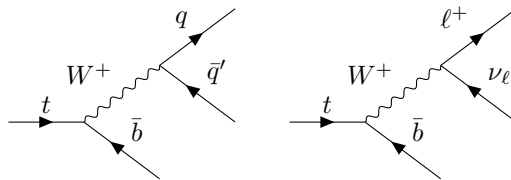

Figure 1.2.1: Representative Feynman diagrams of the two top-quark decay processes taken in consideration for its discovery.

The top-quark phenomenology [15] [16] is very rich, and due to the large top-quark mass a perfect playground for the search of new physics. Before putting our nose inside top-quark phenomenology, we will take a look at top-quark production modes and decays.

1.2.1 Top-quark production at hadron colliders

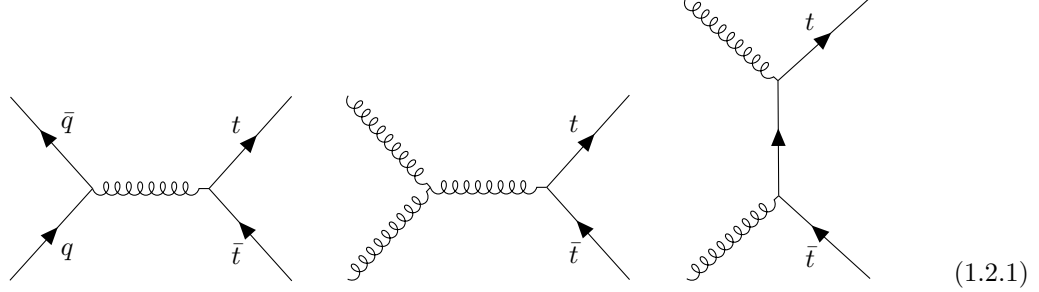The are two partonic processes in hadron colliders, depicted in figure 1.2.2, that can generate a $t\bar{t}$ pair.

$$(1.2.1)$$

Figure 1.2.2: Partonic processes producing a $t\bar{t}$ pair final state.

At low energy, the quark annihilation channel is the favoured one, while at high energy it is the contrary. At the Tevatron ($\sqrt{s} = 1.96$ TeV) 85% of the production cross section is from the quark annihilation, with the remainder from gluon-gluon fusion, at the LHC at $\sqrt{s} = 13$ TeV($\sqrt{s} = 7$ TeV), about 90% (80%) of $t\bar{t}$ production is from gluon-gluon fusion. Predictions for the cross section are computed at the next-to-next-to-leading order (NNLO), meaning two-loop corrections and resumming at all order a class of the logarithmic-enhanced contribution [17]. This is sufficient to give us an idea of how precise the top-quark physics is.

Besides gluon fusion and quark annihilation that produces a $t\bar{t}$ couple, it is possible to produce a single top-quark via EW interactions
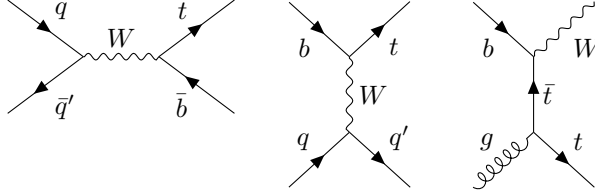

Figure 1.2.3: EW processes producing a single top-quark from an initial QCD state.

the process are $q\bar{q}' \to t\bar{b}$, $qb \to tq'$ and $bg \to Wt$, the so-called associated W production.

The top-quark decays almost immediately due to its large mass, the dominant process is $t \to bW^+$ with a branching ratio BR = 0.998. As we will repeat later the b quark can be experimentally tagged, making the collision event reconstruction very precise. This allows a very accurate measurement of kinematical distributions of the original $t\bar{t}$ couple, in which we can search new-physics signs. The decay chain branching ratios are:

$$\bar{t}t \to W^+bW^-\bar{b} \to q\bar{q}'bq''\bar{q}'''\bar{b} \,(45.7\%)$$
$$\bar{t}t \to W^+bW^-\bar{b} \to q\bar{q}'b\ell^-\bar{\nu}_\ell\bar{b} \,(43.8\%)$$
$$\bar{t}t \to W^+bW^-\bar{b} \to \ell^+\nu_\ell b\ell'^-\bar{\nu}_{\ell'}\bar{b} \,(10.5\%)$$

10

Even if the first process has the highest rate, it is not necessarily the easiest channel to look at, this because in hadron colliders there is a lot of QCD background coming from jet production. For this reason, even if the second and third processes have lower rates, they were considered the golden channels for top-quark discovery.

1.2.2 Relevance of top-quark in EW physics

Although we do not study the top-quark mass in this thesis, we want to motivate why the study of top-quark physics is very important not only for the top-quark sector itself. For this reason, we consider the relation of the top-quark mass with the electroweak sector. Due to its large mass, the top-quark gives the dominant contribution in EW loops, because $y_t \sim m_t/v$ (where v is the Higgs vev and $v \approx 246$ GeV) is by far the largest Yukawa coupling between all the SM fermions. In order to understand how the top-quark corrects the EW observables, we can consider, for example, the two diagrams involving Z and W vector bosons and b and t quarks in figure 1.2.4.
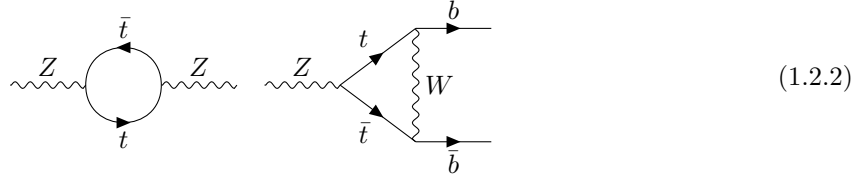

$$(1.2.2)$$

Figure 1.2.4: Top-quark loop correction to Z boson two-point function and to Z decay into a $b\bar{b}$ couple.

Due to the Higgs mechanism, we know that:

$$\rho \equiv \frac{m_W^2}{m_Z^2 \cos^2 \theta_W} \to \rho_{\text{tree}} = 1, \tag{1.2.3}$$

where ρ_{tree} is the theoretical value of ρ at the tree-level and $\cos \theta_W = m_W/m_Z$. The relation $\rho = 1$ is not anymore true once we take into consideration loop corrections

$$\Delta \rho = \frac{1 - \rho}{\rho} = \frac{\Pi_{WW}(0)}{m_W^2} - \frac{\Pi_{ZZ}(0)}{m_Z^2}, \tag{1.2.4}$$

where Π_{VV} is the real part of the transverse component of the self-energy of the vector boson V. The top-quark, due to its large mass, plays a key role in the correction to m_Z through the Z self-energy. This dependence makes the top-quark the game-changer in the whole electroweak precision observable sector, in fact, the parameter $\Delta \rho$ depends almost exclusively on its mass. It has been calculated that

$$\Delta \rho = 3x_t[1 + \Delta \rho^{\text{QCD}} + \Delta \rho^{\text{EW}}], \tag{1.2.5}$$

$$x_t = \frac{G_\mu m_t^2}{8\sqrt{2}\pi^2} \approx 0.3\%. \tag{1.2.6}$$

In equation (1.2.5), $\Delta \rho^{\text{QCD}}$ contains the higher order (NNLO, NNNLO) QCD corrections and $\Delta \rho^{\text{EW}}$ the twoloop electroweak corrections (neglecting the Higgs mass $\Delta \rho^{\text{EW}} \sim -x_t$) [18].

$$(1.2.8)$$

Figure 1.2.5: Fermionic-loop correction to the Higgs 4-point function.

Another important observable in the EW sector is the branching ratio $\mathrm{BR}(Z \to b\bar{b})$ and so from a theoretical point of view $Zb\bar{b}$ vertex corrections are of fundamental importance. Z decay into $b\bar{b}$ is a well-measured process because the b-quark is experimentally distinguishable from light quarks and gluon jets due to its relatively large mass and lifetime. The effect of the one-loop correction to the $Zb\bar{b}$ vertex can be written by shifting the vector coupling to the fermion by a quantity $(\Delta_b/4\sin\theta_{\mathrm{W}})$. The correction Δ_b is proportional to the mass squared of the fermion running inside the loop in the second diagram of 1.2.4, so maximum for the top-quark [18].

$$\Delta_b = -\frac{G_\mu}{4\sqrt{2}\pi^2}\left(m_t^2 + \frac{1}{3}m_W^2(1 + \cos^2\theta_{\mathrm{W}})\ln\frac{m_t^2}{m_W^2}\right). \tag{1.2.7}$$

Another electroweak process in which the top-quark plays a prominent role is the one in figure 1.2.5. This diagram corrects the Higgs self-coupling λ. Renormalizing the EW Lagrangian, the parameter λ runs with the energy Q. Looking at the running of this parameter it is possible to put constraints on the Higgs boson mass assuming the scale in which new physics should emerge. Of course, it is also possible to do the contrary, and find at which scale we expect new physics given the measured Higgs mass. In order to do this is useful to look at what happens at small λ values, where $\lambda \ll \lambda_t, g_1, g_2$. In this case, the RGE for the Higgs self-coupling give us [18]

$$\lambda(Q^2) = \lambda(v^2) + \frac{1}{16\pi^2}\left[-12\frac{m_t^4}{v^4} + \frac{3}{16}(2g_2^4 + (g_2^2 + g_1^2)^2)\right]\ln\frac{Q^2}{v^2}. \tag{1.2.9}$$

If λ becomes negative at a certain energy the Higgs vacuum becomes unstable because it has no minimum anymore. In order to avoid this we can assume the existence of new physics at the scale where this happens, having in mind that this new physics could correct this behaviour. The energy scale at which this happens is strongly dependent on the top-quark mass, in fact for $m_t = 173.1 \pm 2.1\,\mathrm{GeV}$, the error on top-quark mass allows this scale to vary by six orders of magnitude: $10^8\,\mathrm{GeV} < \mu_{\mathrm{neg}} < 10^{14}\,\mathrm{GeV}$ [19].

1.2.3 Top-quark decays, hadronization and spin correlation

There is another reason the top-quark mass plays a key role in phenomenology and it is related to the top-quark decays and hadronization. We can roughly estimate the hadronization time as the inverse of Λ_{QCD}, because it is the characteristic energy for which non-perturbative effects become dominant in a QCD process. A better estimate can be carried out using Non-Relativistic Quantum Mechanics (NRQM), justified by the high top-quark mass. The NRQM QCD potential can be modelled as a Coulomb plus linear potential

$$V(r) = -\frac{4}{3}\frac{\alpha_s}{r} + kr, \tag{1.2.10}$$

12

where the parameter k is independent on the energy scale and can be extracted by fitting the energy levels given by this potential in the Schrödinger equation with the ones measured experimentally in the charmonium ($c\bar{c}$) or in the bottomonium ($b\bar{b}$) mesons. The reason why we discuss it here, will be more clear at the end of this section.

For the first bound state we have a negative energy eigenvalue, this means that the Coulomb-like potential dominates the linear one; the greater the mass and α_s, the better this approximation becomes. So only for the ground state let's suppose that

$$V_0(r) \simeq -\frac{4}{3}\frac{\alpha_s}{r}. \tag{1.2.11}$$

The Schrödinger equation for this potential is analytically solvable, and the ground state energy results to be

$$E_1 = -\frac{\mu}{2}\left(\frac{4}{3}\alpha_s\right)^2, \tag{1.2.12}$$

where μ is the mass of the quarkonium taken into consideration.

We can now use the virial theorem, which for the Coulomb potential leads to

$$\langle T \rangle = -E = \frac{\mu}{2}\left(\frac{4}{3}\alpha_s\right)^2, \tag{1.2.13}$$

and because our treatment is non-relativistic, by (1.2.13) we find that

$$v = \frac{4}{3}\alpha_s. \tag{1.2.14}$$

From the hydrogen atom theory, we also know that the average radius of the ground state is

$$R_0 = \frac{3}{4\mu\alpha_s} = \frac{1}{\mu v}. \tag{1.2.15}$$

Using this information, with a simple approximation

$$\tau_{\text{form}} = \frac{2\pi r_{1S}}{v_{1S}} = \frac{9\pi}{8\mu_{t\bar{t}}\alpha_s^2} \approx \frac{1}{0.6}\text{GeV}^{-1}. \tag{1.2.16}$$

The lifetime of a bounded $t\bar{t}$ state is instead: $1/2\Gamma_t \approx 1/2.8\text{GeV}^{-1}$ and so much smaller than the formation time. Toponium ($t\bar{t}$ bounded state) formation and detection play a key role in the search for new physics, the exchange of new particles could change the formation time, for example at LHC, in which the $gg \to t\bar{t}$ process production mode is the dominant one, we have, between the others, the virtual diagrams in figure 1.2.6.
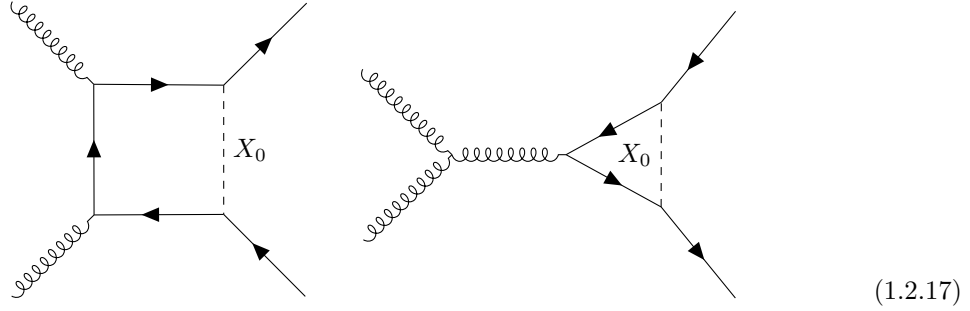
13

$$(1.2.17)$$

Figure 1.2.6

Virtual exchanged particles change the formation time and so the production rate of toponium, these quantities can be measured in order to put constraints on the intensity of new-physics interaction.

The non-hadronization of the top-quark can be exploited for other measurements. The top-quark decay almost exclusively semi-weakly as $t \to W^+ b$, the fact that the top-quark decays before interacting, makes it possible to measure very accurately the CKM value $|V|_{tb}$. New-physics effects could then be searched in anomalies in this coupling.

Yet another way to exploit this property is by studying top-quark pair spin correlation. Light quarks hadronize before decaying allowing depolarization and spin flip. The same does not happen to top quarks. In order to understand why this is the case let's look back at the possible way in which we can produce a $t\bar{t}$ pair in 1.2.2.

In the first diagram, we have $q\bar{q} \to t\bar{t}$. The sub-process $q\bar{q} \to g$ implies the exchange of a spin 1 particle. Due to this fact, the only allowed combinations in the final state are: $q_L \bar{q}_R$, $q_R \bar{q}_L$ and the spins of the two produced top-quark must be aligned [20].

The initial state gluon fusion processes are more complicated: only in one case the s-channel forces the previous situation, but this is not the case for the u and t-channels. We have two possibilities in the initial state: $g_L g_R$ interaction, producing spin-aligned quarks and $g_L g_L, g_R g_R$ interactions, in which spins are in opposite directions [21].

A good observable for this quantity is the correlation

$$C = \frac{\sigma(t_R \bar{t}_R + t_L \bar{t}_L) - \sigma(t_L \bar{t}_R + t_R \bar{t}_L)}{\sigma(t_R \bar{t}_R + t_L \bar{t}_L) + \sigma(t_L \bar{t}_R + t_R \bar{t}_L)}. \tag{1.2.18}$$

Both these quantities have been measured at Tevatron and LHC, the interesting differences arise from the fact that at Tevatron the $q\bar{q} \to t\bar{t}$ dominates over the $gg \to t\bar{t}$ process, while at LHC it is exactly the opposite. At the threshold, at Tevatron, the $t\bar{t}$ pair has zero angular momentum, so it is in the state $^3S_1$, spin eigenstates are:

$$|--\rangle,$$
$$\frac{1}{\sqrt{2}}(|+-\rangle + |-+\rangle),$$
$$|++\rangle.$$

14

Since the t and the $\bar{t}$ move oppositely in the couple centre-of-mass frame, they have opposite helicities if they have the same spin. At the threshold the correlation will be:

$$C = \frac{1}{3} - \frac{2}{3} = -33\%.$$

At high energies, helicity conservation gives instead $C = -100\%$. Adding the gluon contribution and considering PDFs, in average $C \approx -40\%$

At LHC the $t\bar{t}$ pair near the threshold is in the $^1S_0$ state

$$\frac{1}{\sqrt{2}}(|+-\rangle - |-+\rangle)$$

and $C = +100\%$. At high energies, helicity conservation imposes opposite helicities again. Averaging and considering PDFs, $C \approx 31\%$ [22].

NLO contributions enter into the computation of these quantities and can change more or less significantly the spin correlation. This is of course also the case for new-physics interactions. The diagrams shown in figure 1.2.6 are exactly those we are going to calculate in this thesis. We will not investigate and study their impact on spin polarization or on the correlation C, but this kind of study is an example of possible future developments of the results obtained in this thesis. This is the reason why we have introduced this section here.

Chapter 2

Infrared divergences in real emissions

As we have said in the previous chapter, the first possibility to search for new physics consisting of invisible particles is looking at missing transverse energy or momentum. In hadronic colliders due to the partonic structure of the incident particles, the total momentum along the collision axis is unknown. What is known is that the total initial transverse momentum ($\vec{p}_{\mathrm{T,i}}$) is equal to zero. Due to the momentum conservation

$$\vec{p}_{\mathrm{T,i}} = \vec{p}_{\mathrm{T,f}} = 0, \tag{2.0.1}$$

where $\vec{p}_{\mathrm{T,f}}$ is the total final transverse momentum. However, the measured $\vec{p}_{\mathrm{T,f}}$ can be different from zero, because particles that do not interact via QED and QCD, are not visible to detectors. In this case, we will have a missing transverse momentum ($\vec{p}_{\mathrm{T,missing}}$). If in the process $pp \to t\bar{t}X_0$, X_0 is an ALP, it will be invisible to the detectors and we will have $\vec{p}_{\mathrm{T,missing}}$. We can determine its value using (2.0.1).

$$\vec{p}_{\mathrm{T,X_0}} = \vec{p}_{\mathrm{T,missing}} = -\vec{p}_{\mathrm{T,f,visible}} = -\vec{p}_{\mathrm{T,t}} - \vec{p}_{\mathrm{T,\bar{t}}}. \tag{2.0.2}$$

Measuring the $p_{\mathrm{T,missing}}$ it is possible to set bounds on new physics parameters related to the decay of SM particles into invisible particles. The first difficulty, in this kind of procedure, is to obtain a precise measurement of the final transverse momentum in the context of the event reconstruction. Besides this, in colliders, we never detect the produced t and $\bar{t}$ directly, but the product of their decay. The top-quark mainly decays as $t \to W^+b$ and the following $W^+ \to \ell^+\nu_\ell$ produces neutrinos, which are invisible particles. In this case, (2.0.2) must be revised and becomes

$$\vec{p}_{\mathrm{T,missing}} = \vec{p}_{\mathrm{T,X_0}} + \vec{p}_{\mathrm{T,invisible,SM}} = -\vec{p}_{\mathrm{T,f,visible}}. \tag{2.0.3}$$

To overcome this problem we need to simulate the $pp \to t\bar{t}X_0$ process and the top-quark decays in order to predict the transverse momentum distribution of the final invisible SM particles.

As we have said in the introduction, real emission processes like $f\bar{f} \to f\bar{f}\pi$, for π scalar-like or vector-like particle, are characterized by the dependence:

$$\sigma_{f\bar{f}\pi} \propto g_\pi^2 \ln\left(\frac{s}{m_\pi^2}\right), \tag{2.0.4}$$

16

where g_π is the coupling of the π particle to the fermion f and m_π is the π particle mass. The existence of new physics in real emission processes is bounded by experimental measurements, so we cannot have too much large NP effect, because they are excluded by existing measures. Looking at (2.0.4) this implies having a small value of g_π or a large value of the m_π. This well-known behaviour presents an exception for the case of pseudoscalar particles for which, as we will show later, we have no logarithmic infrared divergences when the mass goes to zero, and, in fact, in that limit, the cross section goes like a constant.

In this chapter, we will review the process of real emission for the case of vector, scalar and pseudoscalar particles, and the different behaviours with regard to the energy of the processes, in order to verify in a formal way what we have said before.

In order to make the discussion more fluent here we will only present the main results , the details of the calculations can be found in appendix B.

2.1   Soft vector emission

The interaction Lagrangian for a vector boson A^μ and a fermion ψ is

$$\mathcal{L}_{\text{int}} = -g\bar{\psi}\slashed{A}\psi. \tag{2.1.1}$$

We want to inspect the emission of the vector particle for low momenta, we consider here the following sub-process

$$f \longrightarrow f + \gamma,$$

where f is a generic fermion and γ is the massless vector boson. For this process we have two Feynman diagrams:

$$\tag{2.1.2}$$

$$\tag{2.1.3}$$
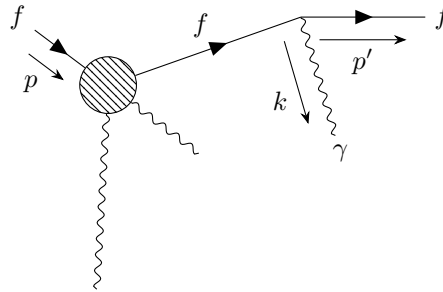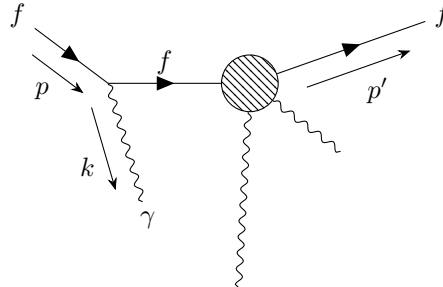
Following [23], we can compute the amplitude as

$$i\mathcal{M} = (ig)\bar{u}(p')\left[\mathcal{M}_0(p',p-k)\left(\frac{\not{p}-\not{k}+m}{(p-k)^2-m^2}\right)\gamma^\mu\epsilon_u^* + \right.$$

$$\left. + \gamma^\mu\epsilon_u^*\left(\frac{\not{p}'+\not{k}+m}{(p'+k)^2-m^2}\right)\mathcal{M}_0(p'+k,p)\right]u(p). \tag{2.1.4}$$

We are interested in the infrared emission case, so taking into account $\left|\vec{k}\right| \ll |\vec{p}-\vec{p'}|$, we will have $M_0(p'+k,p) \simeq M_0(p',p-k) \simeq M_0(p',p)$ and the momentum $\not{k}$ will be negligible in the numerators.

With these tricks and using the fact that $k^2 = 0$ and $p^2 = p'^2 = m^2$, we are able to write

$$i\mathcal{M} = (ig)\bar{u}(p')\left[\mathcal{M}_0(p',p)\left(-\frac{\not{p}+m}{2p\cdot k}\right)\gamma^\rho\epsilon_\rho^* + \gamma^\mu\epsilon_\mu^*\left(\frac{\not{p}'+m}{2p'\cdot k}\right)\mathcal{M}_0(p',p)\right]u(p). \tag{2.1.5}$$

Then we can work on the numerator to obtain

$$i\mathcal{M} = (ig)\bar{u}(p')\mathcal{M}_0(p',p)u(p)\left[\left(-\frac{p^\mu\epsilon_\mu^*}{p\cdot k}\right)+\left(\frac{p'^\mu\epsilon_\mu^*}{p'\cdot k}\right)\right]. \tag{2.1.6}$$

In this way, we have obtained a factorization of the process, in which the massless vector emission part stands alone. We now choose a frame in which $p^0 = p'^0 = E$ and we define the 4-vectors explicit as:

$$k^\mu = (E_k, \vec{k}), \quad p^\mu = E(1, \vec{v}), \quad p'^\mu = E(1, \vec{v}'). \tag{2.1.7}$$

Summing over polarization and spins we obtain

$$\frac{1}{(2\pi)^3}\frac{d^3k}{2E_k}|\mathcal{M}|^2 = |\mathcal{M}_0|^2 \, dF_{f\to f\gamma}. \tag{2.1.8}$$

The differential form factor in this frame is

$$dF_{f\to f\gamma} = \frac{d^3k}{2E_k}\frac{g^2}{(2\pi)^3}\left[-\frac{m^2}{(p\cdot k)^2}-\frac{m^2}{(p'\cdot k)^2}+\frac{2p\cdot p'}{(p\cdot k)(p'\cdot k)}\right] = \frac{\alpha}{2\pi}dE_k\frac{1}{E_k}\mathrm{I}_\gamma(\vec{v},\vec{v}'), \tag{2.1.9}$$

where the full form of $\mathrm{I}(v,v')$ and all the calculations can be found in appendix B .

The $\mathrm{I}_\gamma(\vec{v},\vec{v}')$ term does not depend on E_k, so we can integrate the momentum of the vector boson that should go from 0 to $\Delta E = |\vec{p}-\vec{p'}|$

$$dF_{f\to f\gamma} \propto \int_0^{\Delta E}\frac{1}{E_k}dE_k \to \infty. \tag{2.1.10}$$

This is the term that contains the infrared divergence. In order to obtain a finite result one can regulate the integral giving the photon a small mass m_γ. This can be done at the end of the calculation because if we consider high energetic processes, the kinetic part dominates over the mass in the denominator of (2.1.4)

$$dF_{f\to f\gamma} \propto \int_{m_\gamma}^{\Delta E}\frac{1}{E_k}dE_k = \log\left(\frac{\Delta E}{m_\gamma}\right). \tag{2.1.11}$$

Now we look at the term $I_\gamma(\vec{v}, \vec{v}')$. We consider the case in which $E \gg m$, so that

$$I_\gamma(\vec{v}, \vec{v}') \simeq \int d(\cos\theta) \left[\frac{2(1 - \vec{v}\vec{v}')}{(1 - \hat{k}\vec{v}')(1 - \hat{k}\vec{v})} \right]. \tag{2.1.12}$$

The integral peak when $\hat{k}$ is parallel to $\vec{v}$ or $\vec{v}'$ so we can compute it around that value choosing to integrate from $\hat{k}\vec{v} = \vec{v}\vec{v}'$ to $\cos\theta = 1$ and from $\hat{k}\vec{v}' = \vec{v}\vec{v}'$ to $\cos\theta = 1$.

$$I_\gamma(\vec{v}, \vec{v}') \simeq 2 \left[\int_{\hat{k}\vec{v}=\vec{v}\vec{v}'}^{t=1} dt \frac{(1 - \vec{v}\vec{v}')}{(1 - v't)(1 - \hat{k}\vec{v})} + \int_{\hat{k}\vec{v}'=\vec{v}\vec{v}'}^{t=1} dt \frac{(1 - \vec{v}\vec{v}')}{(1 - \hat{k}\vec{v}')(1 - vt)} \right]. \tag{2.1.13}$$

In order to compute this integral we can substitute the lower extreme of integration inside it and use the fact that $v \simeq v'$ so that $p \simeq p' \simeq E$, obtaining

$$I_\gamma(\vec{v}, \vec{v}') \simeq \frac{4}{v} \log \left[\frac{2p \cdot p'}{(E^2 - p^2)} \right] = \frac{4}{v} \log \left[\frac{2p \cdot p'}{m^2} \right] \approx \frac{4}{v} \log \left(\frac{\Delta E^2}{m^2} \right), \tag{2.1.14}$$

where $\Delta E^2 = (p' - p)^2$. We can now write the cross section of the event as

$$\sigma_{f \to f\gamma} \approx \sigma_{f \to f} \frac{\alpha}{v\pi} \log \left(\frac{\Delta E^2}{m_\gamma^2} \right) \log \left(\frac{\Delta E^2}{m^2} \right), \tag{2.1.15}$$

where the dependence on ΔE^2 is called Sudakov double logarithm and it is a very well-known result.

2.2 Soft scalar emission

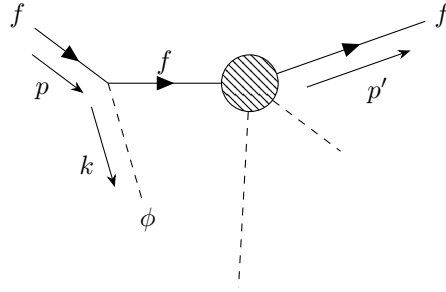The interaction Lagrangian for a scalar ϕ and a fermion ψ is

$$\mathcal{L}_{\text{int}} = -g\bar{\psi}\psi\phi. \tag{2.2.1}$$
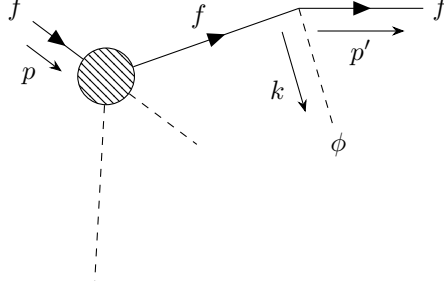
We want to inspect the emission of the scalar for low momenta, we consider here the following sub-process:

$$f \longrightarrow f + \phi,$$

where f is a generic fermion and ϕ is the massless scalar. For this process we have two Feynman diagrams:

$$\tag{2.2.2}$$

19

$$\text{(2.2.3)}$$

and we can compute the amplitude as

$$i\mathcal{M} = (ig)\bar{u}(p')\left[\mathcal{M}_0(p', p - k)\left(\frac{\not{p} - \not{k} + m}{(p - k)^2 - m^2}\right) + \right.$$
$$\left. + \left(\frac{\not{p}' + \not{k} + m}{(p' + k)^2 - m^2}\right)\mathcal{M}_0(p' + k, p)\right]u(p). \tag{2.2.4}$$

We are interested in the infrared emission case, so taking into account $\left|\vec{k}\right| \ll |\vec{p} - \vec{p}'|$, we will have $M_0(p' + k, p) \simeq M_0(p', p - k) \simeq M_0(p', p)$ and the momentum $\not{k}$ will be negligible in the numerators.

With these tricks and using the fact that $k^2 = 0$ and $p^2 = p'^2 = m^2$, we are able to write

$$i\mathcal{M} = (ig)\bar{u}(p')\left[\mathcal{M}_0(p', p)\left(-\frac{\not{p} + m}{2p \cdot k}\right) + \left(\frac{\not{p}' + m}{2p' \cdot k}\right)\mathcal{M}_0(p', p)\right]u(p), \tag{2.2.5}$$

we can now compute

$$|\mathcal{M}|^2 = |\mathcal{M}_0|^2 g^2\left[\frac{m^2}{(p \cdot k)^2} + \frac{m^2}{(p' \cdot k)^2} - \frac{2m^2}{(p \cdot k)(p' \cdot k)}\right]. \tag{2.2.6}$$

We proceed now with the same parametrization of (2.1.7), the differential form factor becomes

$$dF_{f \to f\phi} = \frac{d^3k}{2E_k}\frac{g^2}{(2\pi)^3}\left[\frac{m^2}{(E_kE - \vec{k}\vec{v}E)^2} + \frac{m^2}{(E_kE - \vec{k}\vec{v}'E)^2} - \frac{2m^2}{(E_kE - \vec{k}\vec{v}E)(E_kE - \vec{k}\vec{v}'E)}\right] =$$
$$= \frac{dk}{E_k}\frac{\alpha}{2\pi}\frac{m^2}{E^2}\mathrm{I}_\phi(\tilde{\mathrm{v}}, \tilde{\mathrm{v}}'), \tag{2.2.7}$$

again for the detailed calculations and the full form of $\mathrm{I}_\phi(\tilde{\mathrm{v}}, \tilde{\mathrm{v}}')$ we refer to the appendix B. Now we need to spend again some words on (2.2.7): first all we can see again that $\mathrm{I}_\phi(\tilde{\mathrm{v}}, \tilde{\mathrm{v}}')$ does not depend on k so we can integrate the momentum out and we will obtain the same logarithmic divergences as before, regulated by a fictional low scalar mass.

$$dF_{f \to f\phi} \propto \int_{m_\phi}^{\Delta E}\frac{1}{E_k}dE_k = \log\left(\frac{\Delta E}{m_\phi}\right). \tag{2.2.8}$$

This form factor differs from the one in (2.1.9) from another point of view: here the whole term is suppressed by $\frac{m^2}{E^2}$ term.

20

The integration of $I_\phi(v, v')$ is almost identical to the vector case, here we will put only the result, while the procedure is in appendix B.

$$I_\phi(\tilde{v}, \tilde{v}') \approx \frac{2}{1 - v^2} + \frac{2}{1 - v'^2} + \frac{1}{1 - \vec{v}\vec{v}'} \frac{4}{v} \log\left(\frac{\Delta E^2}{m^2}\right). \tag{2.2.9}$$

We can look again at the asymptotic behaviour in ΔE, for which we obtain again the Sudakov double logarithm suppressed by a multiplicative factor m^2/E^2.

$$\sigma_{f \to f\phi} \propto \sigma_{f \to f} \frac{m^2}{E^2} \frac{1}{1 - \vec{v}\vec{v}'} \frac{\alpha}{v\pi} \log\left(\frac{\Delta E^2}{m_\phi^2}\right) \log\left(\frac{\Delta E^2}{m^2}\right). \tag{2.2.10}$$

2.3 Soft pseudoscalar emission

The interaction Lagrangian for a pseudo-scalar $\tilde{\phi}$ and a fermion ψ is:

$$\mathcal{L}_{\text{int}} = -g\bar{\psi}\gamma_5\psi\tilde{\varphi}. \tag{2.3.1}$$

We want to inspect the emission of the pseudoscalar for low momenta, we consider here the following sub-process

$$f \longrightarrow f + \tilde{\varphi},$$

where f is a generic fermion and $\tilde{\varphi}$ is the massless pseudoscalar. For this process, we have two Feynman diagrams
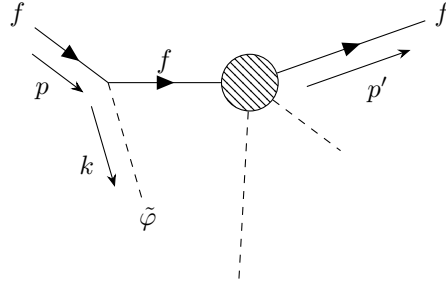
$$(2.3.2)$$

$$(2.3.3)$$

We can compute the amplitude as

$$i\mathcal{M} = (ig)\bar{u}(p')\left[\mathcal{M}_0(p',p-k)\left(\frac{\not{p}-\not{k}+m}{(p-k)^2-m^2}\right)\gamma_5 + \gamma_5\left(\frac{\not{p}'+\not{k}+m}{(p'+k)^2-m^2}\right)\mathcal{M}_0(p'+k,p)\right]u(p).$$
(2.3.4)

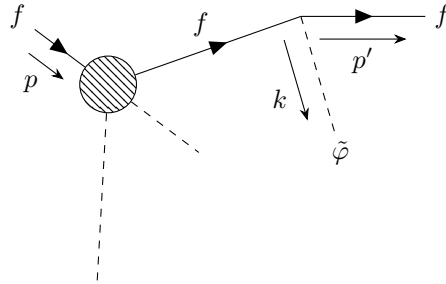We are interested in the infrared emission case, so taking into account $\left|\vec{k}\right| \ll |\vec{p}-\vec{p'}|$, we will have $M_0(p'+k,p) \simeq M_0(p',p-k) \simeq M_0(p',p)$ and the momentum $\not{k}$ will be negligible in the numerators.

With these tricks and using the fact that $k^2 = 0$ and $p^2 = p'^2 = m^2$, we are able to write

$$i\mathcal{M} = (ig)\bar{u}(p')\left[\mathcal{M}_0(p',p)\left(-\frac{\not{p}+m}{2p\cdot k}\right)\gamma_5 + \gamma_5\left(\frac{\not{p}'+m}{2p'\cdot k}\right)\mathcal{M}_0(p',p)\right]u(p).$$
(2.3.5)

Mow we can use (A.0.6) to transform the amplitude as

$$i\mathcal{M} = (ig)\bar{u}(p')\left[\mathcal{M}_0(p',p)\gamma_5\left(\frac{\not{p}-m}{2p\cdot k}\right) + \left(\frac{-\not{p}'+m}{2p'\cdot k}\right)\gamma_5\mathcal{M}_0(p',p)\right]u(p) = 0,$$
(2.3.6)

where in the last step we have used the equation of motion (A.0.21). We have no divergence in the soft emission case for the pseudoscalar massless particle, this is also true for the massive particles because only the denominator changes.

2.4   Numerical checks for scalar and pseudoscalar

In order to check the results expressed in the previous section we have simulated the process

$$pp \to t\bar{t}X_0,$$
(2.4.1)

at $\sqrt{s} = 13\,\text{TeV}$ for the X_0 scalar and X_0 pseudoscalar cases.

The results of the simulations are shown in figure 2.4.1. In the left plot, the cross section of the real scalar emission process is plotted as a function of the logarithm of the scalar mass m_{X_0}. The behaviour is the one predicted above: for small masses, the cross section diverges in a logarithmic way. In the right plot, we consider instead a pseudoscalar particle; for small masses the cross section remains constant, giving no infrared divergences.
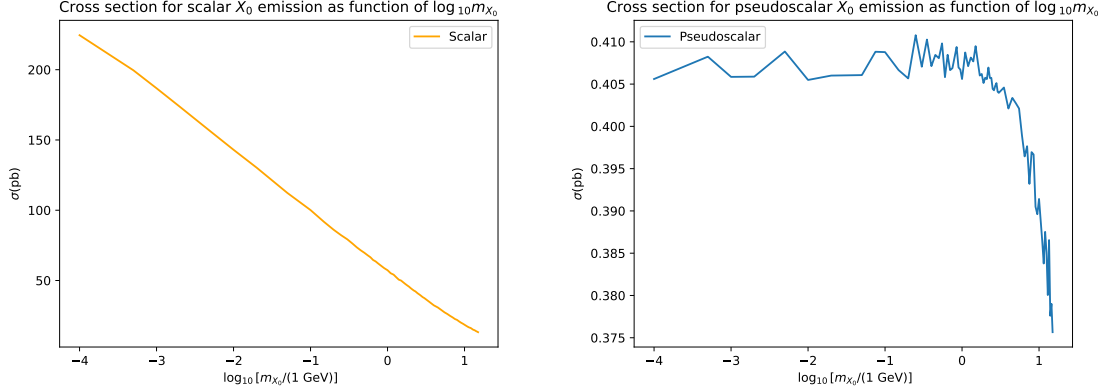
Figure 2.4.1: Cross section for the emission of a scalar (left) and a pseudoscalar particle (right) at $\sqrt{s} = 13\text{TeV}$, on the x-axis we have put a logarithmic scale.

For this and all the other simulations, we have used MadGraph5_aMC@NLO [24, 25] an open-source framework that provides tools for computing cross sections and simulating collision events at LO, and in some cases, at NLO accuracy. One of the many good features of MadGraph5_aMC@NLO is the possibility to import user-defined models in the UFO (Universal FeynRules Output) format to include new interactions. We have produced our own UFO model based on the Lagrangian

$$\mathcal{L}_{\text{model}} = \mathcal{L}_{\text{QCD}} + \mathcal{L}_{\text{int}}, \tag{2.4.2}$$

where $\mathcal{L}_{\text{int}}$ is the one in (1.0.1), which we report for simplicity here:

$$\mathcal{L}_{\text{int}} = -\bar{t}(g + i\tilde{g}\gamma_5)tX_0.$$

The corresponding Feynman rules for $\mathcal{L}_{\text{int}}$ is

$$= -ig + \tilde{g}\gamma_5 \tag{2.4.3}$$

The UFO model was produced using FeynRules[26][27], a dedicated MATHEMATICA package, and validated at the tree-level in the way exposed in appendix C. For our model, the scalar case is obtained setting $\tilde{g} = 0$, while the pseudoscalar one setting $g = 0$.

2.5   ALP emission with top antitop

We will analyze here the process $pp \to t\bar{t}X_0$, where X_0 is an ALP. As we have said in the introduction to this chapter, it is possible to put constraints on the X_0 interaction with the top by looking at the

23

transverse missing momentum in this kind of process. There are four types of diagrams in the process, shown in figure 2.5.1
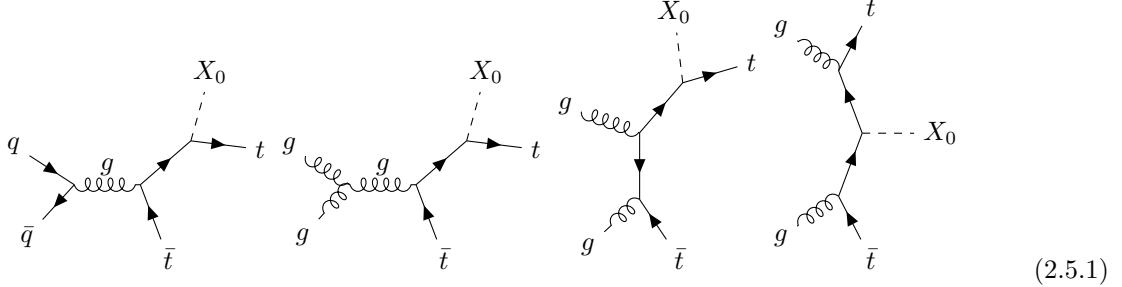

$$(2.5.1)$$

Figure 2.5.1

The first analysis we have realized is the behaviour of the cross section with respect to the mass of the particle m_{X_0} and the coupling $\tilde{g}$ in the process $pp \to t\bar{t}X_0$ at $\sqrt{s} = 13$ TeV. To compute the full cross section we have used MadGraph5_aMC@NLO[24]. We report the results we have obtained in table 2.5.1.

$\tilde{g}$	$\sigma_{t\bar{t}X_0}(pb)$	$\sigma_{t\bar{t}X_0,\tilde{g}}/\sigma_{t\bar{t}X_0,\tilde{g}=m_t/v}$		$\tilde{g}$	$\sigma_{t\bar{t}X_0}(pb)$	$\sigma_{t\bar{t}X_0,\tilde{g}}/\sigma_{t\bar{t}X_0,\tilde{g}=m_t/v}$
m_t/v	0.457	1		m_t/v	0.0054	1
$2m_t/v$	1.836	4.02		$2m_t/v$	0.0216	4
$3m_t/v$	4.131	9.04		$3m_t/v$	0.0486	9
$5m_t/v$	11.47	25.1		$5m_t/v$	0.1356	25.1

Table 2.5.1: Dependence of the cross section with respect to the coupling $\tilde{g}$ at fixed mass. In the first table $m_{X_0} = 10$GeV, in the second one $m_{X_0} = 700$GeV. The third column, in both tables, is the ratio between the cross section in the row and the one in the first row.

The dependence of the cross section with respect to the couplings is $\sigma_{t\bar{t}X_0} \propto \tilde{g}^2$, we have chosen as reference the value $m_t/v \approx 0.7$ because it has the same strength of the coupling of the top-quark to the Higgs boson in the SM.

In 2.5.2 we have plotted the dependence of the cross section of the process $pp \to t\bar{t}X_0$ on m_{X_0} for different values of $\tilde{g}$ and of the mass m_{X_0}. The same kind of plot is presented both with the linear and logarithmic scale for both axes, in order to stress again the constant behaviour for small m_{X_0} masses, and the dependence on the squared coupling.

In figure 2.5.3 we have computed the cross section at different energies for both the scalar and the pseudoscalar case. The cross section increases by increasing the energy and decreases by increasing m_{X_0}. We have compared the scalar and pseudoscalar processes in order to underline two important differences: for the same coupling m_t/v, the cross section of the scalar is more than one order of magnitude greater than the one of the pseudoscalar. In addition, the pseudoscalar cross section is less sensitive to the emitted particle mass with respect to the scalar one, we want to underline this behaviour because we will see it again in the last chapter, where we will present results for the counterpart from the virtual corrections.
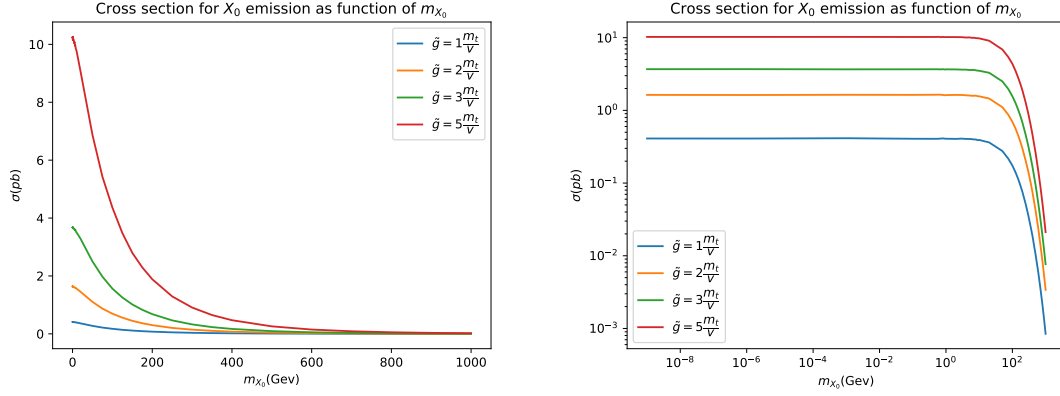
Figure 2.5.2: Plot of the cross section for different couplings $\tilde{g}$ with respect to the mass. **Left:** linear scale on the x-axis. **Right:** logarithmic scale on the x-axis.
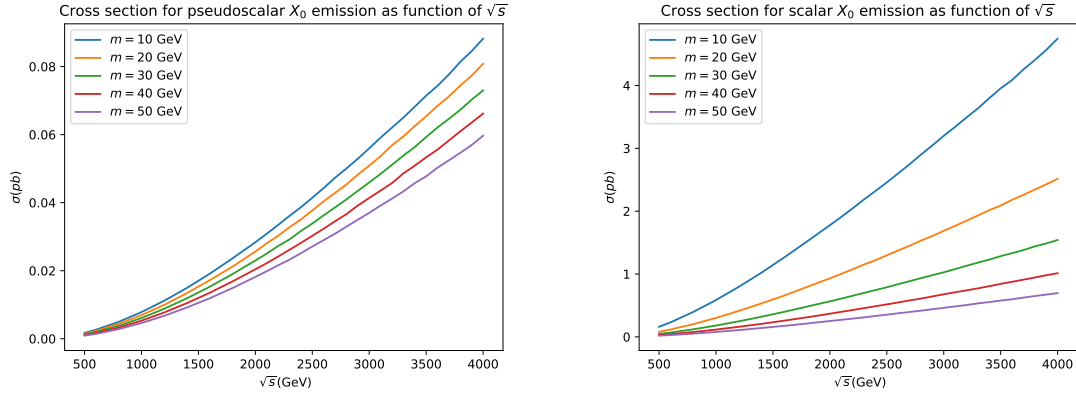

Figure 2.5.3: Cross section of X_0 emission for different masses and different centre-of-mass energies keeping $\tilde{g} = m_t/v$ constant. **Left:** pseudoscalar case. **Right:** scalar case.

Chapter 3

NLO calculation and model validation

As we have said in the introduction new physics can also be searched by looking at how virtual corrections would affect the kinematic distribution of a specific production process.

The final aim of this thesis is to be able to look at the effect of the virtual contribution of new physics on the kinematical distributions for the process $pp \to t\bar{t}$. All the diagrams that contribute to the process at the NLO in NP are depicted in appendix G. Our work has moved in parallel along two directions: writing a MATHEMATICA code using FeynRules and NLOCT [28] packages to produce the final UFO format to use in MadGraph5_aMC@NLO, and the handmade calculation of the one-loop corrections to the process $q\bar{q} \to t\bar{t}$ due to the presence of a X_0 spin-0 particle with the coupling of equation (1.0.1) to the top-quark. We will later use the result of this calculation to validate the produced UFO model.

We have chosen the $q\bar{q} \to t\bar{t}$ process because it contains only two one-loop diagrams: the corrections to the three-point and to the two-point functions shown in figure 3.0.1 together with the tree-level diagram. The calculation becomes even easier in the on-shell renormalization scheme in which the external legs do not receive any correction due to the two-point function.
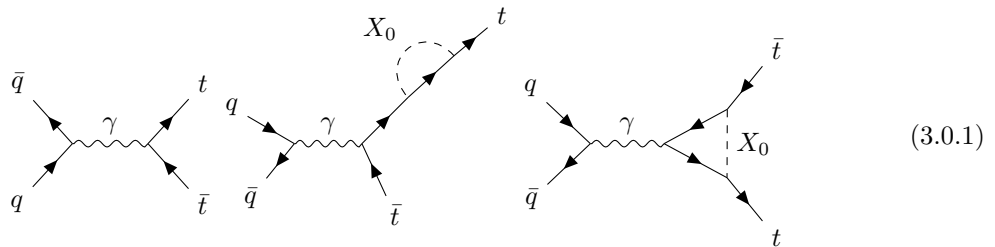
$$\tag{3.0.1}$$

Figure 3.0.1: Tree-level and one-loop X_0 Feynman diagrams for the process $q\bar{q} \to t\bar{t}$ process.

In the diagrams, we have chosen a photon instead of a gluon in the s-channel for convenience. The reason is explained at the beginning of the next section.

3.1 On-shell renormalization

In order to calculate the process

$$q\bar{q} \to t\bar{t}$$

at NLO with X_0 running through the loops we need to proceed with choosing a renormalization scheme and apply it to our theory. In renormalizing the Lagrangian (2.4.2) we will need to compute the correction to the three-point function due to the $A^\mu \bar{t} \gamma_u t$ interaction term. For the sake of clarity in the notation, in this chapter we will denote the fermion field t as ψ. Moreover, in order to simplify the calculations we will consider the vector A^μ as a photon, instead of a gluon, avoiding the colour matrices in the amplitudes. When we will need them, we will reintroduce colour factors inside the computations to obtain the right value for the amplitudes. The most suitable renormalization scheme for the computation of this process is the on-shell one for what we have stated in the introduction to this chapter about the two-point function. In order to renormalize the Lagrangian we need to connect the bare fields and couplings to the renormalized ones:

$$\begin{cases} \psi_0 & = \sqrt{Z_\psi}\psi = (1 + \frac{1}{2}\delta_\psi)\psi, \\ A_0 & = \sqrt{Z}_A A = (1 + \frac{1}{2}\delta_A), \\ m_{X_0} & = Z_m m = (1 + \delta_m)m, \\ e_0 & = Z_e e = (1 + \delta_e)e, \\ Z_1 & = \sqrt{Z}_A Z_e Z_\psi, \\ \delta_1 & = \frac{1}{2}\delta_A + \delta_e + \delta_\psi. \end{cases}$$

The renormalized Lagrangian relevant for the diagrams in figure 3.0.1 is:

$$\begin{aligned} \mathcal{L} \supset & = i Z_\psi \bar{\psi} \slashed{\partial} \psi - Z_\psi Z_m \bar{\psi} \partial \psi m_r - e Z_e \sqrt{Z}_A Z_\psi \bar{\psi} \gamma^\mu \psi A_\mu \\ & = \mathcal{L}_R + i\delta_\psi \psi \slashed{\partial} \psi - (\delta_\psi + \delta_m) m_R \bar{\psi}\psi - e\delta_1 \bar{\psi}\gamma^\mu \psi A_\mu. \end{aligned} \tag{3.1.1}$$

Because there are no tree-level interaction between X_0 and A_μ, A_μ two-point function will receive no correction from new physics at one-loop, the same is valid for the electric charge, so we expect $\delta_1 = \delta_\psi$. This is also expected considering the Ward-Takahashi identity in combination with the conservation of the $U(1)_{\text{em}}$ symmetry. The counterterms for the photon(gluon) are the ones of QED(QCD), for the moment we are not interested in them, we want to look at counterterms useful for the diagrams in figure 3.0.1 .

$$= i(\slashed{p}\delta_\psi - (\delta_\psi + \delta_m)m_R), \tag{3.1.2}$$

$$= -ie_R\delta_1\gamma^\mu \tag{3.1.3}$$

Looking at the two-point function, at one loop the full propagator is

$$iG(\slashed{p}) = \frac{i}{\slashed{p} - m_R + \Sigma(\slashed{p})}, \tag{3.1.4}$$

where:
$$\Sigma(\not{p}) = \Sigma_{X_0}(\not{p}) + \not{p}\delta_\psi - (\delta_\psi + \delta_m)m_R. \tag{3.1.5}$$

The two on-shell renormalization conditions are

$$\Sigma|_{\not{p}=m_t} = 0, \qquad \frac{d}{d\not{p}}\Sigma|_{\not{p}=m_t} = 0, \tag{3.1.6}$$

using (3.1.5) these conditions, following [29], become

$$\text{Re}\left(\Sigma_{X_0}|_{\not{p}=m_t}\right) = \delta_m m_t, \qquad \text{Re}\left(\frac{d}{d\not{p}}\Sigma_{X_0}|_{\not{p}=m_t}\right) = -\delta_\psi. \tag{3.1.7}$$

In the three-point function, the one-loop interaction corrected term can be written as

$$\Gamma^\mu(p) = (1 + f_1(p^2))\gamma^\mu, \tag{3.1.8}$$

if we want to have the electric charge as the one measured by the Coulomb law at large distances we need to put

$$\Gamma^\mu(0) = \gamma^\mu \quad \rightarrow \quad f(0) = -\delta_1. \tag{3.1.9}$$

3.1.1 FF two-point function

We start computing the correction to the 2-point function of the fermion using the Feynman rule in (2.4.3).
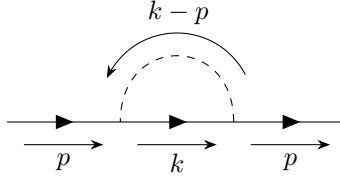
$$(3.1.10)$$

we write this in a general form not asking the fermion outside being on-shell. In this context, we can write this diagram as:

$$iG_0(\not{p})\left[i\Sigma_{X_0}(\not{p})\right]iG_0(\not{p}) \tag{3.1.11}$$

and

$$i\Sigma_{X_0}(\not{p}) = \int \frac{d^4k}{(2\pi)^4}(-ig + \tilde{g}\gamma_5)\frac{i(\not{k}+m_t)}{k^2 - m_t^2 + i\epsilon}(-ig + \tilde{g}\gamma_5)\frac{i}{(p-k)^2 - m_{X_0}^2 + i\epsilon} \tag{3.1.12}$$

the result of this integral, computed in dimensional regularization will be (detail in appendix E)

$$\begin{aligned}
\Sigma_{X_0}(\not{p}) =& \frac{1}{(4\pi)^2}\int_0^1 dx[(g^2 - \tilde{g}^2)m_t + 2ig\tilde{g}m_t\gamma_5 + (g^2 + \tilde{g}^2)x\not{p}]\left[\frac{1}{\epsilon} + \log\left(\frac{\tilde{\mu}^2}{\Delta(x)}\right)\right] = \\
=& \frac{1}{(4\pi)^2}\left[[(m_t + \frac{\not{p}}{2})g^2 + (\frac{\not{p}}{2} - m_t)\tilde{g}^2 + 2ig\tilde{g}m_t\gamma_5]\frac{1}{\epsilon} + \right. \\
& \left. + \int_0^1 dx[(m_t + \not{p}x)g^2 + (\not{p}x - m_t)\tilde{g}^2 + 2ig\tilde{g}m_t\gamma_5]\log\left(\frac{\tilde{\mu}^2}{(1-x)(m_t^2 - p^2x) + m_{X_0}^2 x}\right)\right]
\end{aligned}$$
$$(3.1.13)$$

As usual, we have a UV-divergent part and a scale-dependent logarithm. We know that, in the on-shell scheme, both the scale dependence and the UV term will disappear once we will add the counterterm to the diagram.

3.1.2 Three-point function VFF

In general, the three-point function can be put in the form

$$i\bar{u}(q_2)\Gamma^\mu_\gamma u(q_1) = (-ie)\bar{u}(q_2)[F_1(p^2)\gamma^\mu + i\frac{\sigma^{\mu\nu}}{2m_t}p_\nu F_2(p^2)]u(q_1), \tag{3.1.14}$$

where

$$F_1(p^2) = 1 + f(p^2). \tag{3.1.15}$$

is the tree-level term, plus all the loop contributions inside $f(p^2)$. The UV divergent terms are in $f(p^2)$, this is quite reasonable for the fact that we have defined the counterterm in (3.1.9) by it.

The other term in the decomposition is $F_2(p^2)$, we expect this term not to be UV divergent because there are no terms proportional to $\sigma^{\mu\nu}p_\nu$ in the Lagrangian, from which we could extract a counterterm. The $F_2(p^2)$ term plays a key role in lepton physics, it is in fact responsible for the anomalous magnetic moment. The Hamiltonian of an elementary particle with spin different from 0 in a magnetic field $\vec{B}$, contains a term of the type:
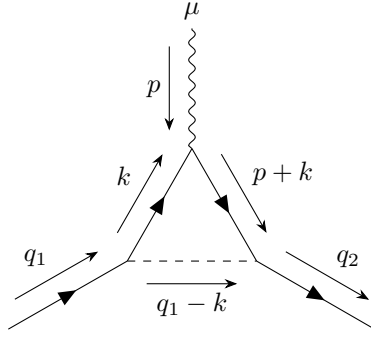
$$\mathcal{H} \supset \frac{e}{2m}g_{\rm em}\vec{B}\cdot\vec{S},$$

where the term $g_{\rm em}$ is called magnetic moment and it is corrected by F_2, at one-loop, in the following manner:

$$g_{\rm em} = 2 + 2F_2(0).$$

Measuring the value of $(g-2)$ is a way to test SM. This means that, although we do not study it, our model will lead to a modification of the $g-2$ of the top.

In order to find $f(p^2)$ and $F_2(p^2)$ we can compute the correction to the three-point function in dimensional regularization.

$$\tag{3.1.16}$$

We consider the photon off-shell and the two fermions on-shell, the amplitude for the virtual X_0 exchange, in this case, will result in

$$i\mathcal{M}^\mu_{X_0} = \int \frac{d^4k}{(2\pi)^4}\frac{i}{(q_1-k)^2-m^2_{X_0}+i\epsilon}\bar{u}(q_2)(-ig+\tilde{g}\gamma_5)\frac{i(\not{p}+\not{k}+m_t)}{(p+k)^2-m^2_t+i\epsilon}(-ie\gamma^\mu)$$
$$\frac{i(\not{k}+m)}{k^2-m^2_t+i\epsilon}(-ig+\tilde{g}\gamma_5)u(q_1). \tag{3.1.17}$$

Solving this integral we find the function $f(p^2)$ and $F_2(p^2)$ in the decomposition(3.1.14).

$$f(p^2) = \frac{1}{16\pi^2}\left[\int_0^1 dxdydz\delta(1-x-y-z)\frac{g^2[(z+1)^2m_t^2 + xyp^2] + \tilde{g}^2[(z-1)^2m_t^2 + xyp^2]}{m_t^2(1-z)^2 - p^2yx + m_{X_0}^2 z} + \right.$$
$$\left. +(g^2 + \tilde{g}^2)\int_0^1 dxdydz\delta(1-x-y-z)\left[-1 + \frac{1}{\epsilon} + \log\left(\frac{\tilde{\mu}^2}{m_t^2(1-z)^2 - p^2yx + m_{X_0}^2 z}\right)\right]\right].$$
$$(3.1.18)$$

We can look at the massless X_0 limit in the $f(p^2)$ piece. We know that IR divergent terms come from the part proportional to m_t^2. For simplicity consider $p^2 = 0$, because the term proportional to p^2 does not carry infrared divergences.

$$f(0)|_{m_{X_0}=0} = \frac{1}{16\pi^2}\int_0^1 dz\int_0^{1-z} dy\left[\frac{g^2m_t^2(z+1)^2 + \tilde{g}^2m_t^2(z-1)^2}{m_t^2(1-z)^2}\right] =$$
$$= \frac{1}{16\pi^2}\int_0^1 dz\left[g^2\frac{(z+1)^2}{z-1} + \tilde{g}^2(1-z)\right] =$$
$$= \frac{1}{16\pi^2}\left[-g^2\frac{1}{2}\left(7 - 6z - z^2 - 8\log(z-1)\right)|_0^1 + \frac{\tilde{g}^2}{2}\right] =$$
$$= \frac{1}{16\pi^2}\left[g^2\left(\frac{7}{2} + 4\log(z-1)|_0^1\right) + \frac{\tilde{g}^2}{2}\right]. \qquad (3.1.19)$$

This confirms our intuition, the scalar part, proportional to g presents an IR divergence represented by the logarithm in (3.1.19), while the pseudoscalar part, proportional to $\tilde{g}$ gives a constant value.

The $\sigma^{\mu\nu}$ term proportional to $F_2(p^2)$ vanishes in the high energy limit due to the absence of a p^2 term in the numerator. From the integral we obtain

$$F_2(p^2) = \frac{m_t^2}{8\pi^2}\int_0^1 dxdydz\,\delta(1-x-y-z)\frac{\left[g^2(1-z^2) - \tilde{g}^2(z-1)^2 + 2ig\tilde{g}\gamma_5(1-z)\right]}{m_t^2(1-z)^2 - p^2xy + m_{X_0}^2 z}. \qquad (3.1.20)$$

The contribution to $(g-2)$ is given by:

$$F_2(0) = \frac{m_t^2}{8\pi^2}\int_0^1 dxdydz\,\delta(1-x-y-z)\frac{\left[g^2(1-z^2) - \tilde{g}^2(z-1)^2 + 2ig\tilde{g}\gamma_5(1-z)\right]}{m_t^2(1-z)^2 + m_{X_0}^2 z}. \qquad (3.1.21)$$

As we can see there are no UV-divergences. The reason for which it happens is how this term appears in dimensional regularization. To look at the detailed calculations we refer to appendix E.

3.1.3 Explicit counterterms

If we define

$$\alpha = \frac{g^2}{4\pi}, \qquad \tilde{\alpha} = \frac{\tilde{g}^2}{4\pi},$$

we can write δ_ψ and δ_m combining (3.1.7) and (3.1.13) and δ_1 combining (3.1.9) and (3.1.18) as

$$\delta_\psi = -\frac{1}{4\pi}\left[(\alpha+\tilde{\alpha})\frac{1}{2\epsilon} + \int_0^1 [(1+x)\alpha + (x-1)\tilde{\alpha}]\frac{2m_t^2 x(1-x)}{m_t^2(1-x)^2 + xm_{X_0}^2} + \right.$$
$$\left. + (\alpha+\tilde{\alpha})x\log\left(\frac{\tilde{\mu}^2}{m_t^2(1-x)^2 + xm_{X_0}^2}\right)dx\right], \tag{3.1.22}$$

$$\delta_m = \frac{1}{4\pi}\left[(3\alpha-\tilde{\alpha})\frac{1}{2\epsilon} + \int_0^1 dx[(1+x)\alpha + (x-1)\tilde{\alpha}]\log\left(\frac{\tilde{\mu}^2}{m_t^2(1-x)^2 + xm_{X_0}^2}\right)\right], \tag{3.1.23}$$

$$\delta_1 = -\frac{1}{4\pi}\left[\int_0^1 dz \int_0^{1-z} dy\, m_t^2 \frac{\alpha(z+1)^2 + \tilde{\alpha}(z-1)^2}{m_t^2(1-z)^2 + m_{X_0}^2 z} + \right.$$
$$\left. + (\alpha+\tilde{\alpha})\left(\frac{1}{2\epsilon} - \frac{1}{2} + \int_0^1 dz \int_0^{1-z} dy\log\left(\frac{\tilde{\mu}^2}{m_t^2(1-z)^2 + m_{X_0}^2 z}\right)\right)\right]. \tag{3.1.24}$$

We expect the integrals in δ_ψ and δ_1 to give the same results in order to have the equality $\delta_1 = \delta_\psi$. Unfortunately solving them is not so easy, but we can see this equality by looking at an approximate form. Considering m_{X_0} small it is possible to perform the integration and then expand in $m_{X_0}^2/m_t^2$ obtaining simpler expressions:

$$\delta_\psi = -\frac{1}{4\pi}\left[\alpha\left(\frac{1}{2\epsilon} + \frac{1}{2}\log\frac{\tilde{\mu}^2}{m_t^2} - 2\log\frac{m_{X_0}^2}{m_t^2} - \frac{7}{2}\right) + \tilde{\alpha}\left(\frac{1}{2\epsilon} + \frac{1}{2}\log\frac{\tilde{\mu}^2}{m_t^2} + \frac{1}{2}\right)\right], \tag{3.1.25}$$

$$\delta_m = \frac{1}{4\pi}\left[\alpha\left(\frac{3}{2\epsilon} + \frac{3}{2}\log\frac{\tilde{\mu}^2}{m_t^2} + \frac{7}{2}\right) + \tilde{\alpha}\left(-\frac{1}{2\epsilon} - \frac{1}{2}\log\frac{\tilde{\mu}^2}{m_t^2} - \frac{1}{2}\right)\right], \tag{3.1.26}$$

$$\delta_1 = -\frac{1}{4\pi}\left[\alpha\left(-\frac{7}{2} - 2\log\frac{m_{X_0}^2}{m_t^2} + \frac{1}{2}\log\frac{\tilde{\mu}^2}{m_t^2} + \frac{1}{2\epsilon}\right) + \tilde{\alpha}\left(\frac{1}{2} + \frac{1}{2\epsilon} + \frac{1}{2}\log\frac{\tilde{\mu}^2}{m_t^2}\right)\right]. \tag{3.1.27}$$

As expected, for all the reasons we have stated at the beginning, we have found $\delta_1 = \delta_\psi$. Also in this approximation is immediate to see that the terms proportional to $\tilde{\alpha}$ (related to the pseudoscalar interaction) in the counterterms do not carry any infrared divergence, while the counterterms δ_1 and δ_ψ proportional to α (related to the scalar interaction) have a $\log(m_{X_0}^2/m_t^2)$ in it, divergent for $m_{X_0}=0$.

3.2   NLO computation for the $q\bar{q} \to t\bar{t}$ process

We want to look at

$$q\bar{q} \to t\bar{t},$$

at NLO considering the X_0 virtual exchange. We do not need to take into account the diagrams as the second of figure 3.0.1 because the corrections are in the external legs. The three diagrams involved are

$$(3.2.1)$$

where the third one includes the vertex counterterm. We write the amplitude as

$$iM = i\frac{e_q e_t}{p^2} \bar{v}(p_2)\gamma_\mu u(p_1)\bar{u}(p_3)\Gamma_\gamma^\mu v(p_4). \tag{3.2.2}$$

and we split it into the tree-level amplitude plus the one-loop corrected amplitude: $M = M_0 + M_{X_0}$. When we square the amplitude, stopping at the next-to-the-leading, order we find

$$|M|^2 = |M_0|^2 + 2\text{Re}\left[M_{X_0}^\dagger M_0\right] + \text{h.o.} \tag{3.2.3}$$

where M_0 is the tree-level amplitude and M_{X_0} is the renormalized one loop amplitude. Using (A.0.29) and (A.0.30) and the property of γ-matrices traces, we find that:

$$\sum_s M_{X_0}^\dagger M_0 = \frac{e_q^2 e_t^2}{p^4}\left(\text{Tr}\left[\not{p}_2\gamma_\rho\not{p}_1\gamma_\mu\right] - 4m_q^2 g_{\rho\mu}\right)\left(\text{Tr}\left[\not{p}_3\gamma^\rho\not{p}_4\left(f_1^*(p^2)\gamma^\mu\right)\right] - 4m_t^2 f_1^*(p^2)g^{\rho\mu}+\right.$$

$$\left.+\frac{i}{2}\text{Tr}\left[\not{p}_3\gamma^\rho F_2^\dagger(p^2)\sigma^{\mu\nu} - \gamma^\rho\not{p}_4 F_2^\dagger(p^2)\sigma^{\mu\nu}\right]p_\nu\right), \tag{3.2.4}$$

where we have defined

$$f_1(p^2) = f(p^2) + \delta_1.$$

The details of the calculation can be found in F

This expression, and in particular the counterterm, is easier to compute in the high energy limit $p^2 \gg m^2$, for which the (3.2.4) becomes

$$\sum_s M_{X_0}^\dagger M_0 = \frac{e_q^2 e_t^2}{p^4}f_1^*(p^2)\text{Tr}\left[\not{p}_2\gamma_\rho\not{p}_1\gamma_\mu\right]\text{Tr}\left[\not{p}_3\gamma^\rho\not{p}_4\gamma^\mu\right] \tag{3.2.5}$$

In this way (3.2.3) becomes

$$|M|^2 = \frac{1}{4}\sum_s|M_0|^2\left(1 + 2\text{Re}[f_1(p^2)]\right) + \text{h.o.} \tag{3.2.6}$$

This formula does not take into account the $F_2(p^2)$ term because as we have said in the previous section it vanishes in the high energy limit, if we want an expression valid at all energy we need to

compute the full correction from (3.2.4)

$$|\mathcal{M}|^2 = \frac{1}{4}\sum_s |\mathcal{M}_0|^2 (1 + 2\mathrm{Re}[f_1(p^2)]) + \text{h.o.}$$

$$+ \frac{1}{4}\frac{e_q^2 e_t^2}{p^4}\left[\left(\mathrm{Tr}\left[\not{p}_2\gamma_\rho\not{p}_1\gamma_\mu\right] - 4m_q^2 g_{\rho\mu}\right)\frac{i}{2}\mathrm{Tr}\left[\not{p}_3\gamma^\rho F_2^\dagger(p^2)\sigma^{\mu\nu} - \gamma^\rho\not{p}_4 F_2^\dagger(p^2)\sigma^{\mu\nu}\right]p_\nu\right) + \text{h.c.}\right] \quad (3.2.7)$$

This term requires many calculations in order to be transformed in a proper way. A general treatment can be done if the F_2 term is simply a number and does not contain any other matrices. This is the case of the scalar interaction ($\tilde{g} = 0$) or of the pseudoscalar interaction ($g = 0$). With some patience is possible to compute all the γ-traces to find

$$|\mathcal{M}|^2 = \frac{1}{4}\sum_s |\mathcal{M}_0|^2 (1 + 2\mathrm{Re}[f_1(p^2) + F_2(p^2)]) +$$

$$+ \frac{2\mathrm{Re}[F_2]}{p^4}e_q^2 e_t^2\left(-4sm_t^2 + s^2 - t^2 + 2tu - u^2\right) + \text{h.o.} \quad (3.2.8)$$

In appendix F we have worked out this expression to obtain

$$|\mathcal{M}|^2 = \frac{1}{4}\sum_s |\mathcal{M}_0|^2 (1 + 2\mathrm{Re}[f_1(p^2)]) + 2\mathrm{Re}[F_2(p^2)]e_q^2 e_t^2\left(2 + 4\frac{m_q^2}{s}\right). \quad (3.2.9)$$

Note that the term proportional to m_q^2 is not present in the $pp \to t\bar{t}$ process, because in the parton model quarks inside protons are considered massless.

We have a slightly different case if we have a mixed scalar-pseudoscalar term, in that case inside F_2 there is also a γ_5 term, as can be seen in its general form written in (3.1.20). The same process in QCD differs only by a overall multiplicative colour factor. We know by Fierz-identity for SU(N) that the colour matrices T_{ij}^a obey:

$$\sum_a T_{ij}^a T_{kl}^a = \frac{1}{2}(\delta_{il}\delta_{kj} - \frac{1}{N}\delta_{ij}\delta_{kl}). \quad (3.2.10)$$

In the process $qq \to \bar{t}t$ when we square the amplitude and average over the initial colour, summing over colours we find the colour factor

$$c = \frac{1}{9}\sum_{a,b}\sum_{i,j}\sum_{k,l}(T^a T^b)_{ij}(T^a T^b)_{kl} = \frac{2}{9},$$

the detail of this calculation can be found in appendix F.

3.2.1 Explicit expression of the form factors in the pseudoscalar case

The general expression of the photon-fermion vertex is given in (3.1.14). Adding the counterterm we can write, taking $g = 0$:

$$f_1(p^2) = -\frac{\tilde{\alpha}}{4\pi}\left[\int_0^1 dz \int_0^{1-z} dy \log\left(\frac{m_t^2(1-z)^2 - p^2(1-y-z)y + m_{X_0}^2 z}{m_t^2(1-z)^2 + m_{X_0}^2 z}\right) + \right.$$

$$\left. + \frac{m_t^2(1-z)^2}{m_t^2(1-z)^2 + m_{X_0}^2 z} - \frac{m_t^2(1-z)^2 + (1-y-z)yp^2}{m_t^2(1-z)^2 - (1-y-z)yp^2 + m_{X_0}^2 z}\right]. \quad (3.2.11)$$

33

First of all, we can look at this term in the high energy limit. The integral becomes:

$$f_1^{\text{h.e.}}(p^2) = -\frac{\tilde{\alpha}}{4\pi} \left[\int_0^1 dz \int_0^{1-z} dy \, \log\left(\frac{-p^2(1-y-z)y}{m_t^2(1-z)^2 + m_{X_0}^2 z} \right) + \frac{2m_t^2(1-z)^2 + m_{X_0}^2 z}{m_t^2(1-z)^2 + m_{X_0}^2 z} \right]. \qquad (3.2.12)$$

Solving the integral, for high momenta we have:

$$f_1^{\text{h.e.}}(p^2) = -\frac{\tilde{\alpha}}{16\pi} \left[2\log\left(-\frac{p^2}{m_t^2} \right) + \frac{m_{X_0}^2}{m_t^4} \left(m_t^2 - 3m_{X_0}^2 \log\frac{m_{X_0}^2}{m_t^2} - 4m_t^2 \log\frac{m_t^2}{m_{X_0}} + \right.\right.$$

$$\left.\left. + \frac{2m_{X_0}\left(10m_t^2 - 3m_{X_0}^2\right)\left(\tanh^{-1}\left(\frac{m_{X_0}}{\sqrt{m_{X_0}^2 - 4m_t^2}} \right) - \coth^{-1}\left(\frac{m_{X_0}\sqrt{m_{X_0}^2 - 4m_t^2}}{m_{X_0}^2 - 2m_t^2} \right) \right)}{\sqrt{m_{X_0}^2 - 4m_t^2}} \right) \right].$$

$$(3.2.13)$$

In the limit $m_{X_0} = 0$ we finally find

$$f_1^{h.e.}(p^2)_{m_{X_0}=0} = -\frac{\tilde{\alpha}}{8\pi} \log\left(-\frac{p^2}{m_t^2} \right), \qquad (3.2.14)$$

and again we can see that we have no infrared divergences. The minus sign in the logarithm needs no additional discussion because it will disappear once we will take the real part of f_1 as in (3.2.9). In figure 3.2.1 we plotted $f_1^{h.e}$ on m_{X_0} for $\tilde{\alpha} = 8\pi$ with a linear scale on the x-axis. On the right, we have plotted the same quantity with a logarithmic scale on the x-axis. For $m_{X_0} \to 0$ there is not an infrared divergence and $f_1^{h.e}$ goes like a constant, as it happens in the real emission process.
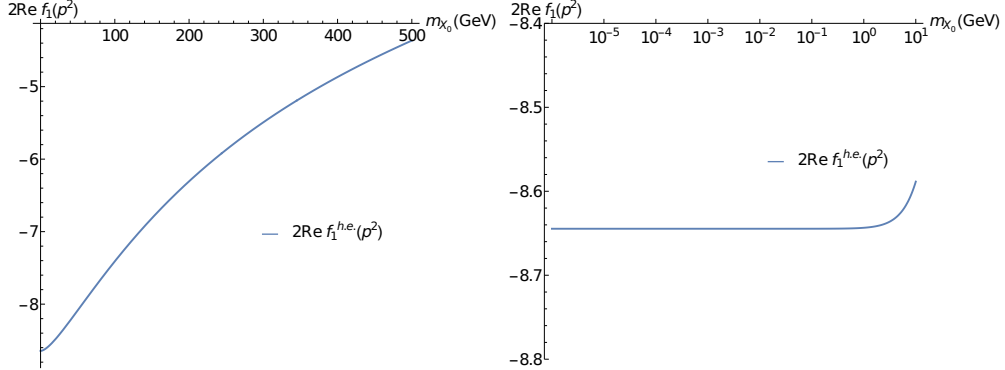

Figure 3.2.1: Left: dependence of $f_1(p^2)$ on m_{X_0} in the high energy limit, for a centre of mass of 13 TeV and $m_t = 172.5$ GeV. **Right:** the behaviour of the same quantity for small X_0 masses with a logarithmic scale on the x-axis.

We can go further and look how is the general form of $f_1(p^2)$ without any approximation:

$$f_1(p^2) = -\frac{\tilde{\alpha}}{4\pi}\int_0^1 dz \frac{2\left(p^2(z-1)^2 - 2m_{X_0}^2 z\right)\tan^{-1}\left(\frac{p(z-1)}{\sqrt{4(z-1)^2 m_t^2 + 4m_{X_0}^2 z - p^2(z-1)^2}}\right)}{p\sqrt{4(z-1)^2 m_t^2 + 4m_{X_0}^2 z - p^2(z-1)^2}} + \frac{m_{X_0}^2(z-1)z}{(z-1)^2 m_t^2 + m_{X_0}^2 z},$$

(3.2.15)

this integral is not easy to be solved, so we will compute it numerically using MATHEMATICA. In figure 3.2.2 we have plotted $f_1(p^2)$ for $\sqrt{s} = 13$ TeV with respect to m_{X_0}, in the high energy limit and in the general case. Looking at the relative difference one can see that the predictions are very similar when $m_{X_0}^2 \ll p^2$. In figure 3.2.3 the same comparison is plotted but now $f_1(p^2)$ is plotted against $\sqrt{p^2}$ and $m_{X_0} = 0$.

Being the top quark very heavy we cannot neglect the contribution given by F_2.

We find (for $m_{X_0} = 0$):

$$F_2(p^2) = -\tilde{g}^2 \frac{m_t^2}{8\pi^2} 2\frac{\arctan\left(\frac{p}{\sqrt{4mt^2 - p^2}}\right)}{(p\sqrt{4m_t^2 - p^2})}.$$

(3.2.16)

Figure 3.2.2: Left: comparison between the real part of $f_1(p^2)$ in the high energy approximation with the exact $f_1(p^2)$ depending on m_{X_0} mass at $\sqrt{s} = 13$ TeV. **Right**: relative difference between the real part of $f_1(p^2)$ in the high energy approximation with the exact $f_1(p^2)$ depending on m_{X_0} mass at $\sqrt{s} = 13$ TeV
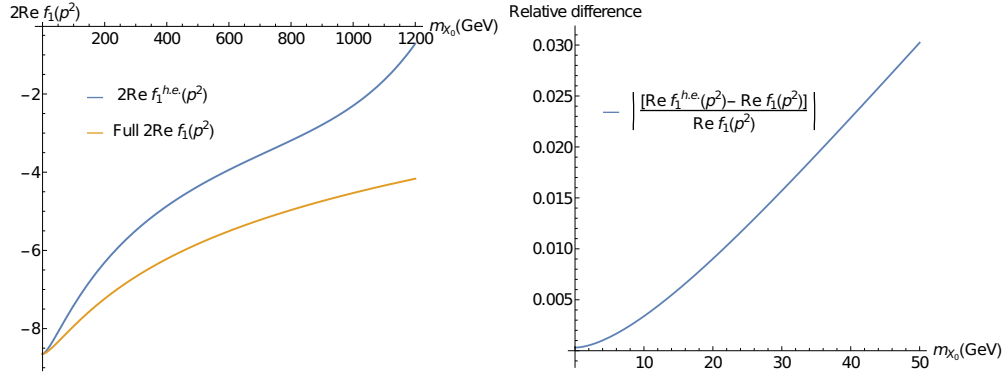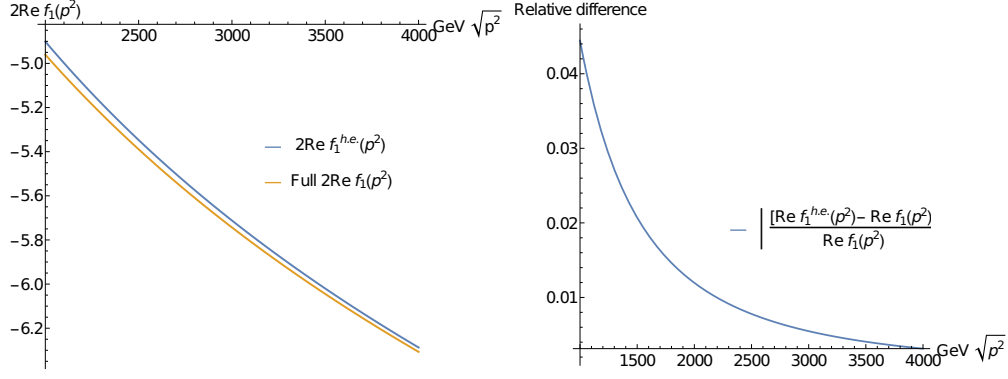
.

35

Figure 3.2.3: Left: comparison between the real part of $f_1(p^2)$ in the high energy approximation with the exact $f_1(p^2)$ depending on p with $m_{X_0} = 0$. **Right**: relative difference between the real part of $f_1(p^2)$ in the high energy approximation with the exact $f_1(p^2)$ depending on p with $m_{X_0} = 0$

.

3.2.2 Explicit expression of the form factors in the scalar case

In the scalar case $\tilde{g} = 0$ we will have:

$$f_1(p^2) = -\frac{\alpha}{4\pi} \left[\int_0^1 dz \int_0^{1-z} dy \, \log\left(\frac{m_t^2(1-z)^2 - p^2(1-y-z)y + m_{X_0}^2 z}{m_t^2(1-z)^2 + m_{X_0}^2 z} \right) + \right.$$
$$\left. + \frac{m_t^2(1+z)^2}{m_t^2(1-z)^2 + m_{X_0}^2 z} - \frac{m_t^2(1-z)^2 + (1-y-z)yp^2}{m_t^2(1+z)^2 - (1-y-z)yp^2 + m_{X_0}^2 z} \right]. \tag{3.2.17}$$

At high energies the expression (3.2.17) becomes

$$f_1^{h.e.}(p^2) = -\frac{\alpha}{4\pi} \left[\int_0^1 dz \int_0^{1-z} dy \, \log\left(\frac{-p^2(1-y-z)y}{m_t^2(1-z)^2 + m_{X_0}^2 z} \right) + \frac{2m_t^2(1+z^2) + m_{X_0}^2 z}{m_t^2(1-z)^2 + m_{X_0}^2 z} \right]. \tag{3.2.18}$$

The result of this integral reads

$$f_1^{h.e.}(p^2) = \frac{\alpha}{8\pi} \left[8 + \log\left(-\frac{m_{X_0}^8}{p^2 m_t^6} \right) - \frac{3m_{X_0}^2}{m_t^2} + \frac{3m_{X_0}^4 \log\left(\frac{m_{X_0}}{m_t} \right)}{m_t^4} + \frac{12m_{X_0}^2 \log\left(\frac{m_t}{m_{X_0}} \right)}{m_t^2} + \right.$$

$$\left. + \frac{3\sqrt{m_{X_0}^2 - 4m_t^2} \left(m_{X_0}^3 - 2m_{X_0}m_t^2 \right) \left(\tanh^{-1}\left(\frac{m_{X_0}}{\sqrt{m_{X_0}^2 - 4m_t^2}} \right) - \coth^{-1}\left(\frac{m_{X_0}\sqrt{m_{X_0}^2 - 4m_t^2}}{m_{X_0}^2 - 2m_t^2} \right) \right)}{m_t^4} \right].$$

$$\tag{3.2.19}$$

In this case, we cannot have a simple expression at $m_{X_0} = 0$ because we have an infrared divergence. What we can do is expand this expression around $m_{X_0}/\sqrt{p^2}$, for which we obtain

$$f_1 = \frac{\alpha}{4\pi}\left[\frac{1}{2}\left(8 + \log - \left(\frac{m_{X_0}^8}{p^2 m_t^6}\right)\right) - 3\pi\frac{m_{X_0}}{\sqrt{p^2}} - \frac{3}{2}\left(4\log\frac{m_{X_0}}{m_t} - 1\right)\frac{m_{X_0}^2}{p^2}\right] + \mathcal{O}\left(\frac{m_{X_0}^3}{\sqrt{p^2}^3}\right). \quad (3.2.20)$$

$f_1^{h.e}$ is plotted in figure 3.2.4 for $\tilde{\alpha} = 8\pi$ with respect to the mass m_{X_0}. At the left we have plotted the same quantity with a logarithmic scale on the x-axis, we can see that the infrared divergence is present and it goes as the $\log m_{1/X_0}$ as in the case of the real emission.
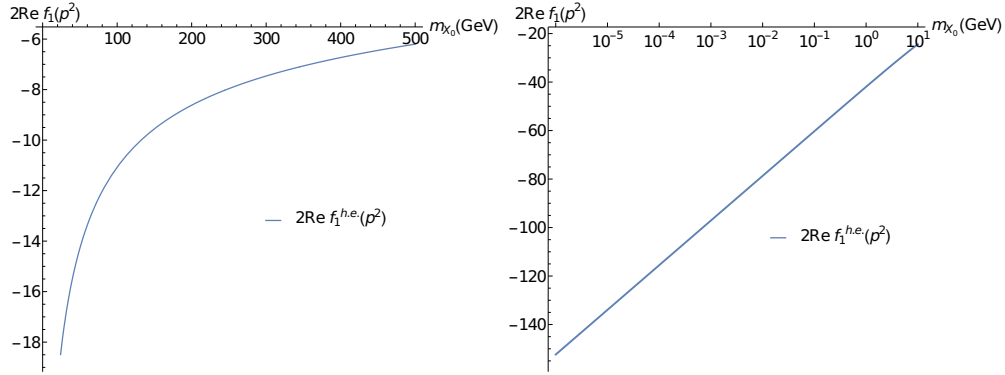
Figure 3.2.4: Left: dependence of $f_1(p^2)$ on m_{X_0} in the high energy limit, for a centre of mass of 13 TeV and $m_t = 172.5$GeV. **Right:** the behaviour of the same quantity for small X_0 masses with a logarithmic scale on the x-axis.

We can go further and look how is the general form of f_1 without any approximation:

$$f_1(p^2) = -\frac{\alpha}{4\pi}\int_0^1 \frac{2\left(8zm_t^2 - 2m_{X_0}^2 z + p^2(z-1)^2\right)\tan^{-1}\left(\frac{p(z-1)}{\sqrt{4(z-1)^2 m_t^2 + 4m_{X_0}^2 z - p^2(z-1)^2}}\right)}{p\sqrt{4(z-1)^2 m_t^2 + 4m_{X_0}^2 z - p^2(z-1)^2}} +$$

$$+ \frac{(z-1)z\left(m_{X_0}^2 - 4m_t^2\right)}{(z-1)^2 m_t^2 + m_{X_0}^2 z}dz. \quad (3.2.21)$$

This integral is not easy to be solved, so we will compute it numerically with MATHEMATICA. In figure 3.2.5 we have plotted $f_1(p^2)$ for $\sqrt{s} = 13$ TeV with respect to m_{X_0}, in the high energy and in the general case. Looking at the relative difference one can see that the predictions are very similar when $m_{X_0}^2 \ll p^2$. They are overall smaller than in the pseudoscalar case, we can argue that this will imply that the high energy approximation in the case of the scalar works better. We will see this in

37

practice in the next section. In figure 3.2.6 the same comparison is plotted but now $f_1(p^2)$ is plotted against $\sqrt{p^2}$ with $m_{X_0} = 10$ GeV.

Figure 3.2.5: Left: comparison between the real part of $f_1(p^2)$ in the high energy approximation with the exact $f_1(p^2)$ depending on m_{X_0} mass at $\sqrt{s} = 13$ TeV. **Right**: relative difference between the real part of $f_1(p^2)$ in the high energy approximation with the exact $f_1(p^2)$ depending on m_{X_0} mass at $\sqrt{s} = 13$ TeV.

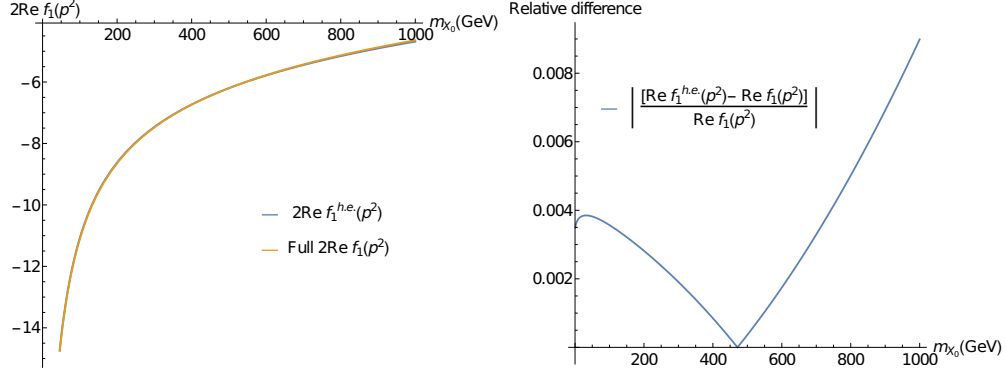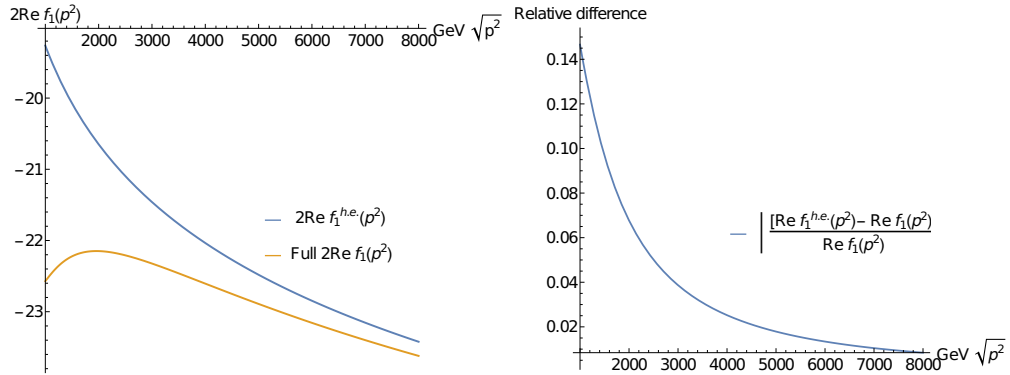**Figure 3.2.6: Left**: comparison between the real part of $f_1(p^2)$ in the high energy approximation with the exact $f_1(p^2)$ depending on p with $m_{X_0} = 10$GeV. **Right**: relative difference between the real part of $f_1(p^2)$ in the high energy approximation with the exact $f_1(p^2)$ depending on p with $m_{X_0} = 10$GeV.

Again the top quark is very heavy so we need also the consider the F_2 term, for which we find:

$$F_2(p^2) = g^2 \frac{m_t^2}{8\pi^2} \int dz \frac{4\left(z^2-1\right)\tan^{-1}\left(\frac{p(z-1)}{\sqrt{4m_{X_0}^2 z + 4m_t^2(z-1)^2 - p^2(z-1)^2}}\right)}{p\sqrt{4m_{X_0}^2 z + 4m_t^2(z-1)^2 - p^2(z-1)^2}} \tag{3.2.22}$$

3.2.3 NLO Validation

As we have stated at the beginning of the chapter our purpose is to validate the UFO model produced with NLOCT in order to automatize the NLO computation for $pp \to t\bar{t}$ and possibly other processes.

In order to do this, we can compare the corrections to the Born amplitude computed by MadGraph using our UFO model and the corrections to the Born amplitude that we have computed theoretically in this chapter. It is important to underline that the results of the theoretical computation and the one obtained by MadGraph are totally independent.

In order to compare the results we define the quantity $\Delta_\mathcal{M}$:

$$\Delta_\mathcal{M} = \frac{2\mathrm{Re}[\mathcal{M}_0 \mathcal{M}_{X_0}^\dagger]}{|\mathcal{M}|_0^2 \frac{\alpha_s}{2\pi}} \tag{3.2.23}$$

where the squared amplitudes are intended averaged and summed over the spins.

If we are at high energies, using (3.2.6), it is immediate to find

$$\Delta_{\mathcal{M}_{he}} = \frac{2\mathrm{Re}\left[f_1(p^2)\right]}{\frac{\alpha_s}{2\pi}} \tag{3.2.24}$$

As we have said, being the top very heavy, we will not have a precise result neglecting spin-interactions, so it is needed to consider the full correction. In the parton model in which light quarks masses are equal to zero the correction becomes:

$$\Delta_\mathcal{M} = \frac{2\pi}{\alpha_s}\left(2\mathrm{Re}\left[f_1(p^2)\right] + 2\frac{2}{9}(\alpha_s 4\pi)^2 \frac{2\mathrm{Re}\left[F_2(p^2)\right]}{|\mathcal{M}|_0^2}\right) \tag{3.2.25}$$

The results we have found are reported in table 3.2.1 in which we have looked at the case $g = 0$ and $\tilde{g} = 0.1$ and in table 3.2.2in which we have looked at the case $g = 0.1$ and $\tilde{g} = 0$.

$\sqrt{s}$ (GeV)	$\Delta_{\mathcal{M}}$ MadGraph5_aMC@NLO (10^{-2})	$\Delta_{\mathcal{M}_{he}}(10^{-2})$	$\Delta_{\mathcal{M}}(10^{-2})$	$\left\|\frac{\Delta_{\mathcal{M}_{he}}-\Delta_{\mathcal{M}}}{\Delta_{\mathcal{M}_{he}}}\right\|$
500	-0.333918	-0.851680	-0.333918	0.602
1000	-1.005070	-1.237798	-1.005070	0.188
1500	-1.356298	-1.486193	-1.356298	0.130
2000	-1.585412	-1.668796	-1.585412	0.083
2500	-1.754552	-1.812970	-1.754552	0.032
3000	-1.888581	-1.931992	-1.888581	0.022
3500	-1.999640	-2.03329	-1.999640	0.017
4000	-2.094511	-2.121435	-2.094511	0.013
4500	-2.177356	-2.19944	-2.177356	0.010
5000	-2.250910	-2.269379	-2.25091	0.008
10000	-2.726512	-2.732085	-2.726512	0.002

Table 3.2.1: Pseudoscalar case ($g = 0$, $\tilde{g} = 0.1$), $m_{X_0} = 0$. In the first column $\Delta_{\mathcal{M}}$ automatically computed by MadGraph5_aMC@NLO, in second and third columns the computation obtained using equation (3.2.24) and (3.2.25) using $f_1(p^2)$ and $F_2(p^2)$ found in previous sections.

$\sqrt{s}$ (GeV)	$\Delta_{\mathcal{M}}$ MadGraph5_aMC@NLO (10^{-1})	$\Delta_{\mathcal{M}_{he}}(10^{-1})$	$\Delta_{\mathcal{M}}(10^{-2})$	$\left\|\frac{\Delta_{\mathcal{M}_{he}}-\Delta_{\mathcal{M}}}{\Delta_{\mathcal{M}_{he}}}\right\|$
500	-1.771673	-1.61915	-1.771673	0.094
1000	-1.547723	-1.478421	-1.547723	0.046
1500	-1.445103	-1.406358	-1.445103	0.026
2000	-1.403109	-1.378219	-1.403109	0.018
2500	-1.384205	-1.366759	-1.384205	0.013
3000	-1.375607	-1.362639	-1.375607	0.010
3500	-1.372150	-1.362095	-1.372150	0.007
4000	-1.371452	-1.363406	-1.371452	0.006
4500	-1.372308	-1.365708	-1.372308	0.005
5000	-1.367061	-1.368542	-1.374063	0.004
10000	-1.400979	-1.399313	-1.400979	0.001

Table 3.2.2: Scalar case ($g = 0.1$, $\tilde{g} = 0$), $m_{X_0} = 1$GeV. In the first column $\Delta_{\mathcal{M}}$ automatically computed by MadGraph5_aMC@NLO, in second and third columns the computation obtained using equation (3.2.24) and (3.2.25) using $f_1(p^2)$ and $F_2(p^2)$ found in previous sections.

The results obtained by our model in MadGraph5_aMC@NLO (second column) and the ones obtained by the theoretical computation (fourth column) are the same at least up to the seventh decimal digit. Again we stress the fact that these two results are independent because the counterterms for the UFO model are computed by the NLOCT package in MATHEMATICA instead of being inserted by hand. Another interesting point is the fact that looking at the tables the spin corrections related to F_2 dominates the pseudoscalar case at low energies, while they are less important in the scalar case, confirming our intuition of the previous section, made by looking at the relative difference between $f_1^{h.e.}(p^2)$ and the exact form of $f_1(p^2)$. In particular, at 500 **GeV** $\sim 3m_t$ the relative error made in the high energy approximation for the scalar is only the 9.4% while for the pseudoscalar case the relative error is 60.2%.

Chapter 4

Kinematical Distributions

In this chapter, we present predictions for the cross section of $pp \to t\bar{t}$ at $\sqrt{s} = 13$ TeV. We show differential distributions both at the tree level and including the effect of X_0 from the loops, which we call NLO corrections. To this aim, we have exploited the UFO model produced with NLOCT and simulated the process $pp \to t\bar{t}$ at NLO accuracy using MadGraph5_aMC@NLO. In particular, we have considered the following observables:

- the invariant mass of the $t\bar{t}$ pair $(m_{t\bar{t}})$;

- the top-quark transverse momentum $(p_T(t))$;

- the rapidity of the top-quark (y_t);

- the difference in the rapidity between t and $\bar{t}$ $(\Delta y_{t\bar{t}} = y_t - y_{\bar{t}})$.

We have briefly introduced p_T as a key observable at hadron colliders in chapter 2, and we will now briefly introduce the invariant mass and the rapidity.

The invariant mass of a pair of particles (in our case $t\bar{t}$) is defined as:

$$m_{t\bar{t}}^2 = (p_t + p_{\bar{t}})^2 = (E_t + E_{\bar{t}})^2 - (\vec{p}_t + \vec{p}_{\bar{t}})^2, \tag{4.0.1}$$

where p_t is the top-quark four-momentum.

The rapidity of a particle is defined as

$$y = \frac{1}{2} \log \frac{E + p_z}{E - p_z}. \tag{4.0.2}$$

The distributions were obtained simulating $pp \to t\bar{t}$ at $\sqrt{s} = 13$ TeV, with $m_t = 172$ GeV, we have used the built-in MadGraph5_aMC@NLO PDF set nn23nlo from NNPDF [30], the strong coupling $\alpha_s(m_Z) = 0.1190$. Factorization and renormalization scales are automatically set on event-by-event basis by MadGraph5_aMC@NLO using the default dynamical scale $H_T/2$ corresponding in this case to $\sqrt{m_t^2 + p_T^2(t)}$.

In the first part, the distributions are plotted keeping $m_{X_0} = 125$ GeV, the same mass of the SM Higgs, and changing the values of the parameters g and $\tilde{g}$. As a reference, we have used the Higgs coupling to the top in the SM, $m_t/v \approx 0.7$. Several benchmark points are selected:

- scalar ($g = m_t/v, \tilde{g} = 0$), short-noted as (1,0);

- pseudoscalar ($g = 0, \tilde{g} = m_t/v$), short-noted as (0,1);

- mixed, concordant signs ($g = m_t/v, \tilde{g} = m_t/v$), short-noted as (1,1);

- mixed, discordant signs ($g = m_t/v, \tilde{g} = -m_t/v$), short-noted as (1,-1).

Our motivation is twofold. First, we want to study in general what happens to the kinematical distributions in different scenarios, both in the normalisation as well as in the shapes. To this aim, we use the quantity

$$\Delta_{\mathrm{NLO}} = \frac{\sigma_{\mathrm{NLO}} - \sigma_{\mathrm{LO}}}{\sigma_{\mathrm{LO}}}, \tag{4.0.3}$$

namely the relative correction, which we will show in the inset of each plot in this chapter.

Second, starting from the four benchmark points, it will be straightforward to predict the more generic cases, with $(g, \tilde{g})$ arbitrary. This can be done by looking at the analytic expression of the relative correction Δ_{NLO}

$$\Delta_{\mathrm{NLO}} = g^2 F_{g^2} + \tilde{g}^2 F_{\tilde{g}^2} + g\tilde{g} F_{\mathrm{interference}}, \tag{4.0.4}$$

with $F_{g^2}, F_{\tilde{g}^2}, F_{\mathrm{interference}}$ to be considered placeholders for the contribution from the full computation (and not the ones computed in chapter 3), including both $q\bar{q}, gg \to t\bar{t}$ partonic processes. The (1,0) and (0,1) benchmark points provide us with the size of F_{g^2} and $F_{\tilde{g}^2}$. For example, in the case $g = n\frac{m_t}{v}$ and $\tilde{g} = 0$, $\Delta_{\mathrm{NLO}}|_{g=n\frac{m_t}{v}, \tilde{g}=0} = n^2 \Delta_{\mathrm{NLO}}|_{g=\frac{m_t}{v}, \tilde{g}=0}$. They also fully determine the component $F_{\mathrm{interference}}$ via the relation

$$g\tilde{g} F_{\mathrm{interference}} = \frac{1}{2} \left(\Delta_{\mathrm{NLO}}(1,1) - \Delta_{\mathrm{NLO}}(1,-1) \right), \tag{4.0.5}$$

In the last part, we have investigated the effects of the variation of m_{X_0} on the distributions in each benchmark point, in order to verify the expectation that in the pseudoscalar case, there should be almost no dependence on m_{X_0}, as already observed in the case of the real-emission process plots in chapter 2 and the $f_1(p^2)$ function at 1-loop in chapter 3.

Before discussing the distributions it is important to note that the $gg \to t\bar{t}$ process at one loop receives a contribution from the diagram in Fig. 4.0.1 containing the particle X_0 in an s-channel.

$$\tag{4.0.6}$$

Figure 4.0.1

For resonant $m_{X_0} > 2m_t$, this process is dominated by the resonance X_0 production with its subsequent decay in $t\bar{t}$. This is an interesting process by itself, and worth to be further investigated. However, for the purpose of our analysis that wants to focus on indirect effects, we can defer it. In order to avoid the region of direct X_0 production, we limit m_{X_0} to a maximum of 334 GeV, that is $2m_t - (10\mathrm{GeV})$.
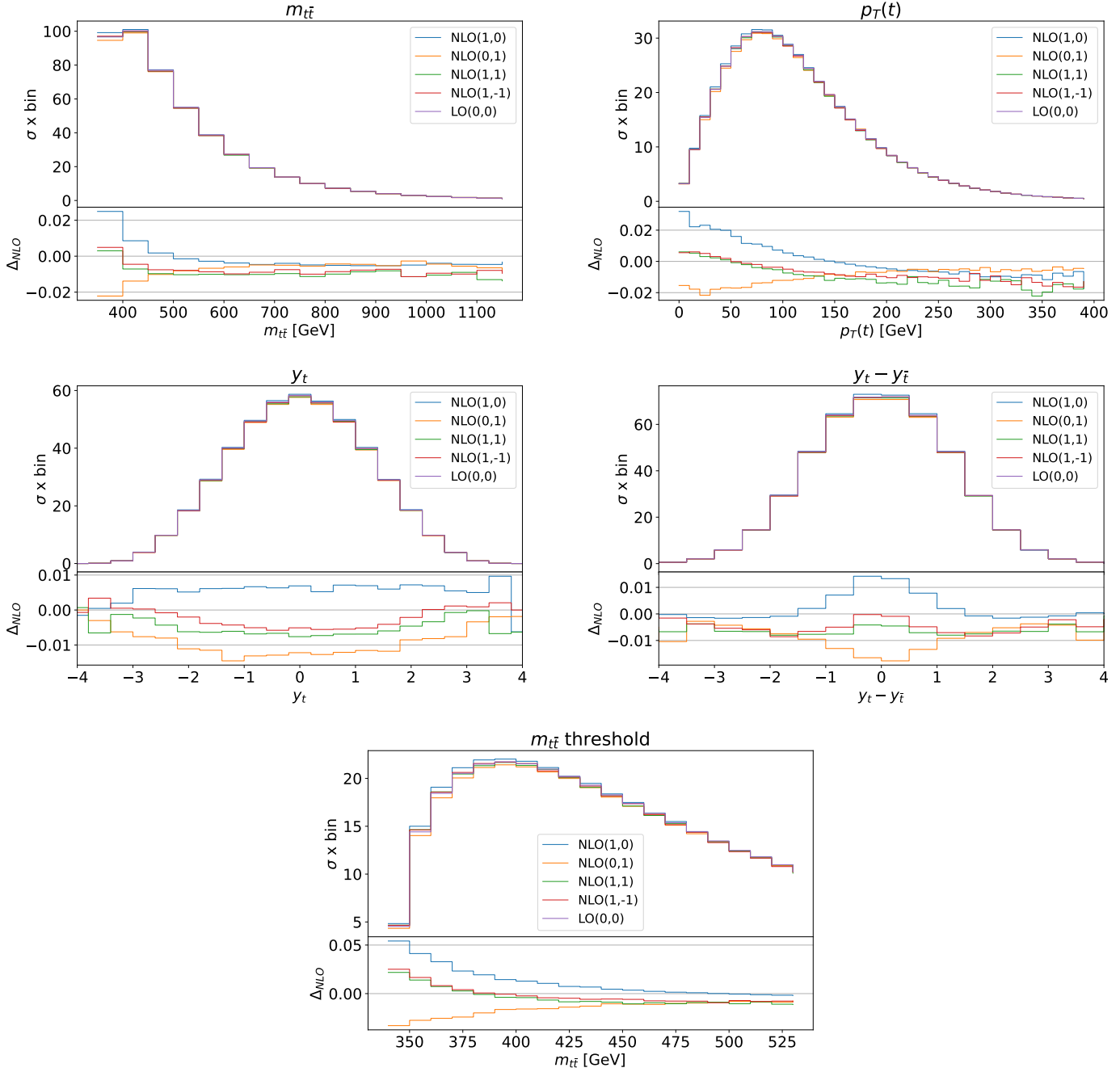
Figure 4.0.2: Plots of the kinematical distributions for each beanchmark point at fixed $m_{X_0} = m_H = 125$ GeV. From left to right, going downwards: the invariant mass distribution $m_{t\bar{t}}$, the transverse momentum distribution $p_T(t)$, the rapidity distribution y_t, the difference between rapidity distribution $y_t - y_{\bar{t}}$ and the invariant mass distribution $m_{t\bar{t}}$ near the threshold at $\sqrt{s} = 13$ TeV. In the inset of each plot is depicted the relative difference Δ_{NLO}, as defined in (4.0.3).

We start by considering the Higgs mass benchmark point for which $m_{X_0} = m_H$. Our results are collected in figure 4.0.2 where are plotted the different kinematical distributions, keeping m_{X_0} fixed but changing the couplings as explained above. We have chosen to study the case $m_{X_0} = m_H = 125$ GeV, in order to validate our results for the case of the Higgs in the SM, (1,0) benchmark point, with the available literature [3]. The cases (0,1), (1,1), (1,-1) are also considered.

From the plots, we can see that the largest corrections are present when the top quarks are produced near the threshold, meaning $m_{t\bar{t}} \simeq 2m_t$. Similarly, corrections are large, in absolute value, for $p_T(t) \simeq 0$

and $\Delta y_{t\bar{t}} = 0$, i.e. near the threshold (this is explicitly shown in appendix H). This behaviour is washed out in the y_t distribution, where the corrections do not peak around a specific value because there is no direct link between the invariant mass and the rapidity of a single particle. For all basic benchmark points, corrections are between 2% and a few per mill, in absolute value.

The different behaviour among the benchmark points is more pronounced for the $m_{t\bar{t}}$ distribution, where at the threshold in the pseudoscalar (0,1) benchmark point we have a negative contribution, while in the scalar (1,0) a positive one. Looking at the $\Delta y_{t\bar{t}}$ distribution, in the pseudoscalar (0,1) there is a negative correction to the central region, and the opposite happens for the scalar (1,0).

A last remark on the mixed term is appropriate: the $(1, 1)$ and the $(1, -1)$ benchmark points give almost the same correction. Looking back at (4.0.5) we can conclude that the interference term $F_{\text{interference}}$ is very small compared to the other two.
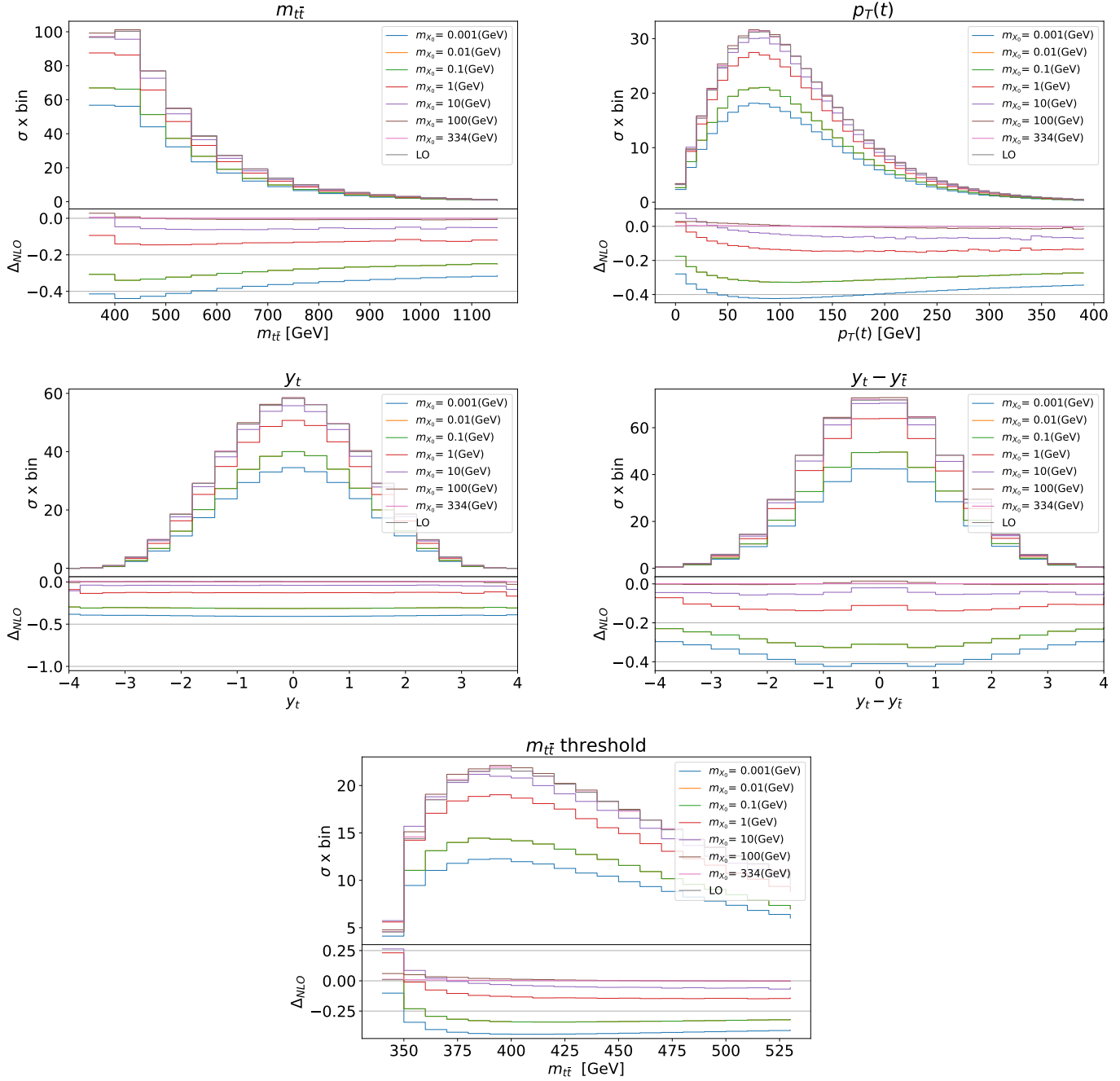
Figure 4.0.3: Plots of the kinematical distributions for the scalar $(1,0)$ benchmark point for different values of m_{X_0}. From left to right, going downwards: the invariant mass distribution $m_{t\bar{t}}$, the transverse momentum distribution $p_T(t)$, the rapidity distribution y_t, the difference between rapidity distribution $y_t - y_{\bar{t}}$ and the invariant mass distribution $m_{t\bar{t}}$ near the threshold at $\sqrt{s} = 13$ TeV. In the inset of each plot is depicted the relative difference Δ_{NLO}, as defined in (4.0.3).

The case of the scalar benchmark point, i.e. $g = m_t/v$, $\tilde{g} = 0$ changing the X_0 mass by logarithmic step, is shown in figure 4.0.3. All the kinematical distributions show a very strong dependence on the mass of X_0. The lower the mass of m_{X_0}, the higher the corrections. This is not surprising: as now mentioned several times, this is the effect of the term

$$\log \frac{s}{m_{X_0}^2},$$

that is present in the scalar case. Note, however, that for a scalar, the coefficient in front of the log

45

is $\frac{m_t^2}{s}$, as calculated in chapter 2. This is the reason why there is no growth for large $m_{t\bar{t}} = s$ value within the distribution.

Corrections for small masses can reach up to the 40% of the LO value near the threshold. As we have seen for the Higgs case, the corrections to y_t are almost flat, because the $t\bar{t}$ produced at the threshold are not produced with a preferred rapidity. The $p_T(t)$ and $\Delta y_{t\bar{t}}$ distributions show the same behaviour as commented before.

We will comment on the behaviour at $m_{X_0} = 334$ GeV in the discussion of the plots in figure 4.0.4 for the pseudoscalar, where the peculiarity of the corrections for $m_{X_0} = 334$ GeV is manifest.
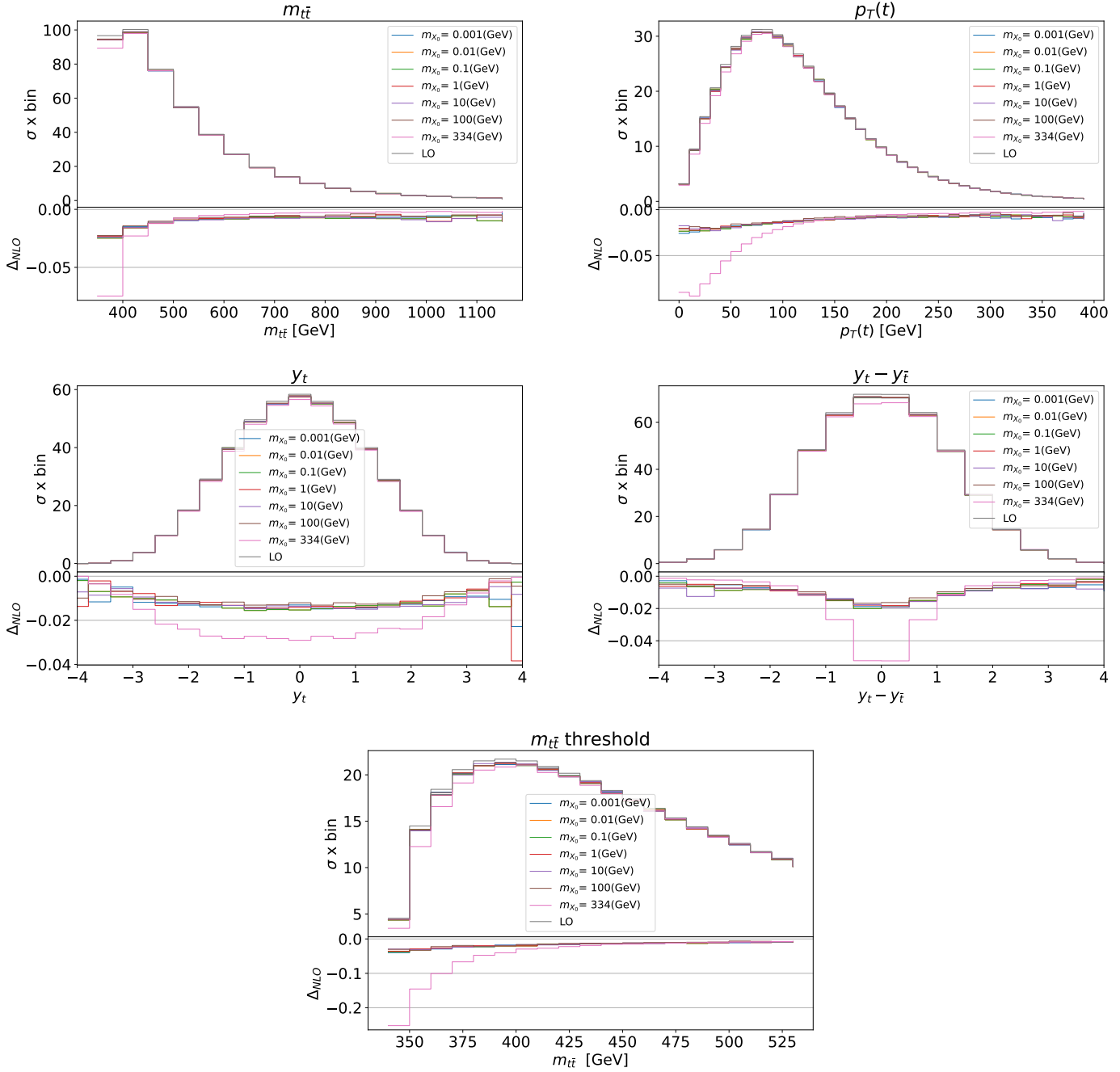
Figure 4.0.4: Plots of the kinematical distributions for the pseudoscalar (0,1) benchmark point for different values of m_{X_0}. From left to right, going downwards: the invariant mass distribution $m_{t\bar{t}}$, the transverse momentum distribution $p_T(t)$, the rapidity distribution y_t, the difference between rapidity distribution $y_t - y_{\bar{t}}$ and the invariant mass distribution $m_{t\bar{t}}$ near the threshold at $\sqrt{s} = 13$ TeV. In the inset of each plot is depicted the relative difference Δ_{NLO}, as defined in (4.0.3).

We now consider the pseudo-scalar case, 4.0.4, (1,0), i.e. $g = 0$, $\tilde{g} = m_t/v$ changing the X_0 mass by logarithmic step. The kinematical distributions show almost no dependence on the mass of X_0. The behaviour with respect to the m_{X_0} is what is expected from our preliminary study on the real radiation in chapter 2: in the limit $m_{X_0} \to 0$ we have found a constant cross section. The same behaviour was noted in the $F_1(p^2)$ computed in chapter 3. We therefore confirm what stated in the introduction to chapter 2: in the case $g = 0$ the possible new physics effect that can be accommodated given the present measurements depend only on $\tilde{g}$ and not on m_{X_0} for $m_{X_0} < 2m_t$. This is the opposite situation

of the scalar ($\tilde{g} = 0$) for which large values of g imply large values of m_{X_0} to not exceed experimental constraints.

Corrections reach up to the 3% of the LO value near the threshold, which is one order of magnitude smaller than the correction for the scalar case. The usual considerations on y_t $p_T(t)$ and $\Delta y_{t\bar{t}}$ are still valid.

Let us now consider the case where $m_{X_0} = 334\text{GeV} = 2m_t - (10\text{GeV})$. This region is important because we are approaching the value of $m_{X_0} = 2m_t$ where the X_0 can be produced on shell and then decay in $t\bar{t}$, i.e., the diagram in 4.0.1 is becoming resonant. In the scalar case the effect is not visible because the corrections for small masses are much higher than the correction given by the diagram becoming resonant and the corrections become smaller for m_{X_0} heavy. On the other hand, in the pseudoscalar case, the corrections do not depend on m_{X_0} and are way smaller than in the scalar case. As a result, the corrections given by the resonance diagram is the dominant effect. It is important to note that the effect is not zero in the scalar case, is only too small to be noted with the scale used in the plot. Moreover, in the appendix I we have calculated the amplitude for the loop induced $gg \rightarrow X_0$ production, with X_0 on-shell, and we have shown how the result is different for the scalar and the pseudoscalar case.

The fact that the pseudoscalar case (0,1) does not depend on the mass implies that we do not need to have a small $\tilde{g}$ for small m_{X_0}. The corrections for a value $\tilde{g} = nm_t/v$ will be, as mentioned before, n^2 the corrections given here. Choosing, for example, $\tilde{g} = g_s(m_Z)$ (where $g_s = \sqrt{4\pi\alpha_s(m_Z)}$), we find that the corrections will be about 12 times larger than those shown here, leading to an overall correction of 24% at the threshold, which is experimentally well observable and therefore can be excluded. However, we should notice that there is not dependence on the mass m_{X_0} in the exclusion limits that could be extracted. If we had extracted from an actual measurement of the $t\bar{t}$ distributions a bound on $\tilde{g}$, we could have set m_{X_0} as small as we want without having an effect on the validity of the bound. This is in contrast to the usual scenario, where larger values of the coupling implies larger values of the mass of the new particle in order to accommodate the effects of new physics in the measurements of kinematical distributions.

Figure 4.0.5: Plots of the kinematical distributions for the mixed (1,1) benchmark point for different values of m_{X_0}. From left to right, going downwards: the invariant mass distribution $m_{t\bar{t}}$, the transverse momentum distribution $p_T(t)$, the rapidity distribution y_t, the difference between rapidity distribution $y_t - y_{\bar{t}}$ and the invariant mass distribution $m_{t\bar{t}}$ near the threshold at $\sqrt{s} = 13$ TeV. In the inset of each plot is depicted the relative difference Δ_{NLO}, as defined in (4.0.3).
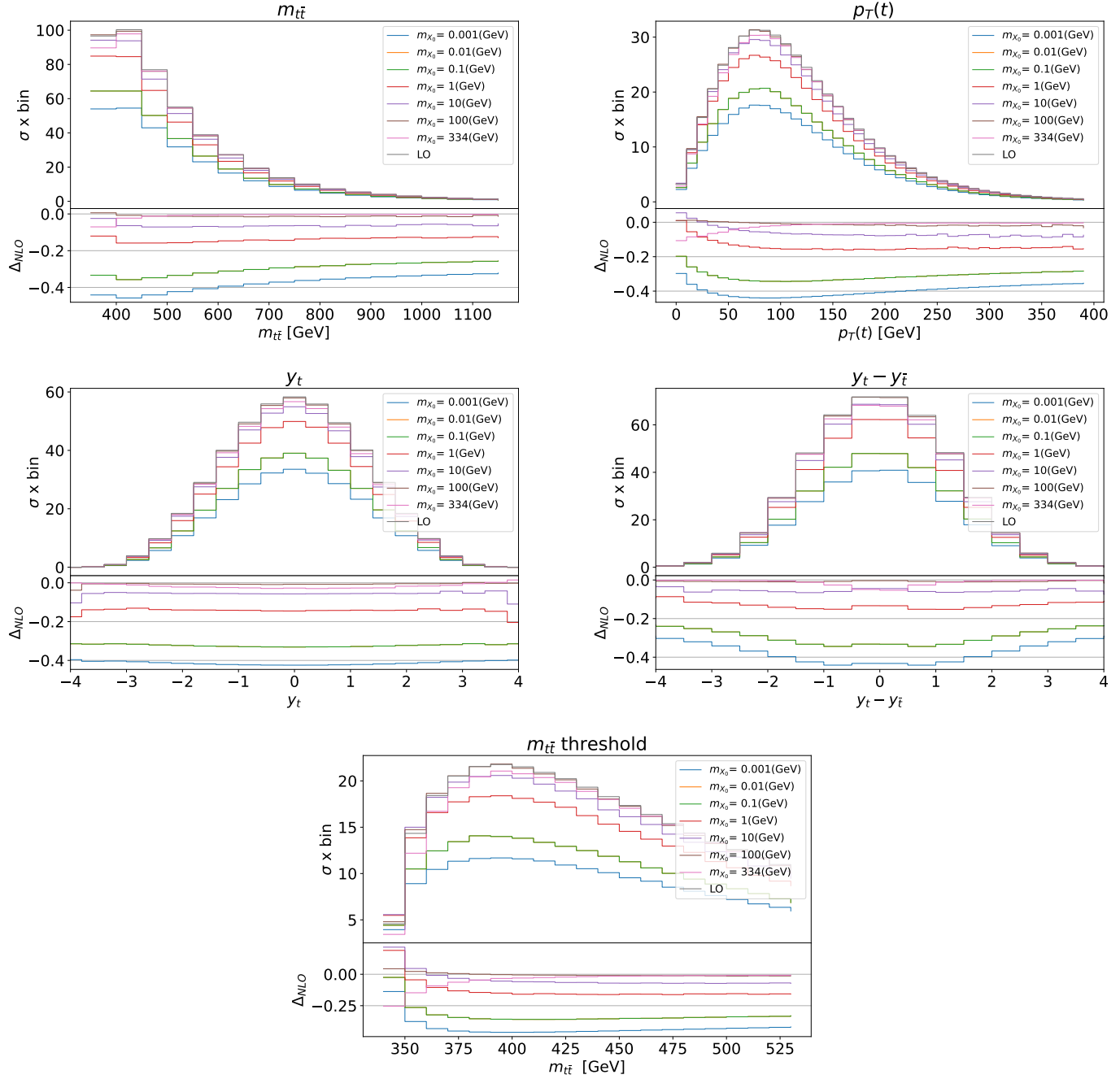
49

Figure 4.0.6: Plots of the kinematical distributions for the mixed benchmark point (1,-1) for different values of m_{X_0}. From left to right, going downwards: the invariant mass distribution $m_{t\bar{t}}$, the transverse momentum distribution $p_T(t)$, the rapidity distribution y_t, the difference between rapidity distribution $y_t - y_{\bar{t}}$ and the invariant mass distribution $m_{t\bar{t}}$ near the threshold at $\sqrt{s} = 13$ TeV. In the inset of each plot is depicted the relative difference Δ_{NLO}, as defined in (4.0.3).
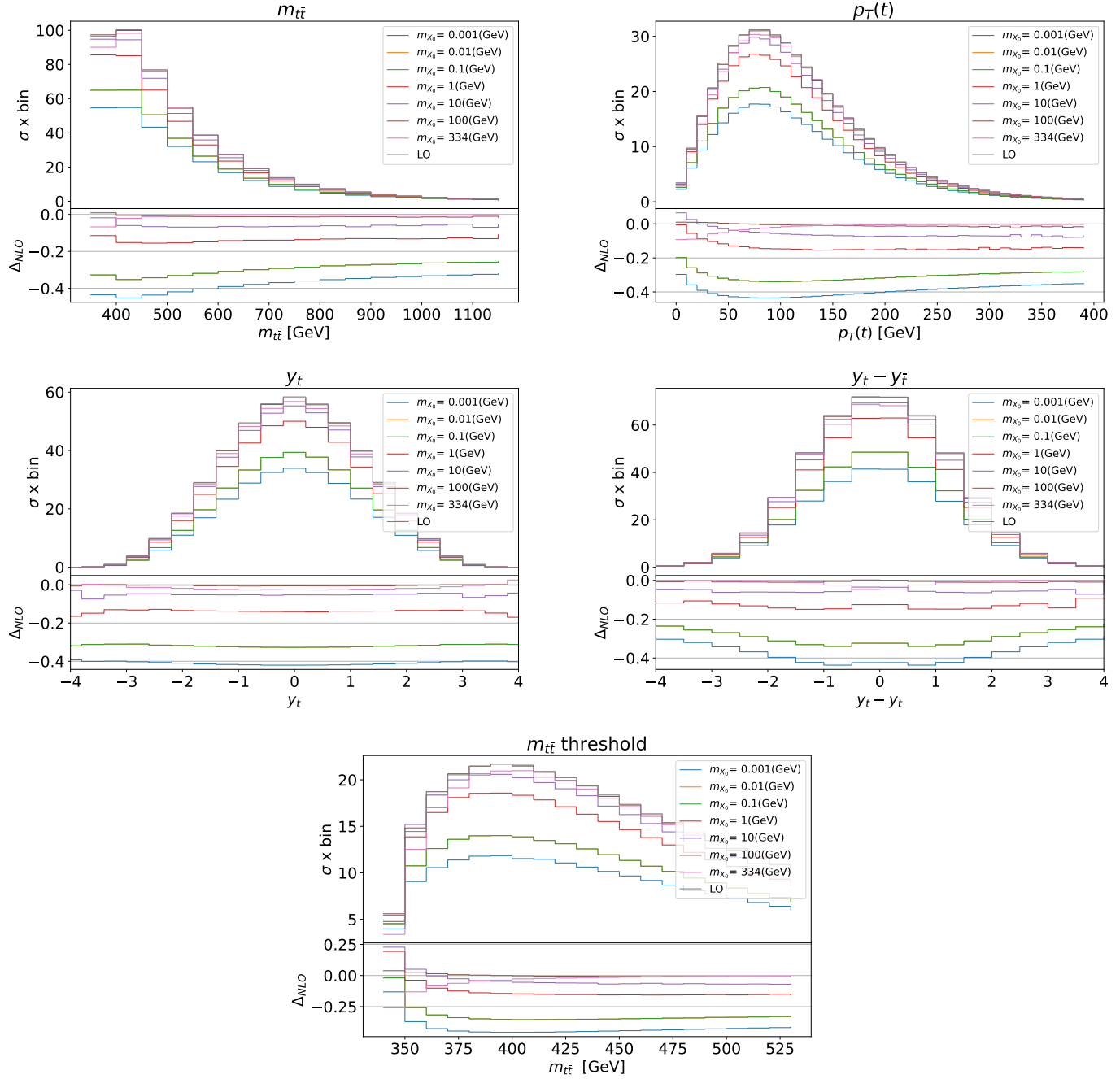
We now consider the kinematical distribution in the mixed (1,1) and (1,-1) benchmark points, i.e. $g = m_t/v$, $\tilde{g} = \pm m_t/v$ changing the X_0 mass by logarithmic step. We have plotted the corresponding results in figures 4.0.5 and 4.0.6.

The shapes of the Δ_{NLO} are similar to the scalar case, the reason being that the scalar corrections are dominant over the pseudoscalar ones. It is very interesting to note the behaviour at $m_{X_0} = 334$ GeV. In this case, both g and $\tilde{g}$ terms are present so, unlike the pure scalar case, at the threshold we have a visible effect. Indeed the correction given by the resonant diagrams is not so small because of the presence of the $\tilde{g}$ term.

Conclusions

In this thesis, we have moved the first steps in the exploration of the phenomenology of a hypothetical new pseudo-scalar state that preferentially couples to the top quark through a generic interaction

$$\mathcal{L}_{\text{int}} = -\bar{t}(g + i\tilde{g}\gamma_5)tX_0.$$

First of all, we have shown that an ALP, i.e. a pseudo-Goldstone boson coupling only derivatively, i.e. at dimension 5, would lead to the same physics. Second, that due to this equivalence, emission of massless (small mass) ALPS, real or virtual, does not lead to any infrared divergence (the soft enhancement). We have explicitly verified this general argument by direct calculation of the soft limits of the real emission processes for vector, scalar and pseudoscalar particles, obtaining the expected results. We have then compared our analytical behaviours by implementing the model into MadGraph5_aMC@NLO via FeynRules at leading order. Using MadGraph5_aMC@NLO package we have simulated the emission processes of a scalar and a pseudoscalar. The simulations confirmed the expectations: the cross section for the emission of a scalar particle has a logarithmic dependence on the scalar mass of the type: $\sigma \propto \log(s/m_{X_0}^2)$, while the pseudoscalar cross section goes like a constant for small m_{X_0} masses. The same behaviour was found by studying the cross section for different masses m_{X_0} and varying the energy of the centre-of-mass: the mass dependence for the scalar is very pronounced, unlike in the pseudoscalar case. After the validation of the picture in the real emission scenario, we have considered the indirect effects of virtual exchanges of ALPs in $pp \to t\bar{t}$ process. For this purpose, we used NLOCT to create a UFO model containing all the ingredients to compute via MadGraph5_aMC@NLO virtual corrections to any process involving top quarks in the final state. To validate the model made with NLOCT, we have calculated analytically the virtual new-physics corrections to the process $pp \to t\bar{t}$ and compared them with the model obtained from NLOCT. The analytic calculation turned out to be useful to check that in virtual processes, the same mass dependence is present as in real emission processes, and to assess how much the low-energy terms can be neglected in the two cases. It turns out that in the scalar case, the approximation for high energies in the calculation of virtual corrections provides a good estimate even for centre-of-mass energies up to about $3m_t$. In the pseudoscalar case, on the other hand, the approximation at high energies for virtual processes, leads to much larger uncertainties, as visible in table 3.2.1. Third, we have used our NLOCT model in MadGraph5_aMC@NLO to simulate the virtual effects of new physics in the process $pp \to t\bar{t}$. To this end, we have studied how key distributions, the invariant mass distribution of the pair $t\bar{t}$, the distribution of the transverse momentum $p_T(t)$ the distribution of the top rapidity y_t and the distribution of the difference $y_t - y_{\bar{t}}$ depend on the parameters g and $\tilde{g}$. The results confirmed our expectations, i.e. that in the scalar interaction case, there is an obvious mass dependence in the virtual corrections of new physics with respect to the LO. In the pseudoscalar case, on the other hand, the corrections are insensitive to the mass, as long as one stays below the $2m_t$ threshold.

Above the threshold, well-known resonance and signal-background interfering effects arise that give very striking signatures. Our implementation has also allowed studying the possible interference effects by the scalar and pseudoscalar components, which are found to be small. Our work opens now the possibility to make a full study of the sensitiveness of $pp \to t\bar{t}$ to new physics effects and to constrain the couplings/mass of the model comparing with available data. In addition, being fully general, the implementation of the UFO model opens the possibility of studying direct and indirect effects in all processes featuring a top in the final state. This is left for future work.

Appendix A

Dirac algebra and spinors identities

In this appendix we will list some useful formulas in the context of Dirac algebra, we will follow the treatment and the notation of [23] and [31] adding other formulae we found ourselves in the context of our computations.

In order to treat spin $\frac{1}{2}$ particles we need to introduce Pauli matrices

$$\sigma^\mu = \left(\begin{pmatrix} 1 & 0 \\ 0 & 1 \end{pmatrix}, \begin{pmatrix} 0 & 1 \\ 1 & 0 \end{pmatrix}, \begin{pmatrix} 0 & -i \\ i & 0 \end{pmatrix}, \begin{pmatrix} 1 & 0 \\ 0 & -1 \end{pmatrix} \right), \tag{A.0.1}$$

so we can define the 4×4 Dirac matrices

$$\gamma^\mu = \begin{pmatrix} & \sigma^\mu \\ \bar{\sigma}^\mu & \end{pmatrix}, \tag{A.0.2}$$

which satisfy the relation

$$\{\gamma^\mu, \gamma^\nu\} = 2g^{\mu\nu}. \tag{A.0.3}$$

In addition to this we introduce Dirac and Dirac adjoint spinor:

$$\psi = \begin{pmatrix} \psi_L \\ \psi_R \end{pmatrix}, \quad \bar{\psi} = \psi^\dagger \gamma^0.$$

Using gamma matrices is possible to build two projector operators, defining $\gamma_5 = i\gamma_0\gamma_1\gamma_2\gamma_3$, namely

$$P_L = \frac{1 - \gamma_5}{2}, \quad P_R = \frac{1 + \gamma_5}{2}, \tag{A.0.4}$$

so that

$$\gamma_5 = \begin{pmatrix} -\mathbb{1} & \\ & \mathbb{1} \end{pmatrix}, \quad P_L = \begin{pmatrix} \mathbb{1} & \\ & 0 \end{pmatrix}, \quad P_R = \begin{pmatrix} 0 & \\ & \mathbb{1} \end{pmatrix}.$$

The projectors act in the following way:

$$P_L\psi = \begin{pmatrix} \psi_L \\ 0 \end{pmatrix}, \quad P_R\psi = \begin{pmatrix} 0 \\ \psi_R \end{pmatrix}.$$

Gamma matrices have some important features useful in computing Feynman amplitudes, we list them here:

$$\gamma_5^2 = \mathbb{1}, \tag{A.0.5}$$

$$\{\gamma_5, \gamma_\mu\} = 0, \tag{A.0.6}$$

$$\gamma^{\mu\dagger} = \gamma^0 \gamma^\mu \gamma^0, \tag{A.0.7}$$

$$\gamma_\mu \gamma^\mu = 4, \tag{A.0.8}$$

$$\gamma_\mu \gamma^\nu \gamma^\mu = -2\gamma^\nu, \tag{A.0.9}$$

$$\gamma_\mu \gamma^\nu \gamma^\rho \gamma^\mu = 4g^{\nu\rho}, \tag{A.0.10}$$

$$\gamma_\mu \gamma^\nu \gamma^\rho \gamma^\sigma \gamma^\mu = -2\gamma^\sigma \gamma^\rho \gamma^\nu, \tag{A.0.11}$$

$$\not{p}\not{p} = p^2, \tag{A.0.12}$$

$$\not{p}\gamma^\mu \not{p} = 2p^\mu \not{p} - \gamma^\mu p^2. \tag{A.0.13}$$

There are also some useful identities involving gamma matrices traces:

$$Tr[\text{odd number of } \gamma] = 0, \tag{A.0.14}$$

$$Tr[\gamma^\mu \gamma^\nu] = 4g^{\mu\nu}, \tag{A.0.15}$$

$$Tr[\gamma^\alpha \gamma^\mu \gamma^\beta \gamma^\nu] = 4(g^{\alpha\mu}g^{\beta\nu} - g^{\alpha\beta}g^{\mu\nu} + g^{\alpha\nu}g^{\mu\beta}), \tag{A.0.16}$$

$$Tr[\gamma_5] = 0, \tag{A.0.17}$$

$$Tr[\gamma_5 \gamma^\mu \gamma^\nu] = 0, \tag{A.0.18}$$

$$Tr[\gamma^\alpha \gamma^\mu \gamma^\beta \gamma^\nu \gamma_5] = -4i\epsilon^{\alpha\mu\beta\nu}. \tag{A.0.19}$$

At this point, we can define the Dirac Lorentz-invariant Lagrangian as

$$\mathcal{L} = \bar{\psi}(i\gamma^\mu \partial_\mu - m)\psi. \tag{A.0.20}$$

Defining the contraction of a four vector with the gamma matrices as $v^\mu \gamma_\mu = \not{v}$, the equations of motion become

$$(i\not{\partial} - m)\psi = 0, \tag{A.0.21}$$

$$\bar{\psi}(i\overleftarrow{\not{\partial}} + m) = 0. \tag{A.0.22}$$

Using the spinor $u^s(p)$ for particles and $v^s(p)$ for antiparticles, the equations of motion become:

$$(\not{p} - m)u^s(p) = \bar{u}^s(p)(\not{p} - m) = 0, \tag{A.0.23}$$

$$(\not{p} + m)v^s(p) = \bar{v}^s(p)(\not{p} + m) = 0. \tag{A.0.24}$$

Spinors can be combined using the following relations:

$$\bar{u}^s(p)u^{s'}(p) = 2m\delta_{ss'}, \qquad (A.0.25)$$

$$\bar{v}^s(p)v^{s'}(p) = -2m\delta_{ss'}, \qquad (A.0.26)$$

$$u_s^\dagger(p)u_{s'}(p) = 2E\delta_{ss'}, \qquad (A.0.27)$$

$$v_s^\dagger(p)v_{s'}(p) = 2E\delta_{ss'}, \qquad (A.0.28)$$

$$\sum_{s=1}^2 u^s(p)\bar{u}^s(p) = \slashed{p} + m, \qquad (A.0.29)$$

$$\sum_{s=1}^2 v^s(p)\bar{v}^s(p) = \slashed{p} - m. \qquad (A.0.30)$$

For on-shell spinors we have the Gordon identity:

$$\bar{u}(q_1)\gamma^\mu u(q_2) = \bar{u}(q_1)\left[\frac{q_1^\mu + q_2^\mu}{2m} + i\frac{\sigma^{\mu\nu}(q_{1\nu} - q_{2\nu})}{2m}\right]u(q_2), \qquad (A.0.31)$$

where

$$\sigma^{\mu\nu} = \frac{i}{2}\left[\gamma^\mu, \gamma^\nu\right]. \qquad (A.0.32)$$

We need another kind of decomposition for our computations:

$$(q_1^\mu + q_2^\mu)\bar{u}(q_1)\gamma_5 u(q_2) = -i\sigma^{\mu\nu}(q_{1\nu} - q_{2\nu})\bar{u}(q_1)\gamma_5 u(q_2). \qquad (A.0.33)$$

The proof is

$$\begin{aligned}
\bar{u}(q_1)i\sigma^{\mu\nu}(q_{1\nu} - q_{2\nu})\gamma_5 u(q_2) =& \bar{u}(q_1)[(-g^{\mu\nu} + \gamma^\nu\gamma^\mu)q_{1\nu} - (g^{\mu\nu} - \gamma^\mu\gamma^\nu)q_{2\nu}]\gamma_5 u(q_2) = \\
=& \bar{u}(q_1)[(-q_1^\mu + \slashed{q}_1\gamma^\mu) - (q_2^\mu - \gamma^\mu\slashed{q}_2)]\gamma_5 u(q_2) = \\
=& \bar{u}(q_1)[(-q_1^\mu + m\gamma^\mu) - (q_2^\mu + \gamma^\mu m)]\gamma_5 u(q_2) = \\
=& (-q_1^\mu - q_2^\mu)\bar{u}(q_1)\gamma_5 u(q_2).
\end{aligned} \qquad (A.0.34)$$

We conclude this appendix by recalling the Feynman rules for external spinor lines:

$$= u^s(p), \qquad (A.0.35)$$

$$= \bar{u}^s(p), \qquad (A.0.36)$$

$$= \bar{v}^s(p), \qquad (A.0.37)$$

$$= v^s(p). \qquad (A.0.38)$$

Appendix B

Detailed calculation of real emission integrals

B.1 Vector emission

We can work out the numerator in the amplitude of equation (2.1.5)

$$\bar{u}(p')\left[\gamma^\mu(\not{p}' + m) - (\not{p} + m)\gamma^\rho\right]u(p). \tag{B.1.1}$$

Using (A.0.3) we can write this as

$$\bar{u}(p')\left[p'_\nu(2g^{\mu\nu} - \gamma^\nu\gamma^\mu) + m\gamma^\mu - (2g^{\rho\nu} - \gamma^\rho\gamma^\nu)p_\nu - m\gamma^\rho\right]u(p) =$$

$$=\bar{u}(p')\left[(2p'^\mu - \not{p}'\gamma^\mu) + m\gamma^\mu - (2p^\rho - \gamma^\rho\not{p}) - \gamma^\rho m\right]u(p) =$$

$$=2\bar{u}(p')(p'^\mu - p^\rho)u(p) + \left[\bar{u}(p')(-\not{p}' + m)\right]\gamma^\mu u(p) + \bar{u}(p')\gamma^\rho\left[(\not{p} - m)u(p)\right]. \tag{B.1.2}$$

Now the terms in square brackets in (B.1.2) vanish thanks to (A.0.23) and relabelling the dummy indices, the amplitude becomes

$$i\mathcal{M} = (ig)\bar{u}(p')\mathcal{M}_0(p',p)u(p)\left[\left(-\frac{p^\mu\epsilon_\mu^*}{p\cdot k}\right) + \left(\frac{p'^\mu\epsilon_\mu^*}{p'\cdot k}\right)\right]. \tag{B.1.3}$$

When we compute $|\mathcal{M}|^2$, summing over the massless vector polarizations we obtain the factorized term as

$$g^2\sum_{\mu\nu}\left[\left(-\frac{p^\mu\epsilon_\mu^*}{p\cdot k}\right) + \left(\frac{p'^\mu\epsilon_\mu^*}{p'\cdot k}\right)\right]\left[\left(-\frac{p^\nu\epsilon_\nu}{p\cdot k}\right) + \left(\frac{p'^\nu\epsilon_\nu}{p'\cdot k}\right)\right], \tag{B.1.4}$$

and replacing $\sum_{\mu\nu}\epsilon_\mu\epsilon_\nu^* \to -g_{\mu\nu}$ we obtain

$$g^2\left[-\frac{m^2}{(p\cdot k)^2} - \frac{m^2}{(p'\cdot k)^2} + \frac{2p\cdot p'}{(p\cdot k)(p'\cdot k)}\right]. \tag{B.1.5}$$

After summing over the polarization, the differential form factor for the cross-section can be written using the parametrization

$$k^\mu = (E_k, \vec{k}), \quad p^\mu = E(1, \vec{v}), \quad p'^\mu = E(1, \vec{v}'), \tag{B.1.6}$$

and will become

$$dF_{f \to f\gamma} = \frac{d^3 k}{2E_k} \frac{g^2}{(2\pi)^3} \left[-\frac{m^2}{(p \cdot k)^2} - \frac{m^2}{(p' \cdot k)^2} + \frac{2p \cdot p'}{(p \cdot k)(p' \cdot k)} \right] =$$

$$= \frac{d^3 k}{2E_k} \frac{g^2}{(2\pi)^3} \left[\frac{2E^2 - 2\vec{v}\vec{v}' E^2}{(E_k E - \vec{k}\vec{v}' E)(E_k E - \vec{k}\vec{v} E)} - \frac{m^2}{(E_k E - \vec{k}\vec{v}' E)^2} - \frac{m^2}{(E_k E - \vec{k}\vec{v} E)^2} \right] =$$

$$= \frac{d\phi}{2E_k} \frac{g^2}{(2\pi)^3} \sin\theta d\theta E_k^2 dk \frac{1}{E_k^2} \left[\frac{2 - 2\vec{v}\vec{v}'}{(1 - \hat{k}\vec{v}')(1 - \hat{k}\vec{v})} - \frac{m^2/E^2}{(1 - \hat{k}\vec{v}')^2} - \frac{m^2/E^2}{(1 - \hat{k}\vec{v})^2} \right] =$$

$$= \frac{\alpha}{2\pi} dk \frac{1}{E_k} I_\gamma(\vec{v}, \vec{v}')$$

$$= \frac{\alpha}{2\pi} dE_k \frac{1}{E_k} I_\gamma(\vec{v}, \vec{v}'), \tag{B.1.7}$$

where the last equality is due to the fact that $k^2 = 0$, so $E_k = |\vec{k}|$. The integral is

$$I_\gamma(\vec{v}, \vec{v}') = \int d\theta \sin\theta \left[\frac{2 - 2\vec{v}\vec{v}'}{(1 - \hat{k}\vec{v}')(1 - \hat{k}\vec{v})} - \frac{m^2/E^2}{(1 - \hat{k}\vec{v}')^2} - \frac{m^2/E^2}{(1 - \hat{k}\vec{v})^2} \right]. \tag{B.1.8}$$

In the high energy limit substituting the lower extreme of integration inside the integral we obtain

$$I_\gamma(\vec{v}, \vec{v}') \simeq \int_{\hat{k}\vec{v}'=\vec{v}\vec{v}'}^{t=1} dt \frac{2}{(1 - v't)} + \int_{\hat{k}\vec{v}'=\vec{v}\vec{v}'}^{t=1} dt \frac{2}{(1 - vt)} =$$

$$= -2 \left[\frac{1}{v'} \log(1 - v't) \right]_{t=\frac{\vec{v}\vec{v}'}{v'}}^1 - 2 \left[\frac{1}{v} \log(1 - vt) \right]_{t=\frac{\vec{v}\vec{v}'}{v}}^1 =$$

$$= 2 \left[\frac{1}{v'} \log\left(\frac{1 - \vec{v}\vec{v}'}{1 - v'} \right) + \frac{1}{v} \log\left(\frac{1 - \vec{v}\vec{v}'}{1 - v} \right) \right]. \tag{B.1.9}$$

Now using the fact that $v \simeq v'$ so that $p \simeq p'$, we can approximate the integral as

$$I_\gamma(\vec{v}, \vec{v}') \simeq \frac{2}{v} \log\left[\frac{(1 - \vec{v}\vec{v}')^2}{(1 - v)(1 - v')} \right] = \frac{2}{v} \log\left[\frac{(E^2 - \vec{p}\vec{p}')^2}{E^2(E - p)^2} \right] =$$

$$= \frac{4}{v} \log\left[\frac{(E^2 - \vec{p}\vec{p}')}{E(E - p)} \right]. \tag{B.1.10}$$

Now in equation (B.1.10), since $p \simeq E$, we can approximate the denominator as $(E^2 - p^2)/2$, in fact $E^2 - p^2 = 2E(E - p)$. In this way

$$I_\gamma(\vec{v}, \vec{v}') \simeq \frac{4}{v} \log\left[\frac{2p \cdot p'}{(E^2 - p^2)} \right] = \frac{4}{v} \log\left[\frac{2p \cdot p'}{m^2} \right] \approx \frac{4}{v} \log\left(\frac{\Delta E^2}{m^2} \right), \tag{B.1.11}$$

where $\Delta E^2 = (p' - p)^2$ and we can proceed as written in the main chapter.

58

B.2 Scalar emission

Working on the amplitude (2.2.5) we can use again (A.0.23) in order to write $\not{p}u(p) = mu(p)$ and $\bar{u}(p')\not{p}' = m\bar{u}(p')$ so that

$$i\mathcal{M} = (ig)\bar{u}(p')\mathcal{M}_0(p',p)u(p)\left[\left(-\frac{2m}{2p\cdot k}\right) + \left(\frac{2m}{2p'\cdot k}\right)\right], \tag{B.2.1}$$

and we can now compute

$$|\mathcal{M}|^2 = |\mathcal{M}_0|^2\, g^2\left[\left(-\frac{m}{p\cdot k}\right) + \left(\frac{m}{p'\cdot k}\right)\right]^2 =$$
$$= |\mathcal{M}_0|^2\, g^2\left[\frac{m^2}{(p\cdot k)^2} + \frac{m^2}{(p'\cdot k)^2} - \frac{2m^2}{(p\cdot k)(p'\cdot k)}\right]. \tag{B.2.2}$$

We need then to work on the form factor, using the same parametrization as before.

$$dF_{f\to f\phi} = \frac{d^3k}{2E_k}\frac{g^2}{(2\pi)^3}\left[\frac{m^2}{(E_kE - \vec{k}\vec{v}E)^2} + \frac{m^2}{(E_kE - \vec{k}\vec{v}'E)^2} - \frac{2m^2}{(E_kE - \vec{k}\vec{v}E)(E_kE - \vec{k}\vec{v}'E)}\right] =$$
$$= \frac{d^3k}{2E_k}\frac{g^2}{(2\pi)^3}\frac{m^2}{E^2}\frac{1}{E_k^2}\left[\frac{1}{(1 - \hat{k}\vec{v})^2} + \frac{1}{(1 - \hat{k}\vec{v}')^2} - \frac{2}{(1 - \hat{k}\vec{v})(1 - \hat{k}\vec{v}')}\right] =$$
$$= d\phi\frac{dk}{2E_k}\frac{g^2}{(2\pi)^3}\frac{m^2}{E^2}\left[\frac{1}{(1 - \hat{k}\vec{v})^2} + \frac{1}{(1 - \hat{k}\vec{v}')^2} - \frac{2}{(1 - \hat{k}\vec{v})(1 - \hat{k}\vec{v}')}\right] =$$
$$= \frac{dk}{E_k}\frac{\alpha}{2\pi}\frac{m^2}{E^2}I_\phi(\vec{v}, \vec{v'}). \tag{B.2.3}$$

From which
$$I_\phi(\vec{v}, \vec{v'}) = \int d\theta \sin\theta\left[\frac{1}{(1 - \hat{k}\vec{v})^2} + \frac{1}{(1 - \hat{k}\vec{v}')^2} - \frac{2}{(1 - \hat{k}\vec{v})(1 - \hat{k}\vec{v}')}\right] \tag{B.2.4}$$

We now integrate $I_\phi(\vec{v}, \vec{v'})$ dividing it into two parts. THe first one is immediate, putting $t = \cos\theta$:

$$\int_{-1}^1 dt\frac{1}{(1 - vt)^2} + \int_{-1}^1 dt\frac{1}{(1 - v't)^2} = \frac{2}{1 - v^2} + \frac{2}{1 - v'^2}, \tag{B.2.5}$$

In order to solve the second part we can use the same tricks of the previous section, but we need to keep in mind the fact that we do not have the numerator so the term with $\vec{v}\vec{v}'$ product does not cancel anymore, in addition to that, we have an overall minus sign. In this case, we need to choose $\hat{k}$ anti-parallel with respect to v or v'.

$$I_\phi(\vec{v}, \vec{v'}) \simeq \frac{2}{1 - v^2} + \frac{1}{1 - v'^2} - 2\left[\int_{t=-1}^{\hat{k}\vec{v}=-\vec{v}\vec{v}'} dt\frac{1}{(1 + v't)(1 - \hat{k}\vec{v})} + \int_{t=-1}^{\hat{k}\vec{v}'=-\vec{v}\vec{v}'} dt\frac{1}{(1 - \hat{k}\vec{v'})(1 + vt)}\right]$$
$$\approx \frac{2}{1 - v^2} + \frac{2}{1 - v'^2} + \frac{1}{1 - \vec{v}\vec{v}'}\frac{4}{v}\log\left(\frac{\Delta E^2}{m^2}\right). \tag{B.2.6}$$

and then we can proceed as explained in the main chapter.

Appendix C

Tree-level validation

To validate the tree-level model we look at the process $pp \to t\bar{t}X_0$ at $\sqrt{s} = 13$ TeV, this process contains all the interaction diagrams and the possible emissions, so it is perfect for our purpose. The cross-sections obtained using our UFO model are compared with the ones obtained by the HCC-NLO-X0 UFO from [3]. The result are presented in table C.0.1, in which we have considered the scalar case ($g = m_t/v, \tilde{g} = 0$) and the pseudoscalar case ($g = 0, \tilde{g} = m_t/v$) C.0.2

m_{X_0} (GeV)	σ HCC (pb)	our σ (pb)
10^{-6}	350.28±0.64	350.39±0.61
10^{-5}	298.22±0.72	298.22±0.72
10^{-4}	249.93±0.59	249.93±0.59
10^{-3}	202.34±0.66	202.34±0.66
10^{-2}	155.71±0.59	155.71±0.59
10^{-1}	108.57±0.25	108.57±0.25
10^{0}	61.53±0.17	61.43±0.17
10^{1}	20.10±0.04	20.10±0.04

Table C.0.1: $pp \to t\bar{t}X_0$ cross-section in the full scalar case, with $g = \frac{m_t}{v}, \tilde{g} = 0$ at $\sqrt{s} = 13$ TeV

m_{X_0} (GeV)	σ HCC (pb)	our σ (pb)
10^{-6}	0.432±0.001	0.432±0.001
10^{-5}	0.433±0.001	0.433±0.001
10^{-4}	0.433±0.001	0.433±0.001
10^{-3}	0.433±0.001	0.433±0.001
10^{-2}	0.432±0.001	0.432±0.001
10^{-1}	0.433±0.001	0.433±0.001
10^{0}	0.457±0.001	0.458±0.002
10^{1}	0.459±0.001	0.459±0.001

Table C.0.2: $pp \to t\bar{t}X_0$ cross-section in the full pseudoscalar case, with $g = 0, \tilde{g} = \frac{m_t}{v}$ at $\sqrt{s} = 13$ TeV

Appendix D

Dimensional regularization

We list here some useful formulae for dimensional regularization.

Feynman parametrization allows us to write

$$\frac{1}{D_1 D_2} = \int_0^1 dx \frac{1}{[D_1 + (D_2 - D_1)x]^2},\tag{D.0.1}$$

$$\frac{1}{D_1 D_2 D_3} = \int_0^1 dxdydz\delta(x + y + z - 1)\frac{2}{[xD_1 + yD_2 + zD_3]^3}.\tag{D.0.2}$$

We need also to look at some important integrals in dimensional regularization, here we will use $d = 4 - 2\epsilon$ and then we will expand around small ϵ values, sending ϵ to zero at the end of the process. We also call $\tilde{\mu}^2 = 4\pi\mu^2 e^{\gamma_E}$.

$$\bullet \, \mu^{4-d} \int \frac{d^d k}{(2\pi)^d} \frac{1}{(k^2 - \Delta + i\epsilon)^2} = \mu^{4-d} \frac{i}{(4\pi)^{\frac{d}{2}}} \frac{1}{\Delta^{2-\frac{d}{2}}} \Gamma\left(\frac{4-d}{2}\right) =$$

$$= \frac{i}{(4\pi)^{2-\epsilon}} \frac{\mu^\epsilon}{\Delta^\epsilon} \Gamma(\epsilon) = \tag{D.0.3}$$

$$= \frac{i}{(4\pi)^2} \left[\frac{1}{\epsilon} + \log\left(\frac{\tilde{\mu}^2}{\Delta}\right)\right].$$

$$\bullet \, \mu^{4-d} \int \frac{d^d k}{(2\pi)^d} \frac{k^2}{(k^2 - \Delta + i\epsilon)^2} = -\mu^{4-d} \frac{d}{2} \frac{i}{(4\pi)^{\frac{d}{2}}} \frac{1}{\Delta^{1-\frac{d}{2}}} \Gamma\left(\frac{2-d}{2}\right) =$$

$$= \mu^\epsilon(\epsilon - 2) \frac{i}{(4\pi)^{2-\epsilon}} \frac{1}{\Delta^{\epsilon-1}} \Gamma(\epsilon - 1) = \tag{D.0.4}$$

$$= \frac{2i\Delta}{(4\pi)^2} \left[\frac{1}{\epsilon} + \frac{1}{2} + \log\left(\frac{\tilde{\mu}^2}{\Delta^2}\right)\right].$$

$$\bullet \, \mu^{4-d} \int \frac{d^d k}{(2\pi)^d} \frac{1}{(k^2 - \Delta + i\epsilon)^3} = \mu^{4-d} \frac{-i}{2(4\pi)^{\frac{d}{2}}} \frac{1}{\Delta^{3-\frac{d}{2}}} \Gamma\left(\frac{6-d}{2}\right) =$$

$$= \mu^\epsilon \frac{-i}{2(4\pi)^{2-\epsilon}} \frac{1}{\Delta^{\epsilon+1}} \Gamma(\epsilon + 1) = \tag{D.0.5}$$

$$= \frac{-i}{2(4\pi)^2} \frac{1}{\Delta}.$$

$$\bullet \, \mu^{4-d} \int \frac{d^d k}{(2\pi)^d} \frac{k^2}{(k^2 - \Delta + i\epsilon)^3} = \mu^{4-d} \frac{d}{4} \frac{i}{(4\pi)^{\frac{d}{2}}} \frac{1}{\Delta^{2-\frac{d}{2}}} \Gamma\left(\frac{4-d}{2}\right) =$$

$$= \mu^\epsilon \frac{i}{(4\pi)^{2-\epsilon}} \left(1 - \frac{\epsilon}{2}\right) \frac{1}{\Delta^\epsilon} \Gamma(\epsilon) = \tag{D.0.6}$$

$$= \frac{i}{(4\pi)^2} \left[\frac{1}{\epsilon} + \log\left(\frac{\tilde{\mu}^2}{\Delta}\right) - \frac{1}{2}\right].$$

Appendix E

Diagram computations in detail

In this appendix, we report the explicit calculation made for the diagrams.

E.1 Mass renormalization

We want to work out the integral:

$$\int \frac{d^4k}{(2\pi)^4}(-ig+\tilde{g}\gamma_5)\frac{i(\slashed{k}+m_t)}{k^2-m_t^2+i\epsilon}(-ig+\tilde{g}\gamma_5)\frac{i}{(p-k)^2-m_{X_0}^2+i\epsilon}. \tag{E.1.1}$$

The denominator with Feynman parametrization transforms into:

$$\frac{1}{k^2-m_t^2+i\epsilon}\frac{1}{(p-k)^2-m_{X_0}^2+i\epsilon} =$$

$$= \int_0^1 dx \frac{1}{[(k^2-m_t^2)+((p-k)^2-m_{X_0}^2-k^2+m_t^2)x]^2}. \tag{E.1.2}$$

We work now on the denominator in order to write it in a useful way to apply dimensional regularization,

$$[(k^2-m_t^2)+((p-k)^2-m_{X_0}^2-k^2+m_t^2)x]^2 =$$
$$=[k^2-m_t^2+p^2x-2p\cdot kx-m_{X_0}^2x+m_t^2x+p^2x^2-p^2x^2]^2 =$$
$$=[(k-px)^2+p^2x-x^2p^2+m_t^2x-m_t^2-xm_{X_0}^2]^2 =$$
$$=[(k-px)^2-\Delta]^2, \tag{E.1.3}$$

where:

$$\Delta = x(xp^2-p^2-m_t^2+m_{X_0}^2)+m_t^2 = (1-x)(m_t^2-p^2x)+m_{X_0}^2x. \tag{E.1.4}$$

We need now to use (A.0.5) and (A.0.6) to work on the numerator, in order to obtain

$$-(-ig+\tilde{g}\gamma_5)(\slashed{k}+m_t)(-ig+\tilde{g}\gamma_5) = \tag{E.1.5}$$

$$=-\left[(-ig+\tilde{g}\gamma_5)^2m_t\right]-|(-ig+\tilde{g}\gamma_5)|^2\slashed{k} =$$

$$=-\left[(-g^2+\tilde{g}^2)m_t-2ig\tilde{g}m_t\gamma_5-(g^2+\tilde{g}^2)\slashed{k}\right]. \tag{E.1.6}$$

Using Feynman parametrization and performing the substitution: $k \to k + px$ we obtainE:

$$\int_0^1 dx \int \frac{d^4k}{(2\pi)^4} \frac{\left[(g^2 - \tilde{g}^2)m_t + 2ig\tilde{g}m_t\gamma_5 + (g^2 + \tilde{g}^2)(\slashed{k} + x\slashed{p})\right]}{[k^2 - \Delta + i\epsilon]^2}, . \tag{E.1.7}$$

We then remove the odd terms in k and we proceed with dimensional regularization choosing $d = 4 - 2\epsilon$. The integral becomes

$$\mu^{(4-d)} \int_0^1 dx \int \frac{d^d k}{(2\pi)^d} \frac{\left[(g^2 - \tilde{g}^2)m_t + 2ig\tilde{g}m_t\gamma_5 + (g^2 + \tilde{g}^2)x\slashed{p}\right]}{[k^2 - \Delta + i\epsilon]^2}; \tag{E.1.8}$$

after using (D.0.3) in (E.1.8) we obtain

$$\Sigma_{X_0}(\slashed{p}) = \frac{1}{(4\pi)^2} \int_0^1 dx[(g^2 - \tilde{g}^2)m_t + 2ig\tilde{g}m_t\gamma_5 + (g^2 + \tilde{g}^2)x\slashed{p}] \left[\frac{1}{\epsilon} + \log\left(\frac{\tilde{\mu}^2}{\Delta(x)}\right)\right].$$

E.2 Three point function

We want to work out the integral:

$$i\mathcal{M}_{X_0}^\mu = \int \frac{d^4k}{(2\pi)^4} \frac{i}{(q_1 - k)^2 - m_{X_0}^2 + i\epsilon} \bar{u}(q_2)(-ig + \tilde{g}\gamma_5) \frac{i(\slashed{p} + \slashed{k} + m_t)}{(p + k)^2 - m_t^2 + i\epsilon}(-ie\gamma^\mu)$$
$$\frac{i(\slashed{k} + m)}{k^2 - m_t^2 + i\epsilon}(-ig + \tilde{g}\gamma_5)u(q_1) \tag{E.2.1}$$

now, this amplitude needs some work to be computed, the first thing we need to do is to work on denominators, using Feynman parametrization:

$$D_1 = (k^2 - m_t^2) + i\epsilon, \tag{E.2.2}$$
$$D_2 = [(p + k)^2 - m_t^2] + i\epsilon, \tag{E.2.3}$$
$$D_3 = [(k - q_1)^2 - m_{X_0}^2] + i\epsilon. \tag{E.2.4}$$

Now, exploiting the fact that the fermions are on-shell ($q_1^2 = q_2^2 = m_t^2$) and $x + y + z = 1$ we find that

$$xD_1 + yD_2 + zD_3 =$$
$$= xk^2 - xm_t^2 + yp^2 + yk^2 + 2yp \cdot k - m_t^2 y + zk^2 + m_t^2 z - 2k \cdot q_1 z - m_{X_0}^2 z + i\epsilon =$$
$$= (k + yp - zq_1)^2 - y^2p^2 - z^2q_1^2 + 2zyp \cdot q_1 + yp^2 - m_t^2 + 2m_t^2 z - m_{X_0}^2 z + i\epsilon =$$
$$= (k + yp - zq_1)^2 - m_t^2(1 - z)^2 + p^2 y(1 - y) + 2zyp \cdot q_1 + i\epsilon =$$
$$= (k + yp - zq_1)^2 - m_t^2(1 - z)^2 + p^2 yx + p^2 yz + 2zyp \cdot q_1 - m_{X_0}^2 z + i\epsilon =$$
$$= (k + yp - zq_1)^2 - m_t^2(1 - z)^2 + p^2 yx + yz((p + q_1)^2 - q_1^2) - m_{X_0}^2 z + i\epsilon =$$
$$= (k + yp - zq_1)^2 - m_t^2(1 - z)^2 + p^2 yx + yz(q_2^2 - q_1^2) - m_{X_0}^2 z + i\epsilon =$$
$$= (k + yp - zq_1)^2 - m_t^2(1 - z)^2 + p^2 yx - m_{X_0}^2 z + i\epsilon =$$
$$= k^2 - \Delta + i\epsilon, \tag{E.2.5}$$

where in (E.2.5) we have made the substitution $k \to k - yp + zq_1$ and

$$\Delta = m_t^2 (1-z)^2 - p^2 yx + m_{X_0}^2 z. \tag{E.2.6}$$

Working on the numerator we obtain

$$
\begin{aligned}
\frac{N^\mu}{2e} &= \bar{u}(q_2)(g + i\tilde{g}\gamma_5)(\slashed{p} + \slashed{k} + m_t)\gamma^\mu(\slashed{k} + m_t)(g + i\tilde{g}\gamma_5)u(q_1) = \\
&= \bar{u}(q_2)(g + i\tilde{g}\gamma_5)(\slashed{p}\gamma^\mu\slashed{k} + \slashed{p}\gamma^\mu m_t + \slashed{k}\gamma^\mu\slashed{k} + \slashed{k}\gamma^\mu m_t + m_t\gamma^\mu\slashed{k} + m_t^2\gamma^\mu)(g + i\tilde{g}\gamma_5)u(q_1) = \\
&= \bar{u}(q_2)[(g^2 + \tilde{g}^2)(\slashed{p}\gamma^\mu\slashed{k} + \slashed{k}\gamma^\mu\slashed{k} + m_t^2\gamma^\mu) + (g^2 - \tilde{g}^2 + 2ig\tilde{g}\gamma_5)(\slashed{p}\gamma^\mu m_t + 2k^\mu m_t)]u(q_1).
\end{aligned}
$$

To proceed with the calculation we will need many properties, in particular, we will use the equations of motion (A.0.21) from which

$$\bar{u}(q_2)\slashed{p}u(q_1) = 0, \tag{E.2.7}$$

and some identities related to γ matrices (A.0.12),(A.0.13) and the usual trick $k^\mu k^\nu \to \frac{1}{d}g^{\mu\nu}k^2$.

In order to put the amplitude in the desired form we have used two decompositions:

$$
\begin{aligned}
\bar{u}(q_2)\slashed{p}\gamma^\mu u(q_1) &= m\bar{u}(q_2)\gamma^\mu u(q_1) - \bar{u}(q_2)\slashed{q}_1\gamma^\mu u(q_1) = \\
&= 2m\bar{u}(q_2)\gamma^\mu u(q_1) - 2\bar{u}(q_2)q_1^\mu u(q_1) = \\
&= 2m\bar{u}(q_2)\gamma^\mu u(q_1) - \bar{u}(q_2)(q_1^\mu + q_2^\mu)u(q_1) + \bar{u}(q_2)p^\mu u(q_1) = \\
&= \bar{u}(q_2)[i\sigma^{\mu\nu}(q_{2\nu} - q_{1\nu}) + p^\mu]u(q_1) = \bar{u}(q_2)[i\sigma^{\mu\nu}p_\nu + p^\mu]u(q_1), \tag{E.2.8}
\end{aligned}
$$

where the last lines equality follows from the Gordon identity (A.0.31).

$$
\begin{aligned}
\bar{u}(q_2)[\slashed{p}\gamma^\mu\gamma_5]u(q_1) &= \bar{u}(q_2)[\slashed{q}_2\gamma^\mu\gamma_5]u(q_1) - \bar{u}(q_2)[\slashed{q}_1\gamma^\mu\gamma_5]u(q_1) = \\
&= m\bar{u}(q_2)\gamma^\mu\gamma_5 u(q_1) - 2q_1^\mu\bar{u}(q_2)\gamma_5 u(q_1) - m\bar{u}(q_2)\gamma^\mu\gamma_5 u(q_1) = \\
&= -2q_1^\mu\bar{u}(q_2)\gamma_5 u(q_1) = (-q_1^\mu - q_2^\mu + p^\mu)\bar{u}(q_2)\gamma_5 u(q_1) = \\
&= \bar{u}(q_2)(p^\mu + i\sigma^{\mu\nu}p_\nu)\gamma_5 u(q_1), \tag{E.2.9}
\end{aligned}
$$

in which we have used (A.0.33).

In order to work with the numerator we separate terms that are multiplied by g^2, $\tilde{g}^2$ and $g\tilde{g}$.

E.2.1 Scalar term

The g^2 term can be computed starting from

$$
\begin{aligned}
g^2\bar{u}(q_2)[&y\gamma^\mu p^2 + z\slashed{p}\gamma^\mu m_t + \frac{2}{d}k^2\gamma^\mu - 2yzm_t p^u + 2z^2 q_1^\mu m_t - \gamma^\mu k^2 - y^2 p^2\gamma^\mu \\
&- z^2 m_t^2\gamma^\mu + 2yzq_1 \cdot p\gamma^\mu + m_t^2\gamma^\mu + \slashed{p}\gamma^\mu m_t - 2yp^\mu m_t + 2zq_1^\mu m_t]u(q_1). \tag{E.2.10}
\end{aligned}
$$

We need now to separate the equation into three parts:

$$
\begin{aligned}
&\left[(1-y)yp^2 - \left(1 - \frac{2}{d}\right)k^2 + m_t^2(1 - z^2)\right]\bar{u}(q_2)\gamma^\mu u(q_1) + \\
&[im_t(z+1)]p_\nu\bar{u}(q_2)\sigma^{\mu\nu}u(q_1) + \\
&\bar{u}(q_2)[2z^2 q_1^\mu m_t + 2yzq_1 \cdot p\gamma^\mu + 2zq_1^\mu m_t + m_t(z + 1 - 2y - 2yz)p^\mu]u(q_1). \tag{E.2.11}
\end{aligned}
$$

65

The last line of (E.2.11) need some work

$$\bar{u}(q_2)[(z+1-2yz-2y)m_t p^\mu + 2z^2 q_1^\mu m_t + 2yzq_1 \cdot p\gamma^\mu + 2zq_1^\mu m_t]u(q_1) =$$
$$= \bar{u}(q_2)\left[(z+1-2yz-2y)m_t p^\mu + (z^2+z)\left(q_1^\mu + q_2^\mu - p^\mu\right)m_t + yz[(p+q_1)^2 - q_1^2 - p^2]\gamma^\mu\right]u(q_1) =$$
$$= \bar{u}(q_2)\left[(z+1-2yz-2y)m_t p^\mu + (z^2+z)m_t\left(2m_t\gamma^\mu - i\sigma^{\mu\nu}p_\nu - p^\mu\right) - yzp^2\gamma^\mu\right]u(q_1), \qquad \text{(E.2.12)}$$

and now rearranging the elements we obtain for the g^2 term

$$g^2\left\{\left[(1-y-z)yp^2 - \left(1-\frac{2}{d}\right)k^2 + m_t^2(z+1)^2\right]\bar{u}(q_2)\gamma^\mu u(q_1)+ \right.$$
$$im_t(1-z^2)p_\nu\bar{u}(q_2)\sigma^{\mu\nu}u(q_1)+$$
$$\left. [-z^2+1-2yz-2y]m_t p^\mu \bar{u}(q_2)u(q_1)\right\}. \qquad \text{(E.2.13)}$$

E.2.2 Pseudoscalar term

The $\tilde{g}^2$ term can be computed starting from:

$$\tilde{g}^2\bar{u}(q_2)(\not{p}\gamma^\mu\not{k} + \not{k}\gamma^\mu\not{k} + m_t^2\gamma^\mu - \not{p}\gamma^\mu m_t - 2k^\mu m_t)u(q_1). \qquad \text{(E.2.14)}$$

We follow the same step as before:

$$\tilde{g}^2\bar{u}(q_2)[y\gamma^\mu p^2 + z\not{p}\gamma^\mu m_t + \frac{2}{d}k^2\gamma^\mu - 2yzm_t p^u + 2z^2 q_1^\mu m_t - \gamma^\mu k^2 - y^2 p^2\gamma^\mu$$
$$-z^2 m_t^2\gamma^\mu + 2yzq_1 \cdot p\gamma^\mu + m_t^2\gamma^\mu - \not{p}\gamma^\mu m_t + 2yp^\mu m_t - 2zq_1^\mu m_t]u(q_1), \qquad \text{(E.2.15)}$$

when we divide it in the three terms, we find:

$$\left[(1-y)yp^2 - \left(1-\frac{2}{d}\right)k^2 + m_t^2(1-z^2)\right]\bar{u}(q_2)\gamma^\mu u(q_1)+$$
$$[im_t(z-1)]p_\nu\bar{u}(q_2)\sigma^{\mu\nu}u(q_1)+ \qquad \text{(E.2.16)}$$
$$\bar{u}(q_2)[(z-1+2y-2yz)m_t p^\mu + 2z^2 q_1^\mu m_t + 2yzq_1 \cdot p\gamma^\mu - 2zq_1^\mu m_t]u(q_1).$$

We need again to work on the last line in (E.2.16)

$$\bar{u}(q_2)[(z-1+2y-2yz)m_t p^\mu + 2z^2 q_1^\mu m_t + 2yzq_1 \cdot p\gamma^\mu - 2zq_1^\mu m_t]u(q_1) =$$
$$= \bar{u}(q_2)\left[(z-1+2y-2yz)m_t p^\mu + (z^2-z)\left(q_1^\mu + q_2^\mu - p^\mu\right)m_t + yz[(p+q_1)^2 - q_1^2 - p^2]\gamma^\mu\right]u(q_1) =$$
$$= \bar{u}(q_2)\left[(z-1+2y-2yz)m_t p^\mu + (z^2-z)m_t\left(2m_t\gamma^\mu - i\sigma^{\mu\nu}p_\nu - p^\mu\right) - yzp^2\gamma^\mu\right]u(q_1). \qquad \text{(E.2.17)}$$

For the $\tilde{g}^2$ term we find

$$\tilde{g}^2\left\{\left[(1-y-z)yp^2 - \left(1-\frac{2}{d}\right)k^2 + m_t^2(z-1)^2\right]\bar{u}(q_2)\gamma^\mu u(q_1)+ \right.$$
$$[im_t(-z^2-1+2z)]p_\nu\bar{u}(q_2)\sigma^{\mu\nu}u(q_1)+$$
$$\left. (2z-1+2y-2yz-z^2)m_t p^\mu \bar{u}(q_2)u(q_1)\right\} \qquad \text{(E.2.18)}$$

66

E.2.3 Mixed term

The last part of the computation includes the mixed term $g\tilde{g}$:

$$2ig\tilde{g}\bar{u}(q_2)(\not{p}\gamma^\mu m_t + 2k^u m_t)\gamma_5 u(q_1) \tag{E.2.19}$$

translating k and removing odd term this becomes:

$$\bar{u}(q_2)(im_t\sigma^{\mu\nu}p_\nu + m_t p^\mu + 2zq_1^\mu m_t - 2yp^\mu m_t)\gamma_5 u(q_1), \tag{E.2.20}$$

we have no term with γ^μ but we still need some work on the term

$$\bar{u}(q_2)[2zq_1^\mu m_t + (1 - 2y)p^\mu m_t]\gamma_5 u(q_1) =$$
$$=\bar{u}(q_2)[z(q_1^\mu - p^\mu + q_2^\mu)m_t + (1 - 2y)p^\mu m_t]\gamma_5 u(q_1) =$$
$$=\bar{u}(q_2)[z(-p^\mu - i\sigma^{\mu\nu}p_\nu)m_t + (1 - 2y)p^\mu m_t]\gamma_5 u(q_1), \tag{E.2.21}$$

so the final term will be

$$2ig\tilde{g}\left[im_t(1 - z)\sigma^{\mu\nu}p_\nu\bar{u}(q_2)\gamma_5 u(q_1)+\right.$$

$$\left. -(z + 2y - 1)p^\mu\bar{u}(q_2)\gamma_5 u(q_1)\right]. \tag{E.2.22}$$

E.2.4 Computing the integral

After the decomposition above we have the following expressions:

$$g^2\bar{u}(q_2)\left\{\left[(1 - y - z)yp^2 - \left(1 - \frac{2}{d}\right)k^2 + m_t^2(z + 1)^2\right]\boldsymbol{\gamma^\mu} + im_t(1 - z^2)p_\nu\boldsymbol{\sigma^{\mu\nu}}\right\}u(q_1), \tag{E.2.23}$$

$$\tilde{g}^2\bar{u}(q_2)\left\{\left[(1 - y - z)yp^2 - \left(1 - \frac{2}{d}\right)k^2 + m_t^2(z - 1)^2\right]\boldsymbol{\gamma^\mu} - im_t(z - 1)^2 p_\nu\boldsymbol{\sigma^{\mu\nu}}\right\}u(q_1), \tag{E.2.24}$$

$$2ig\tilde{g}\left[im_t(1 - z)\boldsymbol{\sigma^{\mu\nu}}p_\nu\bar{u}(q_2)\gamma_5 u(q_1)\right]. \tag{E.2.25}$$

In the previous equations, we have neglected the p^μ terms. They should vanish due to the Ward identity, but we can notice another fact, the integral measure

$$\int dx dy dz \delta(1 - x - y - z), \tag{E.2.26}$$

is symmetric with respect to the exchange $x \leftrightarrow y$ and this is true also for the denominator. The p^μ term can be written as

$$g^2(1 + z)(1 - z - 2y) + \tilde{g}^2(z - 1)(1 - z - 2y) + 2ig\tilde{g}(1 - 2y - z) =$$
$$=g^2(1 + z)(x - y) + \tilde{g}^2(z - 1)(x - y) + 2ig\tilde{g}(x - y), \tag{E.2.27}$$

but this is clearly antisymmetric with respect to the $x \leftrightarrow y$ exchange.

67

In order to put together the terms we need to perform the following transformation:

$$\left(1 - \frac{2}{d}\right)\mu^{4-d} \int \frac{d^d k}{(2\pi)^d} \frac{k^2}{(k^2 - \Delta + i\epsilon)^3} = \left(1 - \frac{2}{d}\right)\mu^{4-d}\frac{d}{4}\frac{i}{(4\pi)^{\frac{d}{2}}}\frac{1}{\Delta^{2-\frac{d}{2}}}\Gamma\left(\frac{4-d}{2}\right) =$$

$$= \frac{1}{2}(1-\epsilon)\mu^{2\epsilon}\frac{i}{(4\pi)^{2-\epsilon}}\frac{1}{\Delta^\epsilon}\Gamma(\epsilon) = \frac{i}{(4\pi)^2}\left[\frac{1}{2\epsilon} + \frac{1}{2}\log\left(\frac{\tilde{\mu}^2}{\Delta}\right) - \frac{1}{2}\right], \tag{E.2.28}$$

where we have used (D.0.6) and expanded in ϵ. The terms proportional to m_t^2, p^2 and the $\sigma^{\mu\nu}$ term do not generate UV divergent contribution and can be computed in dimensional regularization using (D.0.5). Putting together all these terms we find the integral as expressed in the main chapter.

Appendix F

Detailed calculation of the NLO corrected amplitude

The interference term in the $q\bar{q} \to t\bar{t}$ amplitude reads

$$\sum_s \mathcal{M}_{X_0}^\dagger \mathcal{M}_0 \frac{e_q^2 e_t^2}{p^4} \sum_s \left[\bar{u}(p_3) \left[f_1(p^2)\gamma^\mu + i\frac{\sigma^{\mu\nu}}{2m_t} p_\nu F_2(p^2) \right] v(p_4) \bar{v}(p_2)\gamma_\mu u(p_1) \right]^\dagger \bar{u}(p_3)\gamma^\rho v(p_4)\bar{v}(p_2)\gamma_\rho u(p_1)$$

$$= \frac{e_q^2 e_t^2}{p^4} \sum_s \bar{u}(p_1)\gamma_\mu v(p_2)\bar{v}(p_4) \left[f_1^*(p^2)\gamma^\mu - i\frac{\sigma^{\mu\nu}}{2m_t} p_\nu F_2^*(p^2) \right] u(p_3)\bar{u}(p_3)\gamma^\rho v(p_4)\bar{v}(p_2)\gamma_\rho u(p_1)$$

$$= \frac{e_q^2 e_t^2}{p^4} \text{Tr}\left[(\slashed{p}_2 - m_q)\gamma_\rho(\slashed{p}_1 + m_q)\gamma_\mu \right] \text{Tr}\left[(\slashed{p}_3 + m_t)\gamma^\rho(\slashed{p}_4 - m_t)\left(f_1^*(p^2)\gamma^\mu - iF_2^\dagger(p^2)\frac{\sigma^{\mu\nu}}{2m_t}p_\nu \right) \right] =$$

$$= \frac{e_q^2 e_t^2}{p^4} \left(\text{Tr}\left[\slashed{p}_2\gamma_\rho\slashed{p}_1\gamma_\mu \right] - 4m_q^2 g_{\rho\mu} \right)\left(\text{Tr}\left[\slashed{p}_3\gamma^\rho\slashed{p}_4\left(f_1^*(p^2)\gamma^\mu \right) \right] - 4m_t^2 f_1^*(p^2)g^{\rho\mu} + \right.$$

$$\left. + \frac{i}{2}\text{Tr}\left[\slashed{p}_3\gamma^\rho F_2^\dagger(p^2)\sigma^{\mu\nu} - \gamma^\rho\slashed{p}_4 F_2^\dagger(p^2)\sigma^{\mu\nu} \right] p_\nu \right). \tag{F.0.1}$$

We have seen in chapter 3 that

$$|\mathcal{M}|^2 = \frac{1}{4}\sum_s |\mathcal{M}_0|^2 (1 + 2\text{Re}[f(p^2) + \delta_1 + F_2(p^2)]) +$$

$$+ \frac{2\text{Re}[F_2]}{p^4} e_q^2 e_t^2 \left(-4sm_t^2 + s^2 - t^2 + 2tu - u^2 \right). \tag{F.0.2}$$

69

Now we can work on the Mandelstam variables in the second part:

$$2\text{Re}[F_2]\frac{e_q^2 e_t^2}{s^2}\left(-4sm_t^2 + s^2 - t^2 + 2tu - u^2\right) =$$

$$=2\text{Re}[F_2]\frac{e_q^2 e_t^2}{s^2}\left(-2t^2 - 2u^2 - 4sm_t^2 + s^2 + (t+u)^2\right) =$$

$$=2\text{Re}[F_2]\frac{e_q^2 e_t^2}{s^2}\left(-2t^2 - 2u^2 - 4sm_t^2 + s^2 + (s - 2m_q^2 - 2m_t^2)^2\right) =$$

$$=2\text{Re}[F_2]\frac{e_q^2 e_t^2}{s^2}\left(-2t^2 - 2u^2 - 4sm_t^2 + 2s^2 + 4(m_q^2 + m_t^2)^2 - 4s(m_q^2 + m_t^2)\right) =$$

$$=2\text{Re}[F_2]\frac{e_q^2 e_t^2}{s^2}\left(-2t^2 - 2u^2 + 2s^2 + 4(m_q^2 + m_t^2)^2 - 8s(m_q^2 + m_t^2) + 4sm_q^2\right) =$$

$$=2\text{Re}[F_2]\left[-\frac{1}{4}\sum_s \mathcal{M}_0^2 + \frac{e_q^2 e_t^2}{s^2}\left(2s^2 + 4sm_q^2\right)\right].$$

(F.0.3)

Now we can put our result back inside (F.0.2) to obtain:

$$|\mathcal{M}|^2 = \frac{1}{4}\sum_s |\mathcal{M}_0|^2 (1 + 2\text{Re}[f(p^2) + \delta_1]) + 2\text{Re}[F_2(p^2)]e_q^2 e_t^2\left(2 + 4\frac{m_q^2}{s}\right).$$

(F.0.4)

The colour factor in front of $F_2(p^2)$ can be understood by thinking about the fact that the two $gq\bar{q}$ and $gt\bar{t}$ vertices will give a $T_{ij}^a T_{kl}^b$ matrices. The gluon propagator takes with itself a δ^{ab} term, so in the final amplitude, we will have a term like $T_{ij}^a T_{kl}^a$. When we compute the squared amplitude and take the average over the initial colours we find

$$\frac{1}{9}\sum_{a,b}\sum_{i,j}\sum_{k,l} T_{ij}^a T_{kl}^a T_{ij}^b T_{kl}^b = \frac{1}{9}Tr(T^a T^b)Tr(T^a T^b) = \frac{1}{9}\frac{1}{4}\delta^{ab}\delta^{ab} = \frac{1}{9}\frac{1}{4}8 = \frac{2}{9}.$$
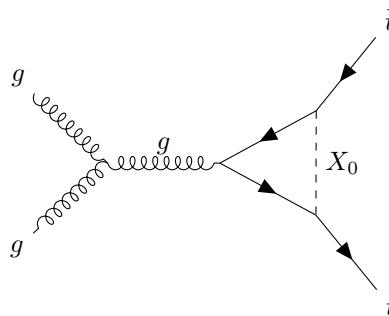
70

Appendix G

NLO process diagrams

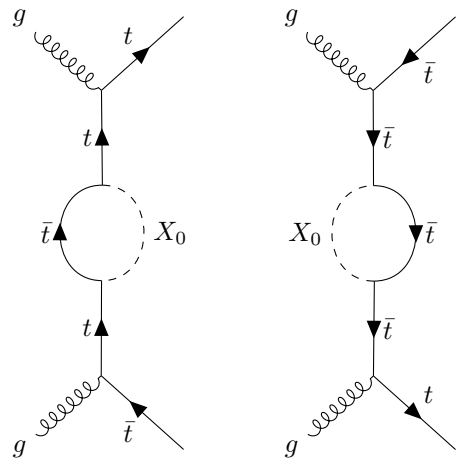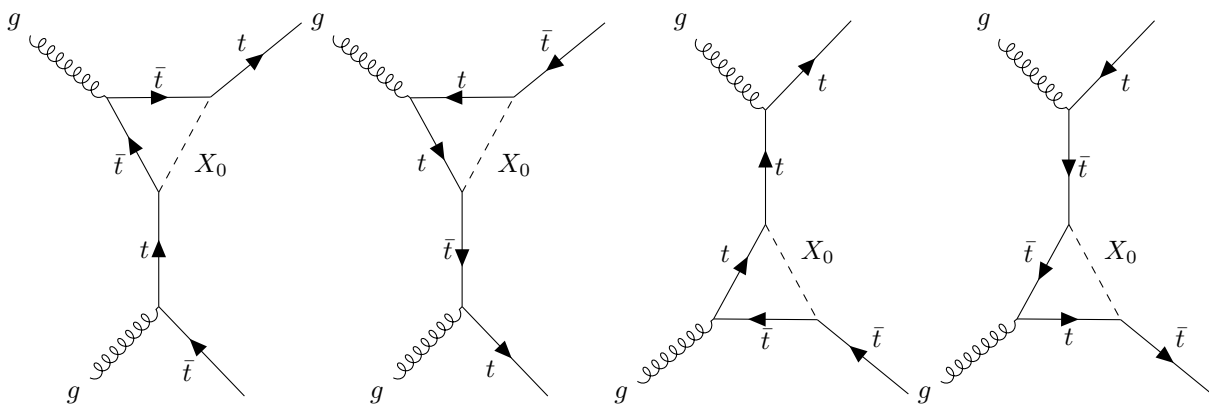For the process $q\bar{q} \to t\bar{t}$ there is only one diagram:
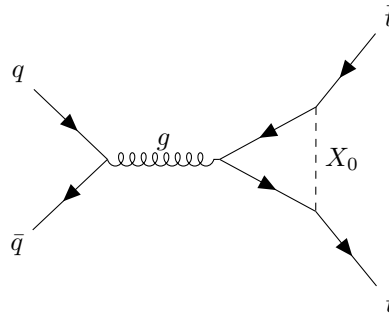
$$(G.0.1)$$

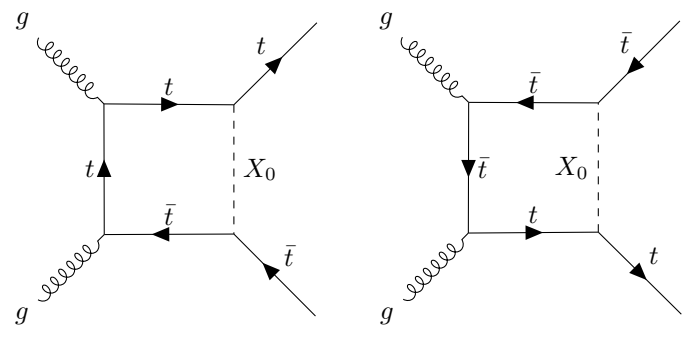For the process $gg \to t\bar{t}$ there are eleven diagrams:
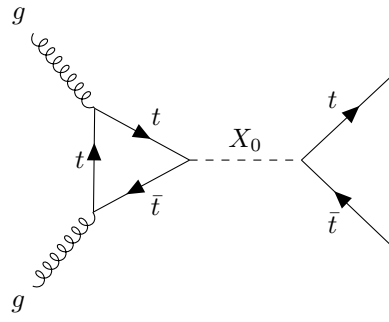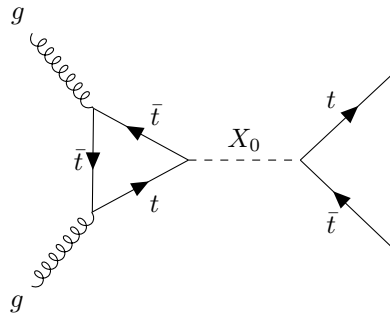

$$(G.0.2)$$

(G.0.3)

(G.0.4)

(G.0.5)

72

$$(G.0.6)$$

Appendix H

Rapidity and transverse momentum at the threshold

The rapidity

$$y = \frac{1}{2} \log \frac{E + p_z}{E - p_z}, \tag{H.0.1}$$

where z is the collision axis, can be used together with the transverse energy

$$E_T = \sqrt{m^2 + p_T^2}, \tag{H.0.2}$$

to express the 4-momentum of a particle as

$$p^\mu = (E_T \cosh y, P_{T,x}, P_{T,y}, E_T \sinh y). \tag{H.0.3}$$

We can now use this parametrization to express the invariant mass in the $t\bar{t}$ production process

$$M_{t\bar{t}} = E_{T,t}^2 + E_{T,\bar{t}}^2 + 2E_{T,t}E_{T,\bar{t}}(\cosh y_t \cosh y_{\bar{t}} - \sinh y_t \sinh y_{\bar{t}}), \tag{H.0.4}$$

where we have used the fact that the total transverse momentum must be equal to zero. We can now look at what happens at the threshold,

$$4m_t^2 = E_{T,t}^2 + E_{T,\bar{t}}^2 + 2E_{T,t}E_{T,\bar{t}}\cosh(y_t - y_{\bar{t}}). \tag{H.0.5}$$

Using the fact that $p_{T,t} = p_{T,\bar{t}} = p_T$ we have:

$$4m_t^2 = 2(m_t^2 + p_T^2)(1 + \cosh(y_t - y_{\bar{t}})), \tag{H.0.6}$$

from which

$$p_T^2(1 + \cosh(y_t - y_{\bar{t}})) + m_t^2(1 - \cosh(y_t - y_{\bar{t}})) = 0, \tag{H.0.7}$$

for which the couple

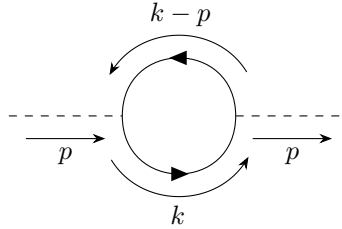$$p_T = 0 \qquad \cosh(y_t - y_{\bar{t}}) = 1 \rightarrow y_t - y_{\bar{t}} = 0 \tag{H.0.8}$$

is a solution.

Appendix I

Other 1-loop interesting diagrams

I.1 Fermionic-loop correction to X_0 two-point function

We compute the correction for the 2-point function of the particle X_0 with a fermion loop

$$\tag{I.1.1}$$

The integral for the loop turns out to be

$$\int \frac{d^4 k}{(2\pi)^4} \frac{i}{(p-k)^2 - m_t^2} \frac{i}{k^2 - m_t^2} \text{Tr}[(g + i\tilde{g}\gamma_5)(\slashed{k} - \slashed{p} + m)(g + i\tilde{g}\gamma_5)(\slashed{k} + m)], \tag{I.1.2}$$

we start the computation looking at the trace and using (A.0.14),(A.0.15),(A.0.17):

$$\text{Tr}[(g + i\tilde{g}\gamma_5)(\slashed{k} - \slashed{p} + m)(g + i\tilde{g}\gamma_5)(\slashed{k} + m)] =$$
$$= \text{Tr}[(g^2 + \tilde{g}^2)(\slashed{k} - \slashed{p})(\slashed{k} + m) + (g^2 - \tilde{g}^2 + 2ig\tilde{g}\gamma_5)(m\slashed{k} + m^2)] =$$
$$= (g^2 + \tilde{g}^2)(4k^2 - 4p \cdot k) + 4g^2 m^2 - 4\tilde{g}^2 m^2. \tag{I.1.3}$$

We turn back at the denominator, using the Feynman parametrization (D.0.1) we have:

$$k^2 - m_t^2 + [(p-k)^2 - m_t^2 - k^2 + m_t^2]x =$$
$$= k^2 - m_t^2 + p^2 x - 2p \cdot kx + p^2 x^2 - p^2 x^2 =$$
$$= (k - px)^2 - m_t^2 + p^2 x - p^2 x^2 =$$
$$= (k - px)^2 - \Delta, \tag{I.1.4}$$

where:

$$\Delta = m_t^2 - p^2 x(1 - x). \tag{I.1.5}$$

In order to use dimensional regularization we need to make the substitution: $k^\mu \rightarrow k^\mu + p^\mu x$.

We can now can turn back to the full integral, with the substitution above, removing odd terms we find:

$$\int_0^1 dx \int \frac{d^4k}{(2\pi)^4} \frac{4(g^2 + \tilde{g}^2)(k^2 + p^2x^2 - xp^2) + 4(g^2 - \tilde{g}^2)m_t^2}{(k^2 - \Delta + i\epsilon)^2}. \tag{I.1.6}$$

We need now to use (D.0.3) and (D.0.4) to obtain:

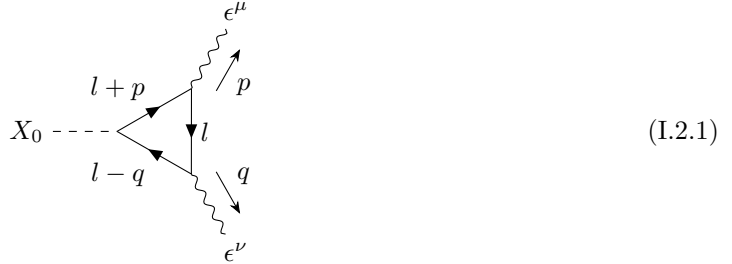$$\Pi_{X_0} = \int_0^1 dx[4(\alpha - \tilde{\alpha})m_t^2 - 4(\alpha + \tilde{\alpha})x(1-x)p^2]\left[\frac{1}{\epsilon} + \log\left(\frac{\tilde{u}^2}{\Delta(x)}\right)\right] +$$

$$+ \int_0^1 dx 8\Delta(\alpha + \tilde{\alpha})\left(\frac{1}{\epsilon} + \frac{1}{2} + \log\left(\frac{\tilde{\mu}^2}{\Delta(x)}\right)\right). \tag{I.1.7}$$

Now integrating Δ when it is possible:

$$\Pi_{X_0} = [2(6m_t^2 - p^2)\alpha + 2(2m_t^2 - p^2)\tilde{\alpha}]\frac{1}{\epsilon} +$$

$$+ (\alpha + \tilde{\alpha})\left(4m_t^2 - \frac{2}{3}p^2\right) +$$

$$+ \int_0^1 dx \left[12(m_t^2 - p^2x(1-x))\alpha + 4(m_t^2 - 3p^2x(1-x)\tilde{\alpha}\right] \log\left(\frac{\tilde{\mu}^2}{m_t^2 - x(1-x)p^2}\right) \tag{I.1.8}$$

I.2 Fermionic triangular diagram

We consider here the case of the X_0 decay into two photons, the gluon case differs only for a colour factor.

$$\tag{I.2.1}$$

We can also exchange the position of the two photons, but the diagram is the same, so we can simply multiply this diagram by a factor 2 in order to obtain the value of the full amplitude.

$$\mathcal{M} = i\epsilon_\mu^* \epsilon_\nu^* (-ie_t)^2 \int \frac{d^4l}{(2\pi)^4} \frac{i(\slashed{l} + m_t)}{l^2 - m_t^2}\gamma^\mu \frac{i(\slashed{l} + \slashed{p} + m_t))}{(l+p)^2 - m_t^2}(-g - i\tilde{g}\gamma_5)\frac{i(\slashed{l} - \slashed{q} + m_t)}{(l-q)^2 - m_t^2}\gamma^\nu. \tag{I.2.2}$$

As usual, we start working on the denominator in order to pass to the form in (D.0.2). What we obtain using the Feynman parametrization is

$$D_1 D_2 D_3 = (l + px - qy)^2 - m_t^2 + xy m_{X_0}^2. \tag{I.2.3}$$

76

We must now work on the numerator, neglecting the photon polarizations

$$N = \text{Tr}\left[(\not{l} + m_t)\gamma^\mu(\not{l} + \not{p} + m_t)(-g - i\tilde{g}\gamma_5)(\not{l} - \not{q} + m_t)\gamma^\nu\right], \tag{I.2.4}$$

we use the γ-matrices identities in A in order to remove trace of odd number of γ-s and solve the other ones:

$$N = -g\text{Tr}\left[\not{l}\gamma^\mu(2\not{l} + \not{p} - \not{q})\gamma^\nu m_t + m_t\gamma^\mu(l^2 + \not{p}\not{l} - \not{l}\not{q} - \not{p}\not{q})\gamma^\nu + m_t^3\gamma^\mu\gamma^\nu\right] + \\ -i\tilde{g}\text{Tr}\left[\not{l}\gamma^\mu(\not{p} + \not{q})\gamma_5\gamma^\nu m_t + m_t\gamma^\mu(-l^2 - \not{p}\not{l} + \not{l}\not{q} + \not{p}\not{q})\gamma_5\gamma^\nu + m_t^3\gamma^\mu\gamma_5\gamma^\nu\right]. \tag{I.2.5}$$

We will work this out keeping the terms in g and $\tilde{g}$ separated. Using the identity with γ traces, we finally obtain:

$$N = -4m_t g\left[2l^\mu l^\nu + l^\nu p^\nu - l^\mu q^\nu - 2g^{\mu\nu}l^2 - g^{\mu\nu}l\cdot p + g^{\mu\nu}l\cdot q + 2l^\mu l^\nu + l^\nu p^\mu - l^\nu q^\mu + l^2 g^{\mu\nu} + \right.$$

$$+ p^\mu l^\nu - l^\mu q^\nu - p^\mu q^\nu - p^\nu l^\mu + l^\nu q^\mu + p^\nu q^\mu + g^{\mu\nu}p\cdot l - g^{\mu\nu}l\cdot q - g^{\mu\nu}p\cdot q + m_t^2 g^{\mu\nu}\bigg] +$$

$$\left. -4m_t\tilde{g}\left[\epsilon^{\alpha\mu\beta\nu}(l_\alpha p_\beta + l_\alpha q_\beta + p_\alpha l_\beta - l_\alpha q_\beta - p_\alpha q_\beta)\right], \right. \tag{I.2.6}$$

now we need to remember that for the Lorentz gauge: $p\cdot\epsilon(p) = 0$, and that being $\epsilon^{\alpha\mu\beta\nu}$ anti-symmetric, we have $\epsilon^{\alpha\mu\beta\nu}(l_\alpha p_\beta + l_\beta p_\alpha) = 0$ so the numerator becomes much easier:

$$N = -4m_t g\left[4l^\mu l^\nu - \frac{m_{X_0}^2}{2}g^{\mu\nu} + m_t^2 g^{\mu\nu} - g^{\mu\nu}l^2 + p^\nu q^\mu\right] + \\ +4m_t\tilde{g}\left[\epsilon^{\alpha\mu\beta\nu}(p_\alpha q_\beta)\right]. \tag{I.2.7}$$

Now the g part is the same one we obtain for the Higgs boson calculation, the result is well known and therefore we will not compute it. Looking at the second term we have no dependence on l at all in the numerator.

We focus only on the $\tilde{g}$ term because the scalar case is the same as the Higgs. What we obtain at the end, shifting the denominator and multiplying by 2, in order to take into account both diagrams is

$$\mathcal{M}|_{\tilde{g}} = im_t\tilde{g}\epsilon_\mu^*\epsilon_\nu^*(-ie_t)^2\int\frac{d^4l}{(2\pi)^4}\int dxdy\frac{8\epsilon^{\alpha\mu\beta\nu}p_\alpha q_\beta}{(l^2 - m_t^2 + xym_{X_0}^2)^3}. \tag{I.2.8}$$

Now the integral in l using (D.0.5) give us

$$\mathcal{M}|_{\tilde{g}} = \tilde{g}m_t\epsilon_\mu^*\epsilon_\nu^*\frac{(-ie_t)^2}{32\pi^2}\int dxdy\frac{8\epsilon^{\alpha\mu\beta\nu}p_\alpha q_\beta}{m_t^2 - xym_{X_0}^2} \tag{I.2.9}$$

$$= m_t\tilde{g}\epsilon_\mu^*\epsilon_\nu^*\frac{(-ie_t)^2}{32\pi^2}8\epsilon^{\alpha\mu\beta\nu}p_\alpha q_\beta\frac{\text{Li}_2\left(\frac{2m_0}{m_0 - \sqrt{m_0^2 - 4m_t^2}}\right) + \text{Li}_2\left(\frac{2m_0}{\sqrt{m_0^2 - 4m_t^2 + m_0}}\right)}{m_0^2} = \tag{I.2.10}$$

$$\xrightarrow{m_t^2 \gg m_{X_0}^2} m_t\tilde{g}\epsilon_\mu^*\epsilon_\nu^*\frac{(-ie_t)^2}{8\pi^2}\epsilon^{\alpha\mu\beta\nu}\frac{p_\alpha q_\beta}{m_t^2}. \tag{I.2.11}$$

Before continuing we compare the integrals in the amplitudes in the pseudoscalar and in the scalar case:

$$\mathcal{M}_{\tilde{g}} = -\,\tilde{g}m_t\epsilon_\mu^*\epsilon_\nu^*\frac{e_t^2}{4\pi^2}\epsilon^{\alpha\mu\beta\nu}p_\alpha q_\beta\int dxdy\,\frac{1}{m_t^2 - xym_{X_0}^2}, \tag{I.2.12}$$

$$\mathcal{M}_{g} = -\,g\epsilon_\mu^*\epsilon_\nu^*m_t\frac{e_t^2}{4\pi^2}\left(g^{\mu\nu}m_{X_0}^2 - 2p^\nu q^\mu\right)\int dxdy\,\frac{1-4xy}{m_t^2 - m_{X_0}^2 xy}. \tag{I.2.13}$$

It is interesting to look what happens at this term when we put $m_{X_0} = 2m_t$.

$$\mathcal{M}_{\tilde{g}} = -\,\frac{\tilde{g}}{m_t}\epsilon_\mu^*\epsilon_\nu^*\frac{e_t^2}{4\pi^2}\epsilon^{\alpha\mu\beta\nu}p_\alpha q_\beta\frac{\pi^2}{8}, \tag{I.2.14}$$

$$\mathcal{M}_{g} = -\,\frac{g}{m_t}\epsilon_\mu^*\epsilon_\nu^*\frac{e_t^2}{4\pi^2}\left(g^{\mu\nu}4m_t^2 - 2p^\nu q^\mu\right)\frac{1}{2}. \tag{I.2.15}$$

I.2.1 Differential decay rate

Now for the decay, we are interested in the quantity $|\mathcal{M}|^2$, for the rest of the computation we will indicate the result of the integral in (I.2.9) as $F(m_t^2, m_{X_0}^2)$. Summing over polarization we obtain

$$
\begin{aligned}
|\mathcal{M}|^2|_{\tilde{g}} &= \frac{m_t^2\tilde{g}^2 e_t^4}{16\pi^4}(\epsilon^{\alpha\mu\beta\nu}p_\alpha q_\beta)(\epsilon^{\gamma\delta\sigma\tau}p_\gamma q_\sigma)g_{\mu\delta}g_{\nu\tau}\left|F(m_t^2, m_{X_0}^2)\right|^2 = \\
&= \frac{m_t^2\tilde{g}^2 e_t^4}{16\pi^4}(\epsilon^{\alpha\beta\mu\nu}p_\alpha q_\beta)(\epsilon_{\gamma\sigma\mu\nu}p^\gamma q^\sigma)\left|F(m_t^2, m_{X_0}^2)\right|^2 = \\
&= -\,\frac{m_t^2\tilde{g}^2 e_t^4}{8\pi^4}(\delta_{\gamma\sigma}^{\alpha\beta}p_\alpha q_\beta p^\gamma q^\sigma)\left|F(m_t^2, m_{X_0}^2)\right|^2 = \\
&= -\,\frac{m_t^2\tilde{g}^2 e_t^4}{8\pi^4}\left|F(m_t^2, m_{X_0}^2)\right|^2(p^2 q^2 - (p\cdot q)^2) = \\
&= \frac{m_t^2\tilde{g}^2 e_t^4}{32\pi^4}m_{X_0}^4\left|F(m_t^2, m_{X_0}^2)\right|^2. \tag{I.2.16}
\end{aligned}
$$

We can finally write

$$d\Gamma = \frac{1}{2m_{X_0}}|\mathcal{M}|^2\,d\Pi_{LIPS} = \frac{m_t^2\tilde{g}^2 e_t^4}{32\pi^4}m_{X_0}^3\left|F(m_t^2, m_{X_0}^2)\right|^2 d\Pi_{LIPS} \tag{I.2.17}$$

$$\xrightarrow{m_t^2 \gg m_{X_0}^2} \frac{\tilde{g}^2 e_t^4}{128\pi^4}\frac{m_{X_0}^3}{m_t^2}d\Pi_{LIPS}. \tag{I.2.18}$$

Ringraziamenti

In questo lungo lavoro di tesi, un ringraziamento è dovuto, più che ad ogni altro, al mio relatore, Davide Pagani. Non solo per le innumerevoli ore dedicate alla rilettura e alla correzione dell'elaborato, senza le quali sarebbe ben lontano dalla forma in cui è stato presentato, ma anche per i numerosi consigli, incoraggiamenti e la passione con cui mi ha accompagnato in tutto il percorso di stesura. Non c'è stata una sola volta in cui io mi sia sentito non ascoltato o ignorato. Un altro grande ringraziamento va al professor Fabio Maltoni, che mi segue dai tempi della tesi triennale, il suo entusiasmo nell'insegnamento e nello studio della fisica sono stati fondamentali durante tutto il mio percorso, mostrandomi come dopo anche anni di ricerca nella stessa materia, sia ancora possibile stupirsi e interrogarsi su nuove questioni. Un ringraziamento speciale va al professor Marco Zaro che ci ha aiutato a modificare i file di MadGraph5_aMC@NLO per poter ottenere le distribuzione cinematiche dell'ultimo capitolo. Non sarebbe giusto non ringraziare anche Maximiliano Sioli, mio tutor presso il Collegio Superiore, uno dei professori più disponibili che abbia incontrato nella mia carriera universitaria e fonte inesauribile di buoni consigli.

In questi anni universitari a fisica ho incontrato molte persone straordinarie, con cui ho condiviso le ansie e le gioie di questo percorso. Ce ne sarebbero molte da ringraziare e un elenco completo può essere trovato in bibliografia[1]. Grazie a Silvia, Stoppi, Diego, Ste, Mati, Bianca, Filippo e tutti gli altri. È stato un bellissimo viaggio da fare insieme, e spero che, anche se in luoghi diversi, continueremo in qualche modo a viaggiare insieme.

Una seconda famiglia l'ho trovata al Collegio Superiore[2]. Anche qui l'elenco sarebbe lungo. Grazie a Puli per essere stato un coinquilino assurdo e per avermi fatto vivere delle vere faide, come si usava tra i banditi della sua terra d'origine. Grazie a Cosmin, Valentina, Manu e Kevin per i bei momenti passati insieme in questi anni, i balli di gruppo e avermi insegnato a prendermi meno sul serio. Grazie ad Agnese, Ivan, Andrea, Lorenzo e Silvia, negli ultimi mesi se non sono affogato nella marea di cose da fare, è stato anche merito vostro. Grazie a Greta, per aver avuto la pazienza di prendere i fili ingarbugliati dei miei pensieri e metterli in ordine.

Grazie ai vecchi amici di Lodi. Elena, Pietro, Bryan, Andre, Gianluca, Secco, Fait e Angy. Anche se vi vedo poco, vi tengo dentro di me.

Grazie alla mia famiglia, a mia madre per aver sopportato i miei orari folli e le mie risposte stressate, a mio padre perché tra una discussione e l'altra mi ha insegnato anche lezioni preziose.

---

[1]Club del Drago (et. al.)

[2]Per un elenco completo si veda in bibliografia: I Prego, Commisione Fuego e Vacanze Selezionatissime

Bibliography

[1] Sven Krippendorf, Fernando Quevedo and Oliver Schlotterer. *Cambridge Lectures on Supersymmetry and Extra Dimensions*. 2010. DOI: `10.48550/ARXIV.1011.1491`. URL: `https://arxiv.org/abs/1011.1491`.

[2] A.M. Sirunyan et al. 'Measurement of the top quark Yukawa coupling from $t\bar{t}$ kinematic distributions in the dilepton final state in proton-proton collisions at $\sqrt{s} = 13\,\textbf{TeV}$'. In: *Physical Review D* 102.9 (Nov. 2020). DOI: `10.1103/physrevd.102.092013`. URL: `https://doi.org/10.1103%5C%2Fphysrevd.102.092013`.

[3] Till Martini et al. 'Probing the CP structure of the top quark Yukawa coupling: Loop sensitivity versus on-shell sensitivity'. In: *Physical Review D* 104.5 (Sept. 2021). DOI: `10.1103/physrevd.104.055045`. URL: `https://doi.org/10.1103%5C%2Fphysrevd.104.055045`.

[4] Federico Demartin et al. 'Higgs characterisation at NLO in QCD: CP properties of the top-quark Yukawa interaction'. In: *The European Physical Journal C* 74.9 (Sept. 2014). DOI: `10.1140/epjc/s10052-014-3065-2`. URL: `https://doi.org/10.1140%5C%2Fepjc%5C%2Fs10052-014-3065-2`.

[5] "De Blasi et al. 'On going on work'. In: ().

[6] F. Wilczek. 'Problem of Strong P and T Invariance in the Presence of Instantons'. In: *Phys. Rev. Lett.* 40 (5 Jan. 1978), pp. 279–282. DOI: `10.1103/PhysRevLett.40.279`. URL: `https://link.aps.org/doi/10.1103/PhysRevLett.40.279`.

[7] R.J. Crewther et al. 'Chiral estimate of the electric dipole moment of the neutron in quantum chromodynamics'. In: *Physics Letters B* 88.1 (1979), pp. 123–127. ISSN: 0370-2693. DOI: `https://doi.org/10.1016/0370-2693(79)90128-X`. URL: `https://www.sciencedirect.com/science/article/pii/037026937990128X`.

[8] Igor G. Irastorza and Javier Redondo. 'New experimental approaches in the search for axion-like particles'. In: *Progress in Particle and Nuclear Physics* 102 (Sept. 2018), pp. 89–159. DOI: `10.1016/j.ppnp.2018.05.003`. URL: `https://doi.org/10.1016%5C%2Fj.ppnp.2018.05.003`.

[9] R. D. Peccei and Helen R. Quinn. 'CP Conservation in the Presence of Pseudoparticles'. In: *Phys. Rev. Lett.* 38 (25 June 1977), pp. 1440–1443. DOI: `10.1103/PhysRevLett.38.1440`. URL: `https://link.aps.org/doi/10.1103/PhysRevLett.38.1440`.

[10] Cumrun Vafa and Edward Witten. 'Parity Conservation in Quantum Chromodynamics'. In: *Phys. Rev. Lett.* 53 (6 Aug. 1984), pp. 535–536. DOI: `10.1103/PhysRevLett.53.535`. URL: `https://link.aps.org/doi/10.1103/PhysRevLett.53.535`.

[11] Murray Gell-Mann and M Levy. 'The axial vector current in beta decay'. In: *Nuovo Cim.* 16 (1960), p. 705. DOI: `10.1007/BF02859738`.

[12] S. Abachi et al. 'Observation of the Top Quark'. In: *Physical Review Letters* 74.14 (Apr. 1995), pp. 2632–2637. DOI: `10.1103/physrevlett.74.2632`. URL: `https://doi.org/10.1103%5C%2Fphysrevlett.74.2632`.

[13] F. Abe et al. 'Observation of Top Quark Production in Pbar-P Collisions'. In: *Physical Review Letters* 74.14 (Apr. 1995), pp. 2626–2631. DOI: `10.1103/physrevlett.74.2626`. URL: `https://doi.org/10.1103%5C%2Fphysrevlett.74.2626`.

[14] R. L. Workman et al. 'Review of Particle Physics'. In: *PTEP* 2022 (2022), p. 083C01. DOI: `10.1093/ptep/ptac097`.

[15] Werner Bernreuther. *Top quark physics at the LHC*. 2008. DOI: `10.48550/ARXIV.0805.1333`. URL: `https://arxiv.org/abs/0805.1333`.

[16] Vittorio Del Duca and Eric Laenen. 'Top physics at the LHC'. In: *International Journal of Modern Physics A* 30.35 (Dec. 2015), p. 1530063. DOI: `10.1142/s0217751x1530063x`. URL: `https://doi.org/10.1142%2Fs0217751x1530063x`.

[17] R. L. Workman et al. 'Review of Particle Physics- Top Review'. In: *PTEP* 2022 (2022), p. 083C01. DOI: `10.1093/ptep/ptac097`.

[18] Abdelhak Djouadi. 'The anatomy of electroweak symmetry breaking'. In: *Physics Reports* 457.1-4 (Feb. 2008), pp. 1–216. DOI: `10.1016/j.physrep.2007.10.004`. URL: `https://doi.org/10.1016%2Fj.physrep.2007.10.004`.

[19] Giuseppe Degrassi et al. 'Higgs mass and vacuum stability in the Standard Model at NNLO'. In: *Journal of High Energy Physics* 2012.8 (Aug. 2012). DOI: `10.1007/jhep08(2012)098`. URL: `https://doi.org/10.1007%5C%2Fjhep08%5C%282012%5C%29098`.

[20] In: *Il Nuovo Cimento C* 35.3 (June 2012), pp. 111–114. ISSN: 03905551. DOI: `10.1393/ncc/i2012-11229-2`. URL: `https://doi.org/10.1393/ncc/i2012-11229-2`.

[21] V Barger, J Ohnemus and RJN Phillips. 'Spin correlation effects in the hadroproduction and decay of very heavy top quark pairs'. In: *International Journal of Modern Physics A* 4.03 (1989), pp. 617–625.

[22] T. Stelzer and S. Willenbrock. 'Spin correlation in top-quark production at hadron colliders'. In: *Physics Letters B* 374.1-3 (May 1996), pp. 169–172. DOI: `10.1016/0370-2693(96)00178-5`. URL: `https://doi.org/10.1016%2F0370-2693%2896%2900178-5`.

[23] Michael E. Peskin and Daniel V. Schroeder. 'An Introduction To Quantum Field Theory'. In: 1995.

[24] J. Alwall et al. 'The automated computation of tree-level and next-to-leading order differential cross sections, and their matching to parton shower simulations'. In: *Journal of High Energy Physics* 2014.7 (July 2014). DOI: `10.1007/jhep07(2014)079`. URL: `https://doi.org/10.1007%5C%2Fjhep07%5C%282014%5C%29079`.

[25] R. Frederix et al. 'The automation of next-to-leading order electroweak calculations'. In: *JHEP* 07 (2018). [Erratum: JHEP 11, 085 (2021)], p. 185. DOI: `10.1007/JHEP11(2021)085`. arXiv: `1804.10017 [hep-ph]`.

[26] Adam Alloul et al. 'FeynRules 2.0 - A complete toolbox for tree-level phenomenology'. In: *Comput. Phys. Commun.* 185 (2014), pp. 2250–2300. DOI: `10.1016/j.cpc.2014.04.012`. arXiv: `1310.1921 [hep-ph]`.

[27] Neil D. Christensen and Claude Duhr. 'FeynRules Feynman rules made easy'. In: *Computer Physics Communications* 180.9 (Sept. 2009), pp. 1614–1641. DOI: `10.1016/j.cpc.2009.02.018`. URL: `https://doi.org/10.1016%5C%2Fj.cpc.2009.02.018`.

[28] Celine Degrande. 'Automatic evaluation of UV and R2 terms for beyond the Standard Model Lagrangians: A proof-of-principle'. In: *Computer Physics Communications* 197 (Dec. 2015), pp. 239–262. DOI: `10.1016/j.cpc.2015.08.015`. URL: `https://doi.org/10.1016%5C%2Fj.cpc.2015.08.015`.

[29] A. Denner. 'Techniques for the Calculation of Electroweak Radiative Corrections at the One-Loop Level and Results forW-physics at LEP 200'. In: *Fortschritte der Physik/Progress of Physics* 41.4 (1993), pp. 307–420. ISSN: 1521-3979. DOI: `10.1002/prop.2190410402`. URL: `http://dx.doi.org/10.1002/PROP.2190410402`.

[30] Richard D. Ball et al. 'Parton distributions with QED corrections'. In: *Nucl. Phys. B* 877 (2013), pp. 290–320. DOI: `10.1016/j.nuclphysb.2013.10.010`. arXiv: `1308.0598 [hep-ph]`.

[31] Matthew D. Schwartz. *Quantum Field Theory and the Standard Model*. Cambridge University Press, 2013. DOI: `10.1017/9781139540940`.